CRANFIELD UNIVERSITY

EDUARDO PILES MONCHOLI

AN EXPERIMENTAL AND NUMERICAL STUDY ON THE EFFECT OF SOME PROPERTIES OF NON-METALLIC MATERIALS ON THE ICE ADHESION LEVEL

SCHOOL EN ENGINEERING
Department of Power and Propulsion
PhD Thesis

2010 - 2013

Supervisor: Dr David W. Hammond

CRANFIELD UNIVERSITY

EDUARDO PILES MONCHOLI

AN EXPERIMENTAL AND NUMERICAL STUDY ON THE EFFECT OF SOME PROPERTIES OF NON-METALLIC MATERIALS ON THE ICE ADHESION LEVEL

SCHOOL OF ENGINEERING
Department of Power and Propulsion
PhD Thesis

2010 - 2013

Supervisor: Dr David W. Hammond

This thesis is submitted in partial fulfilment of the requirements for the degree of PhD

ACKNOWLEDGEMENTS

I would like to thank my supervisor Dr David W. Hammond for his help, wise guidance and teaching skills. He has been and will be an influence in my future. I would like to thank the senior lecturers Dr David Mba and Dr. Joao Amaral Teixeira, who approached me for this PhD position. The experimental part of the Project has been possible thanks to the help of the Tunnel engineer, Mr. Brian Stappleton, his experience and suggestions were important factors in the success of the tests. I would like to thank Mr. Paolo Vanacore, our contact in Rolls Royce, for his interest in this Project, pragmatic suggestions and for being a kind host in the meetings in Derby.

I would like to thank Dr. Marie L. Pervier for her guidance in the first stages of the Project. I would also like to thank to other PhD researchers and MSc students that have been work colleagues during these years: Omid Gohardani, Beñat Gurrutxaga Lerma, Haseeb Shah (nice business trip to China), Vaira Pandian and Marta Esquer Cerezo.

Outside the University, I would like to thank all my friends for their company and nice moments together these years: Rafael López, hope we carry on doing our cultural trips to the best museums in Europe; Alex Escolar (que no pare, nano); Marta Arenas; Gonzalo Fernández, metalheads since 2010; Maria Ángeles Garrido; Mario Carreño, the best person and worst Comunio manager (Mario, paga); Raúl Picón; Rosa Hernández; Javier Rojas; Aleixo González; Carlos Soria and Luis Sánchez.

I would like to thank Leke Babalola, Elena Hatzimihali and the rest of the members of the Cranfield Salsa Society, for all the time and effort spent here. We have been a great team and made the Society to be a nice and warm atmosphere for all the students

Finally, I leave my last thank for the most important people to me, my parents, my sister and the rest of my family, for their support and company in the distance.

TABLE OF CONTENTS

LIST OF FIGURES

LIST OF TABLES

LIST OF EQUATIONS

LIST OF ABBREVIATIONS

A_{FEA}.	Crack developmenta Area in the Finite Elements model
A_{REAL}.	Crack develpment area of a slice of the real model
c [mm].	Defect size
E [GPa].	Young Modulus
FE [J/m^2].	Fracture Energy
FEA	Finite Elements Analysis
G [GPa].	Shear Modulus
h [mm].	Ice thickness
HDPE.	High Density Polyethylene
ISD,	Ice Shedding Device. Fixture employed in Shear Adhesion tests
K_I [Pa $m^{1/2}$].	Stress Intensity Factor, in tensile direction, for bulk materials
K_{IB} [Pa $m^{1/2}$]	Stress Intensity Factor in tensile direction, in a bi-material junction
K_{IB}/σ [Pa $m^{1/2}$].	Stress State in the crack tip, in tensile direction, in a bi-material junction
K_{IB_C} [Pa $m^{1/2}$].	Critical Stress Intensity Factor, in tensile direction, in a bi-material junction
K_{IC} [Pa $m^{1/2}$].	Fracture Toughness
K_{II} [Pa $m^{1/2}$].	Stress Intensity Factor, in shear direction, for bulk materials
K_{IIB} [Pa $m^{1/2}$].	Stress Intensity Factor, in shear direction, in a bi-materail junction
K_{IIB}/σ [$m^{1/2}$].	Stress State in the crack tip, in shear direction, in a bi-material junction
K_{IIB_C} [Pa $m^{1/2}$].	Critical Stress Intensity Factor, in shear direction, in a bi-material interface
LEFM,	Linear Elastic Fracture Mechanics
LWC [g/m^3].	Liquid Water Content
MVD [mm].	Median Volume Diameter
P_A [bar]	Air Pressure in the Tunnel atomizers
P_W [bar]	Water Pressure in the Tunnel atomizers
PP.	Polypropylene
PTFE,	Polytetrafluoroethylene
PVC.	Poly-vinyl-Chloride

r [mm].	Distrance from the crack tip along the crack plane
T [^{0}C].	Total Temperature
t [mm].	Coating thickness
t_{glue} [mm].	Glue layer thickness
τ_{13} [MPa].	Shear Stresses in the interface of a bi-material junction
Y.	Geometric Factor
σ [MPa].	Remote Load
σ_C [MPa]..	Critical Pressure
σ_Y [MPa].	Yield Strength
υ.	Poisson´s ratio

ABSTRACT

The rise of the Environmentalism in every sector of the Industry has lead the aircraft and engine manufacturing companies to develop new generations of more environmentally friendly engines. The companies, encouraged to this purpose, are in a constant research for new manufacturing and production techniques, in order to improve their products, from the environmental point of view, by gaining efficiency in the manufacturing techniques and reduce the fuel consumption and emissions in-flight.

Having in mind this scenario, the sponsor of this Project is interested in understanding how changing the materials of the blades, titanium alloys currently, for other lighter materials, such as composites, is going to have an effect in the overall gas turbine efficiency.

In the particular case of this Project, it will be studied the influence of the Stiffness and coating Thickness of those non-metallic materials suitable to be employed as coatings on gas turbine fan blades, from the icing point of view. The work procedure will be based on a study of Linear Elastic Fracture Mechanics of bi-material junctions and will extrapolate the general problem to the ice-coatings case, by getting experimental data from tests carried out in an Icing Tunnel.

It will be observed that the coating Stiffness has an influence on the Adhesion Level of ice to less stiff materials, if compared with the Adhesion Level of ice to metals. Besides, it will be described how a 0.5 millimetres thin polymeric coating placed over a metallic substrate is enough to reduce the Adhesion Level of ice, hiding any effect that the underneath materials might have on the Adhesion Level.

Keywords:

Icing, polymers, icing tunnel, bi-material junctions, mitigation strategies, elastic properties of materials, coating thickness, LEFM

CHAPTER 1. PRESENTATION

OF THE PROJECT

1.1. Background

This Thesis is a sponsored University Project, under the SAMULET (Strategic Affordable Manufacturing in the UK through Leading Environmental Technologies) Project developed by Rolls-Royce. The aim of SAMULET Project is the research in a range of new Materials, Manufacturing Processes and Techniques that will allow the development of a new generation of more environmentally friendly engines.

Aerospace companies are continuously researching on new improvements that would achieve higher gas turbine performance: reduction of CO_2 emissions and increase the overall efficiency, without compromising the in-flight safety and engine reliability. The sponsor is in the process of development of a new generation of engines. Among other improvement, the company plans to substitute the material of the fan blades. The Titanium alloy that is employed currently is planned to be substituted for composite core blades with Titanium alloy protection on the leading edge. The composite exposed area might be coated with polymeric coating and/or paint.

This project is focused on the icing phenomenon on the gas turbine fan blades. The objective of this Thesis is to study how the Stiffness and Thickness of a polymeric coating might affect the ice adhesion strength to materials that could be candidates to be employed as blades coating. This Thesis will provide Rolls-Royce with a framework of results and conclusions that will help the company to understand how the substrate properties of non metallic materials have an effect on ice adhesion strength. This scheme will be helpful for the Company in order to choose an optimum combination or layout of non-metallic materials for them to study the suitability of using non-metallic fan blades from the icing point of view

This Project has a starting base in the PhD Project by Marie Pervier (Pervier, 2012), who has targeted her project on the mechanisms of ice attachment to Titanium alloys and the physics of ice. The experimental results and the merit of the materials will be compared to the results obtained in that Project on order to estimate the merit of the non metallic material to be employed as a mitigation strategy

1.2. Icing Hazards

Icing in aerospace environment is the accretion of impact ice, under certain conditions of temperature and humidity, on exposed surfaces. It is possible to find it on aircraft exposed parts, ships, overhead lines or building structures affected by icing.

Icing might occur due to the different forms of water. The interest of this work, and how it is reproduced experimentally, is the icing event due to super cooled droplets. These are the conditions that cause the ice to grow in the fan blades whereas icing due to other ice sources is more concerning to other parts of the gas turbine. For instance, the concern of icing due to ice crystals is more focused towards the risk of blockage of measurement devices or ice formation if the first stages of the compressor.

Icing due to super cooled droplets (from now on, referred only as “icing” in this work) occurs when liquid water droplets are suspended in the atmosphere. Liquid water droplets in the atmosphere are known as super-cooled droplets and, as long as water is in super cooled state, it is in active state. When in active state, water tends to attach to any interfering surface. If the surface is at a sub-zero Temperature, the water that adheres freezes and ice grows over the exposed surface. When an aircraft passes through the clouds, provided the aircraft surfaces are below 0^0C, water droplets get in contact with the exposed surfaces and freeze. This is the onset of ice accretion.

The risks of the ice formation on gas turbine fan blades are that ice can shed from the rotating blades and impact on inner components of the gas turbine. There is the possibility of a combination of ambient conditions and rotational speed that allows the ice to grow in large block before the shedding process. If this happens, it can cause damage of the internal parts of the gas turbine, such as the fan track liners or the gas turbine components located behind the fan.

1.3. Icing in fan blades

Ice forms on the leading edge and the pressure surface of the blades. The rotational speed generates centrifugal forces that create a stress field within the ice and in the ice-blade interface. This situation makes the icing hazards especially concerning in taxing, idle (30 % of max power) and hold conditions (60% of max power), since the rotational speed is in a range that the centrifugal forces created allow the ice to form in larger blocks before shedding it. Icing in maximum power regime is not a concern since the centrifugal forces are large enough to cause the ice to shed earlier in smaller pieces. No damage due to the shedding of ice is expected in this regime.

Ice can detach from the blades due centrifugal forces in tensile or shear direction. The regime creates larger centrifugal forces in the tip of the blade, which can create a crack in the interface between the ice and the blade. On the other hand, the geometry of the blade, the twisting and the vibrations can result in scenarios where the ice sheds in tension. The sketch of the forces can be observed in Figure 1.1**,** where σ is the tensile stress and τ the shear stress. This sketch is supported by some pictures obtained from the Icing Department at Rolls Royce (Figure 1.2).

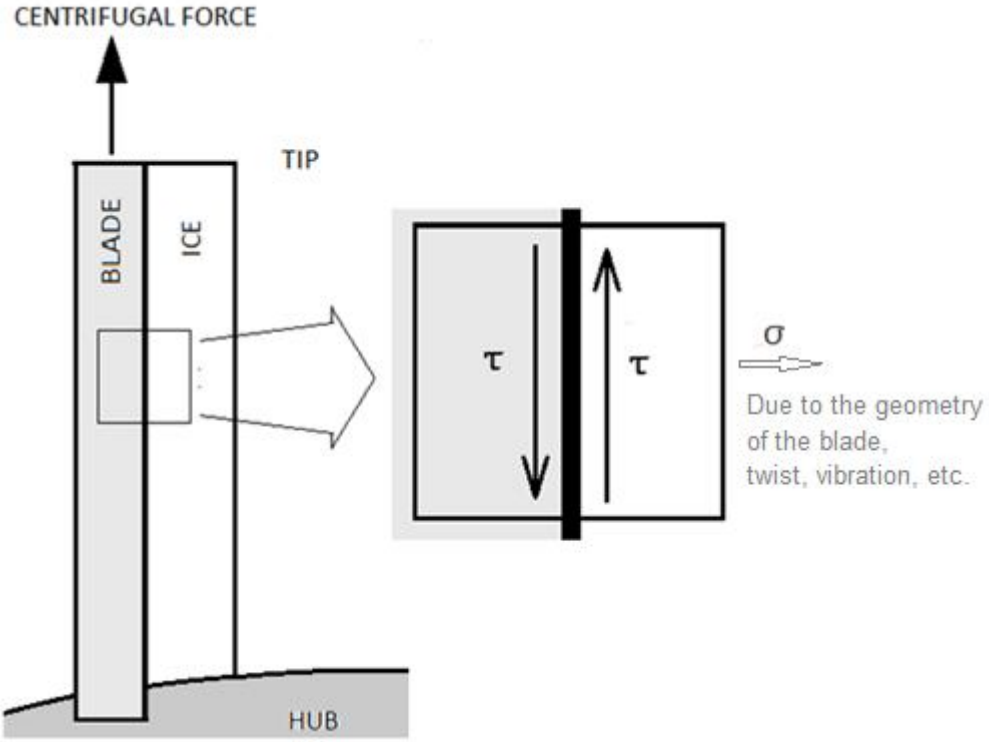

Fig 1.1. Distribution of forces on a fan blade profile

Fig 1.2. Pictures taken from a ground level icing test, supplied by Rolls-Royce©.

The pictures in Figure 1.2 show two cases of a fan after ice release. They belong to a series of ground level icing tests of real gas turbines carried out by Rolls-Royce, for freezing fog conditions and having the turbine the regime it would have in idle, hold and max power conditions.

The picture on top shows a case where the shaft was rotating in hold conditions (60% maximum power), at a temperature of -10^0C and real freezing fog conditions. This is a typical case of shear dominant fracture, the blade areas nearby the hub keep ice attached whereas the tip is free of ice. This occurs since the centrifugal forces caused the crack to start in the tip and develop along the ice-blade interface until the Fracture Toughness of ice is reached; then, the crack develops within the volume of ice.

On the other hand, the bottom picture of Figure 1.2 shows a case where the predominant fracture occurs in tensile direction. This picture was taken in a test in idle conditions, a temperature of -10^0C and freezing fog ambient conditions. Due to the regime, the centrifugal forces did not cause a crack onset in the tip of the blades, but the crack started in tensile direction in zones half distance between the hub and the tip.

Both pictures in Figure 1.2 show that fracture in both tensile and shear direction can occur in gas turbine fan blades, so that, both modes are to be studied equally in this work

1.4. On the Cloud Physics

Water in nature is in continuous motion, causing the water to change the state. Those changes of state generate the hydrologic cycle. Practically, the most vapour water in the atmosphere comes from sea water evaporation and it is spread out to the continental mass through wind currents.

Physically, a cloud is an accumulation of vapour, condensed water droplets and, often, ice particles, suspended in the atmosphere. The growth model employed by various text books is the "Continuous Growth Model". All the drops with the same size grow at the same rate (Mason, 1972). Droplet formation is subjected to a nuclei formation, and no vapour condenses without their presence. These nuclei are particles of any nature, formed from the disintegration of matter of any nature, where the moist condenses into it as liquid water droplets.

Clouds can be found up to an altitude of 6000 metres from sea level. They can be classified according to the processes they generate. These types have different shape, distribution, Liquid Water Concentration, altitude, etc (Mason, 1972):

- Stratus clouds: These clouds are created when a front of warm and moist air passes slowly through a cold air atmospheric layer, at an altitude below 300 meters. These clouds are horizontal and spread out across the sky, covering vast areas (many kilometres). Its aspect is grey and featureless and the LWC is approximately 0.28-0.3 g/m3
- Cumulus clouds: Theses clouds form when warm and moist air lifts at an altitude between 600 and 1000 metres. The cloud aspect is round and deformed (candy floss shape). The variety of cumulonimbus clouds are the typical summer storm clouds that can provoke thunderstorms and can extend hundreds of meters vertically. The typical LWC is 0.25-0.45 g/m^3.
- Cirrus clouds: These are formed by ice crystals, as a result of direct sublimation of vapour particles. These clouds form at about 6000 meters. Its shape is curly and feathery. The LWC is the lowest, around 0.06 g/m^3.

1.5. On the types of Ice

Ice can be classified in many several ways, according to its appearance, density and mechanism of formation. This work will use the suggestions by the New Zealand Aviation Authority to classify the ice that it is likely to form in-flight (Aircraft Icing Handbook., 2000)

- Glaze Ice: Also called Clear Ice or Clean Ice. It is a high-density ice (approx 0'92 g/cm^3), transparent and hard. Glaze ice is formed by slow solidification process, in general, under high temperature and high moisture conditions or large super cooled droplets. At slow solidification processes, only the volume in contact freezes when they contact with sub zero body, while the external side is still liquid and able to run back through the surface before freezing.
- Rime ice. Rime ice is white, opaque, granulated and has a feathery aspect. It is formed when the solidification is immediate. This occurs in general in colder and dryer conditions than the Glaze Ice case. So that, there is a large quantity of trapped air bubbles and rapid dissipation of the latent fusion heat. The bubbles trapped reduce the density and make the rime ice to be lighter, brittle and weak. However, the density may vary, being so slow that the ice can be hand removed or as dense as the glaze ice.
- Mixed ice. A mixture between both previous ice types..

An approximation of icing risk grades according to the temperature is shown in Table 1.1

	Cumulus Clouds	**Stratus Clouds**	**Rain and Drizzle**
High Risk	0 to -20ºC	0 to -15ºC	Below 0ºC
Medium Risk	-20 to -40ºC	-15 to -30ºC	
Low Risk	Lower than -40ºC	Lower than -30ºC	

Table 1.1. Icing risks

The project will study the ice adhesion in those situations where there is a high risk of icing. The tests will be carried out at a set of temperatures between -5 and -20^{0}C. The most common Temperature tested will be -10^{0}C and the most common LWC will be 0.4 g/m^3, the range of LWC found in cumulus clouds.

1.6. Icing Parameters

There are some ambient conditions that have been discussed to have an influence on the icing phenomenon. The parameters are Ambient Temperature, LWC, droplet size and wind speed. (Gent, et al., 2000)

Total Air Temperature (TAT): The ambient has an effect on the Surface Temperature in the exposed surfaces where the ice forms by cooling them down. TAT has also an effect on the type of ice that can form.

Air speed: The higher the speed, the more volume of air intercepted in the same amount of time, what is the same, more quantity of water will contact the exposed surface

MVD (Median Volume Diameter or Droplet size): It has an effect on the mass of the water impinging the surface and in the aerodynamic behaviour of the droplet. A large droplet tends to follow a straight line when forced. A large mass body has larger inertial forces than a small one, so that, aerodynamics are not affecting the trajectory, but these forces. On the other hand, small droplets will tend to follow the streamline since the inertial forces are negligible. To sum up, whether a droplet impacts on a surface or follows the streamline is physically determined by the ratio inertia/aerodynamic forces. The droplet size is linked to ambient temperature, because the probability of finding large droplets decreases as the temperature decreases. The MVD used in this work is common for every test, 20 μm diameter, a typical size of a super cooled droplet

LWC: Since the humidity and the water droplet distribution is not uniform in a cloud, the factor to determine whether the cloud is “wet” or “dry” when compared to others is the LWC. This parameter defines the average mass of liquid water suspended in a volume in a cloud. LWC affects the growth rate, making it to increase as the LWC increases: more quantity of water surrounding makes more frequent the contact between liquid water and the surface. LWC also affects the type of ice, high LWC favours the glaze ice accretion. Rime ice is more likely to generate in drier conditions.

CHAPTER 2. LITERATURE SURVEY

2.1. On the Adhesion of Ice to exposed substrates

Icing phenomenon has been a research topic due to its importance for in-flight safety. This chapter will bring together some observations made by authors on the ice Adhesion Level to metals and non metals, for both tensile and shear direction

The first concept is the attachment mechanism of ice. Landy and Freiberger discussed that ice adheres mechanically and chemically (Landy & Freiberger, 1966).

The mechanical adhesion is based on clamping to irregularities. Water penetrates into the structure through superficial roughness. Once the droplet freezes in a "valley" of the surface, it expands and gets squeezed inside and pushes the sides apart. Then, the trapped ice acts as an anchor of the ice to the substrate.

Chemical adhesion occurs when the ice and the exposed material come close enough for their inner structures to create intermolecular bonds between them. The ice adheres through H-bonds and Van de Waals forces. The authors related the Adhesion Level of ice with the Free Surface Energy and used the wettability of a substrate to evaluate it. The wettability is the capacity of a liquid to spread over a surface. Any liquid must satisfy $\gamma < \gamma_c$ to spread, being γ_c the specific surface tension of the substrate. There are some samples of γ_c for different polymers in Figure 2.1. The polymers with the lowest values of Surface Energy Coefficients are chlorine-carbons, hydrocarbons or fluorocarbons. The strength of the covalent bond of a C-Cl, C-H and C-F makes the surface more inert, so that, the H-bonds to those surfaces are the weakest. This "weakness" of the bond makes the amount of energy necessary to separate the materials in the junction (Free Surface Energy) to be lower

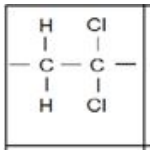	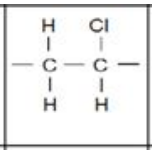	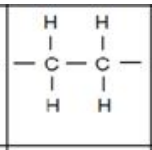	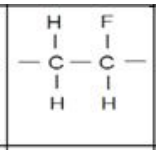	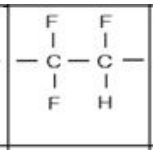	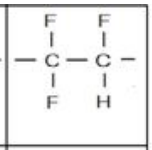
40	39	31	28	22	18

Fig 2.1. Surface Tension Coefficients values at 20^0C (units (mN/m)

This work employs the Critical Stress State in the crack onset to define the Adhesion Level of the ice. Critical Stress and Free Surface Energy are related and both refer to the Adhesion Strength. The Free Surface Energy is the energy per square meter necessary to break the chemical bonds that attach the ice to the accretion surface, whereas the Critical Stress State describes the resistance of a crack to grow and spread until the fracture. Critical Stress state is chosen for this work since the equations to obtain it make the possibility to compare the Critical Stress Intensity Factor in tensile and shear direction.

2.2. On the Tensile Adhesion to bonded joints

Tensile adhesion strength of bonded joints is the resistance to separation of a joint when a remote load σ is applied in perpendicular direction to the junction plane. Several studies have been carried out studying the adhesion strength of ice to different substrates and the effect of ambient conditions. These studies in the Literature use different tools to separate the ice from an external body whose properties and geometry are well known and different technique to estimate the adhesion level. The works surveyed observe, in general, that the materials employed do have an influence in the adhesion.

Jellinek (Jellinek, 1959) is among the first researchers to study the effect of the Temperature on the ice adhesion, in tensile and shear direction. He observed, in the tensile direction scenario, that the cohesive strength of the ice had a constant value and the adhesive strength was observed to depend linearly upon the temperature for both metals and non-metals (Figure 2.3).

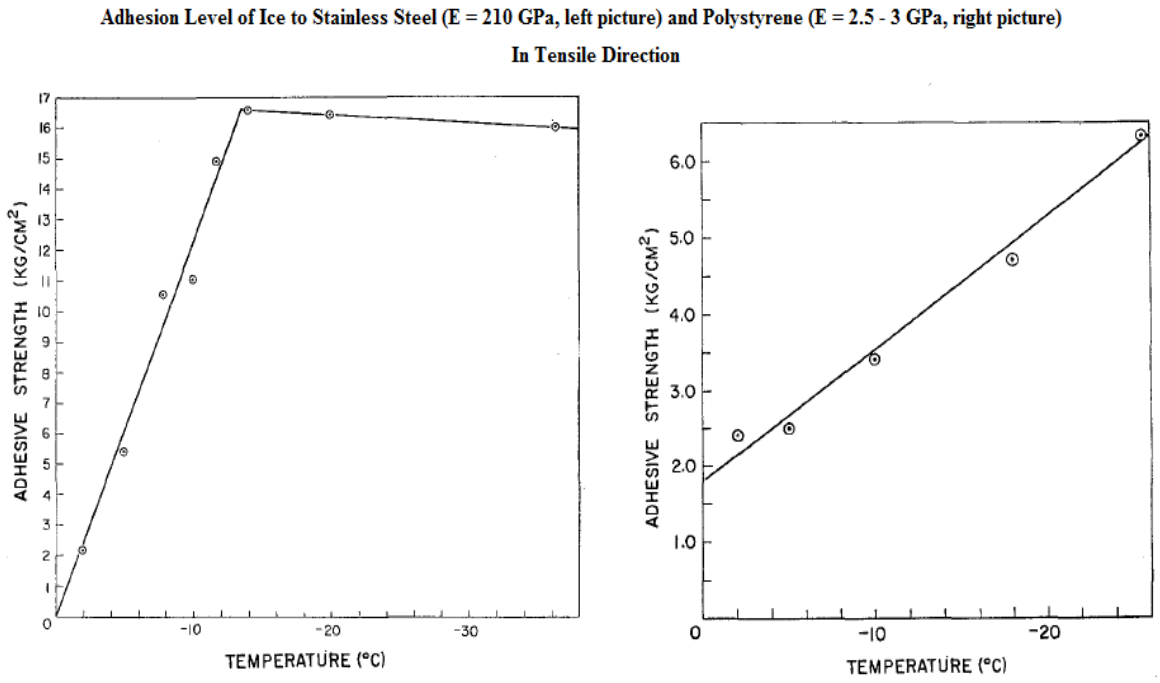

Fig 2.3. Evolution of Fracture Energy with Temperature for Metallic (right) and polymeric Substrates (Jellinek, 1957)

In the case of ice attached to metals, Jellinek observed that the fracture was found to break adhesively until the Temperature was decreased up to certain value. For Temperatures lower than that value, there was a transition between adhesive and cohesive fracture mode. Once that point is overcome, the adhesive strength grows above the cohesive one, so it is first reached the critical fracture toughness of the ice and, consequently, the fracture occurs cohesively. In the case of ice attached to Polystyrene, the fracture strength was observed to be adhesive at every range of temperatures tested (-5 to -20^{0}C). The trend line is different for metals (stiffer than ice) and polymers (less stiff than ice) and the Adhesion Level was found to be larger in metals (stainless steel) compared to non-metal samples (Polystyrene). The results showed in Figure 2.3 were carried out in samples whose area was 1.54 cm^2, at atmospheric pressure and a thickness of ice of 0.1 cm. The results are not entirely comparable to the ones obtained in this work as the ice thickness is in a range that the fracture can be assumed to occur in Plane Stress Conditions, whereas Plane Strain conditions are considered within the ice in this work (15 cm thick in average in my samples), however, some of his conclusions can be employed in this work as a starting point. The fact that the author found that fracture occurs in the polymeric coatings, in adhesive way, led the present author to consider that the least stiff material in a junction has the largest influence in the value of the Adhesion Level.

Raraty and Tabor (Raraty & Tabor, 1958) conducted their research on ice adhesion to polymers and metals. They formed the ice by freezing distilled water on metallic and non-metallic rods and pulled them out of the ice, measuring the tension to remove the rod. One of the observations was that non-metallic rods needed less force to be pulled out. The fracture mode was found to be adhesive for less stiff materials and cohesive for the stiffest ones. In 1981, Frederking and Karri (Frederking & Karri, 1981) studied the fracture criteria in different materials: wood, concrete, steel, PVC, Polyethylene and Inerta 160 (marine coating). Experiments were performed in cylindrical piles of these materials, submerged in a water pool where temperature was decreased until solidification, and pulled up through a rope. The tensile stress that caused the rods to separate was recorded. Results showed that failure in polymers occurred by a sudden separation between ice and material (adhesive failure). On the other hand, the fracture in the metallic materials was cohesive. It was also measured lower Remote Load to extract

the piles in polymers than in the other materials employed. This situation confirmed what was observed by Raraty and Tabor (Raraty & Tabor, 1958) and Jellinek (Jellinek, 1959), the Adhesion Level of ice is lower in the least stiff materials. The reason in this particular case could be the larger capacity of a less stiff material to shrink when a tensile load is applied. Therefore, the elastic properties of the material, Stiffness and Poison's Modulus, had an influence in causing the material to separate from the ice.

Andrews and Stevenson developed a plane-strain-based ice adhesion test to get the fracture energy of ice in Mode I (Andrews & Stevenson, 1978). The test rig employed by the authors has been taken as a base for the experimental rig used in this work, changing the geometry, the materials tested and placing it inside an Icing Tunnel. The Andrews-Stevenson test rig allows placing a defect in a bi material junction and manipulating easily its geometry. A sketch of the Andrews-Stevenson test rig and the two different fracture modes (adhesive and cohesive) is sketched in Figure 2.4 (sketched by David W. Hammond).

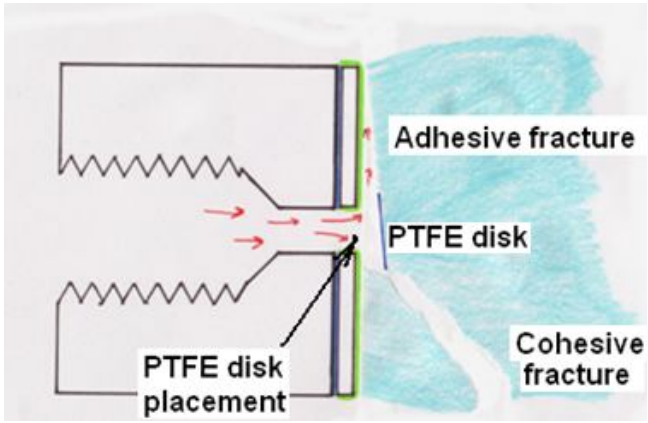

Fig 2.4. Andrews Stevenson test rig sketch and Mode I fracture modes (Hammond)

Using the Andrews-Stevenson test rig, Andrews and Lockington (Andrews & Lockington, 1983) studied the influence of fracture mode, ice thickness, temperature and pressurization rate on the fracture energy of ice added to metallic substrates (Titanium alloy and Stainless Steel). Ice formed from distilled water attached to a metallic substrate and the fracture was driven through applying gas pressure through the ice block formed. The Adhesion Level, represented trough the fracture, was observed to grow linearly until a certain point where it remained steady (cohesive fracture mode transition), as the previous mentioned in this chapter authors observed. This is

represented in Figure 2.5, where the evolution of Adhesion Level (represented by the author as Fracture Energy) is plotted against Temperature and Pressurization Rate. The authors observed that the Pressurization rate affected the slope of the adhesive failure evolution. Nevertheless, the Pressurization rate is kept constant in this Project at 1 MPa/sec. These results showed an Fracture Toughness of ice for Ice-to-Titanium joints of approximately 0.6 J/m^2

The decrement of the Temperature strengthen the chemical bond between ice and exposed surface, so that, the Adhesion Level of the ice increases. This increment continues until the Fracture Toughness of ice is reached, then, the fracture occurs cohesively and the Adhesion Level (represented through the Fracture Energy in their work) has a steady value. This situation is achieved in ice-metals scenarios, where the substrate is much stiffer than ice, so that, the fracture occurs due to the strain fields generated within the volume of the ice, much larger than those generated within the volume of the metallic substrate.

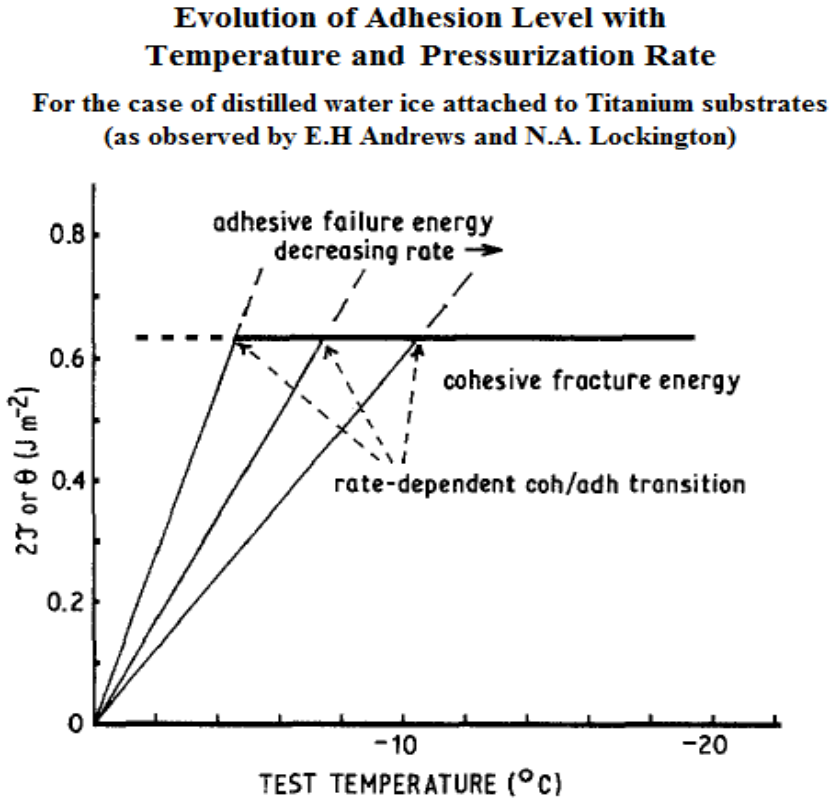

Fig 2.5. Evolution of Adhesion Level with Temperature and Pressurization rate (Andrews & Lockington, 1983)

Andrews, Majid and Lockington studied the effect of substrate thickness on fracture energy of ice attached to polyurethanes (Andrews, et al., 1984). They developed a theory of thickness dependence for coatings placed over stiff substrates by testing a set of coatings of different thickness. The fracture energy of ice was found to decrease as the thickness of the polyurethane increases. On the other hand, for very thin coatings (the order of 0.1 mm) the fracture energy was found to decrease. They concluded that the fracture event was aided by the large energy release from a flexible body, in proportion to the volume of the softest material.

2.3. On the Shear Adhesion to bonded joints

Jellinek (Jellinek, 1959) studied the shear adhesion of ice to metals and polymers and compared it with the tensile adhesion level. The apparatus employed consisted of a stainless steel cylinder and disks of different materials, where ice (snow ice) is sandwiched between both fixtures. The disk is moved in shear direction creating the fracture in the ice. The Adhesion level in shear direction was found to increase as the Temperature decreased. As it happened for the tensile tests, in the ice-metal attachment scenarios, the point for the Fracture Toughness in shear direction of the ice was reached and the fracture occurred cohesively for lower Temperatures, this is, the Adhesion Strength increased as the Temperature decreased until this point was reached, after that, it remained steady. On the other hand, the Adhesion Strength recorded was lower in ice-polymer scenarios and the Fracture Toughness of ice was not reached.

Jellinek (Jellinek, 1959) reported that shear adhesion level to both metals and polymers increased as the Temperature decreased, when adhesive fracture was observed, and was slightly dependent when cohesive fracture occurred. Shear adhesion level was found to be up to 15 times lower than that adhesion level obtained in tensile direction. The author developed a theory of a Liquid-like layer between the ice and substrate, so that, only frictional forces had to be overcome to break the ice, rather than the surface tension forces involved in the fracture in tensile direction. Stallabrass and Price (Stallabrass & Price, 1962) tested the ice shear adhesion level to metallic and non-metallic materials: Aluminium alloy 65ST, Stainless Steel 304, Titanium alloy (metals) and Viton (a fluoro-elastomer) and Teflon, 0.65 mm thick (non metallic coatings). Ice was formed in a cold chamber by freezing a cloud generated within over a set of substrates. The tests consisted in growing ice on rotating blades (70 mm long) and calculating the rotational speed of the ice in the shedding moment due to a sensor deflection. It was found that shear Adhesion Level was larger in metals unless they had surface contamination. In the tests to Viton, the authors observed that the coating was peeling off before the shedding. Due to these observations, it leads the author to consider that the shedding process of ice depends on the Stiffness of the coating for both tensile and shear direction. The least stiff material is the material dominating the Adhesion Level. Anderson et al (Andersson, et al., 1993) studied the shear adhesion of ice to polymers employing a test procedure

designed for this purpose. The test fixture was similar to the one employed by Jellinek (Jellinek, 1957), it consisted of a set of disks where ice grew in between. The separation occurred when a Remote Load was applied. This load pulled a steel rope, causing one of the disks to be displaced aside, generating shear loads in the block of ice formed in between the disks until the fracture occurred. It was found that the substrate thickness had an influence on the adhesion level. Thicker substrates resulted in lower adhesion level, attributed by the authors to the deflection. This situation might be especially influential when one of the substrates is less stiff than ice. The authors also observed that reinforced polymers (black carbon employed) resulted in an increment of shear adhesion level. No correlation between hydrophobicity and adhesion strength was found.

Stallabrass and Price (Stallabrass & Price, 1962) observed and influence of the Stiffness on the Adhesion Level in shear direction, whereas Andersson et al (Andersson, et al., 1993) observed the influence of substrate Thickness on the adhesion level. This work is aimed to relate both properties on the Adhesion Level in both Mode I and Mode II

Fortin and Perron (Fortin & Perron, 1996) studied the shear stresses for helicopter blades using a wind tunnel operating at temperatures below zero, testing a sub-scaled model of an actual helicopter rotor. The shear stresses were calculated at the rotating speed at which the ice shed. It was found that the adhesion shear stress increases linearly as the temperature decreases when ice was attaching to an Aluminium blade. They estimated a Critical adhesion shear stress from 0.07 MPa at -5^0C to 0.26 MPa at -20^0C. A thin icephobic coating was place to benchmark its behaviour compared with bare Aluminium. The icephobic coating was found to reduce the ice accretion rate, but did not reduce the Shear Adhesion stress (0.12 MPa uncoated, 0.10 MPa coated). The coating properties were not disclosed in this study, it is likely that its Stiffness and Thickness had small influence on the Adhesion Level of ice. Laforte et al (Laforte, et al., 2002) studied the ice adhesion to several hydrophobic coatings. The authors studied the effect of a solid coating on ice adhesion. The ice formed over stripes of painted Aluminium through precipitation at -10^0C and a MVD 200 µm. The pressure was applied to one of the sided of the strip through a screw, generating shear forces in the junction until the ice shed.. Ice adhesion in their work was found to depend highly on

the roughness, whereas hydrophobicity was not considered to have a remarkable effect. It was found that Roughness was the most affecting factor in the adhesion strength whereas hydrophobicity was not observed to make a difference. The coatings were painted over the coupons, it was expected that the thickness is very small, so that, the adhesion level might experience an effect of the underneath material. Laforte and Beisswenger (Laforte & Beisswenger, 2005) employed a rotating test rig to calculate the shear adhesion level of ice. They calculated the shear adhesion level through the rotating speed like Fortin and Perron did. Ice was grown in bars by submerging them in cold water and letting it to freeze afterwards. Once the ice was formed, the bars were spin until the ice shed. Seven bars were tested: Three Aluminium bars and three Aluminium bars coated with greases or non-permanent icephobic material. It was observed the reduction of adhesion in icephobic coatings, compared to metals. Laforte and Laforte (Laforte & Laforte, 2009) related strain and stress at the fracture of ice with icing parameters such as surface roughness, ice block thickness and the mode of solicitation (tensile, shear and bending). The experimental rigs consisted of a conventional tensile test rig for tensile tests. Shear test were performed through a torsion machine. The specimens were tested at -10^0C. The stress and strain registered increased as surface roughness increased. In their work, the bending stress was studied as a combination of both tensile and shear stresses, having as a result that this combination of forces reduced considerably the strain required for ice failure.

These latest works cited have been carried out by focusing the research on the icephobic / hydrophobic capacity of a coating. The application of these coatings affected the thickness of the ice grown on the test rigs; however, the authors did not find a considerable reduction on the Adhesion Level. This Project is meant to study how the Stiffness and Thickness of non icephobic / hydrophobic materials can indeed reduce the Adhesion level of ice to exposed surfaces due to its Mechanical Properties, rather than its Chemical properties. Further chapters will disclose some the materials employed and its properties and the reduction of the Adhesion level will be evaluated considering these factors

CHAPTER 3. PROJECT PROCEDURE

This short Chapter is made in order to clarify the Project procedure. The results of this Project are going to be obtained following this four steps route:

3.1. Experimental Routine in the Icing Tunnel:

This Project comprises the use of the Cranfield University Icing Tunnel Facilities for the experimental work. In the tunnel, sets of materials were tested in tensile and shear fracture modes. The output from these tests is the Critical Pressure, this is, the pressure recorded in the piping system in the moment the ice shed. Chapter 4 will describe entirely the Facilities and tests carried out there

3.2. Numerical Work carried out in Finite Elements:

The samples tested in the laboratory are modelled in Finite Elements to understand how the Stiffness and the Coating Thickness affect the Stress State in the vicinity of the crack tip. A number of numerical simulations are carried out, in tensile and shear direction having the target to extract the stress field generated by any Remote Load, in the bi-material junction interface. Chapter 5 will describe the FEA models designed

3.3. Mathematical Methodology to post-process the Numerical Results

The results obtained in the Finite Elements work are employed to obtain the Stress State in the vicinity of the crack tip, through a series of equations that are adapted to the particular case of ice-to-polymers studied in this project. These equations will be used to calculate the Stress Intensity Factor per unit of Remote Load. Chapter 6 will describe the equations employed.

3.4. Obtaining the Adhesion Level for each scenario

The metric considered as representative of the Adhesion Level, employed in this work, is the Critical Stress Intensity factor in the interface between ice and coating. This value is going to be obtained combining the experimental results from the Icing tunnel and Stress State results obtained through the Mathematical Methodology. The Adhesion Level will be calculated to study the effect of material properties in Chapters 8 and 9

CHAPTER 4. EXPERIMENTAL ROUTINE IN THE ICING TUNNEL

4.1. Icing Tunnel Description

The experimental routine is carried out at the Cranfield University Icing Tunnel Facilities, described by Hammond (Hammond, et al., 2003). A sketch of the Tunnel can be found in Figure 4.1

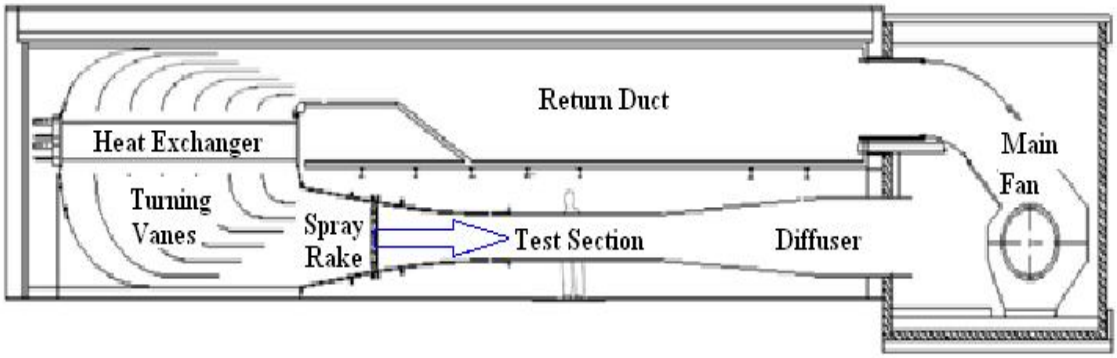

Fig 4.1. Sketch of the Ice Tunnel (sketched by Hammond)

The Tunnel comprises of a circuit where air flows pulled by a fan, that is driven by a diesel engine. The most crucial Icing Parameters regulated in the Icing Tunnel are Temperature, air speed and LWC.

The Temperature within the Tunnel is recorded upstream the spray rakes, where the air speed is low. When the air flow is driven towards the Test section the Total Air Temperature is assumed to remain the same. The Temperature is regulated through a refrigeration pump connected to the 400kW Heat exchanger.

The air speed in the test section is controlled by the regime of the Main Fan

The Tunnel has a spray grid where a set of atomizers are placed. These atomizers expel a fine mist that will generate the cloud downstream. The constitution of this cloud is controlled by manipulating the Water and Air Pressure (P_W and P_A respectively) in the atomizers. By manipulating P_A and P_W, for a given conditions of air speed, will result in a LWC estimated for the cloud. However, the LWC is not regular along the whole volume of the cloud; it is assumed that the dispersion of the LWC values is around ±0.1 g/m^3. Moreover, this dispersion makes the cloud not to be regular at any point in the Test Section. The test specimens are not placed randomly in the bars in the Test section, but in those areas where the LWC is similar. The position of those nozzles depends on

the mode to be tested. Tensile and Shear tests have different fixtures and, therefore, the LWC in the cloud that impacts on it changes as the flow of air encounters different opposition bodies on its circuit.

The work to estimate the LWC average concentration in the whole cloud, the estimation of the distribution LWC at the Test Section and the work to establish the positions of the atomizers in the spray rake is disclosed in Appendix A

When the Temperature inside the tunnel reaches the desired value and stabilizes, the water is sprayed from the atomizers towards the testing section. This water is atomized into fine mist to conform the cloud and follows the air stream towards the section Area to grow over the exposed specimens ready to be tested. The water employed is de-ionised water from an 8000 litres tank.

The test section has a square shape, whose area is 760 mm^2. The test fixtures for tensile and shear fracture modes are placed in this section.

A sketch of the pneumatic map of the installation is showed in Figure 4.2.

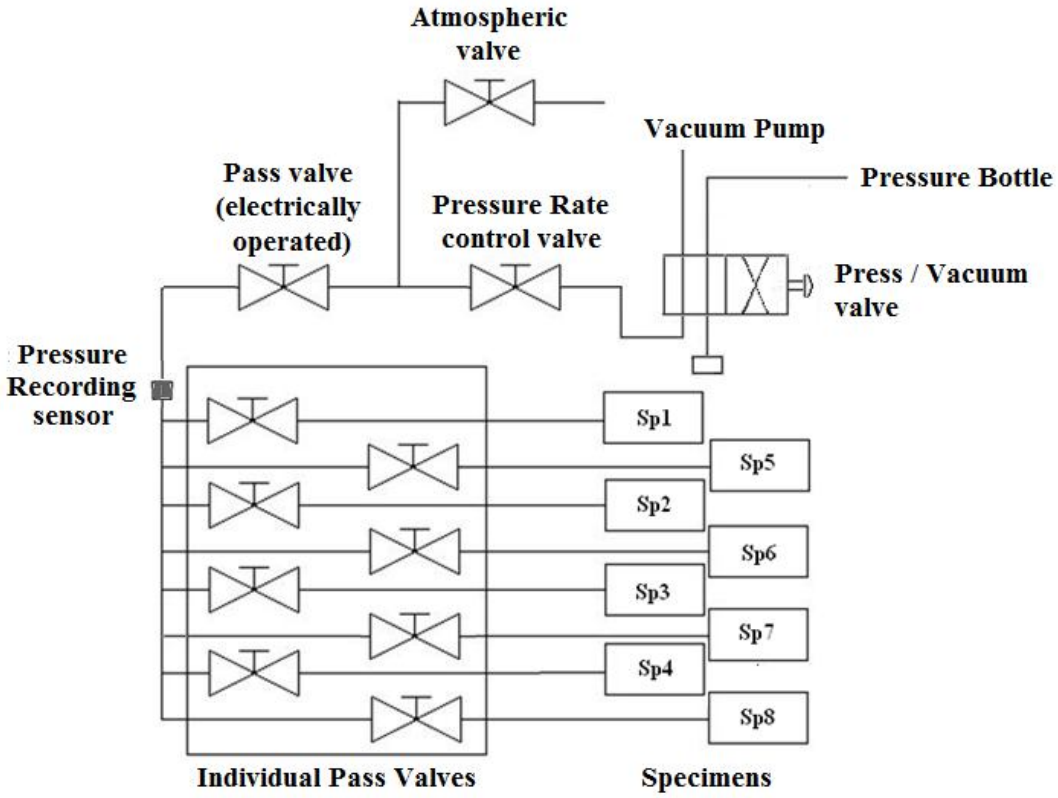

Fig 4.2. Pneumatic map of the installation

The tests target is to grow ice on the exposed specimens and cause the fracture to obtain the Critical Pressure necessary to shed the ice. The external source of pressure is pressurized gas coming from a gas bottle towards the samples through a piping system. The pressure pipe ramifies to derive the pressure to every one of the specimens to be tested, named as Sp# in Figure 4.2. Individual pass valves are used to control which is the specimen to be tested. A real picture from the Test Control Panel is showed in Figure 4.3.

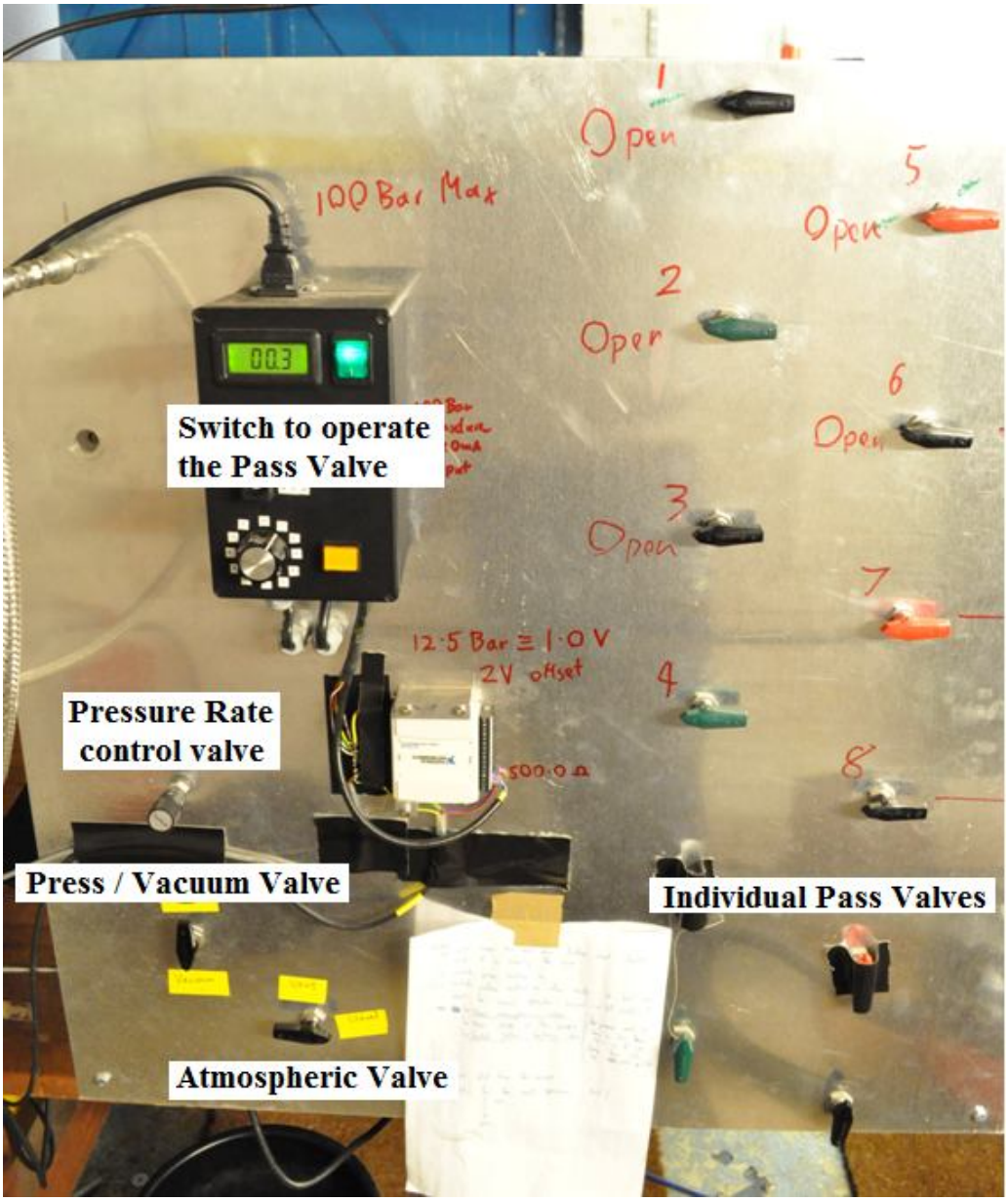

Fig 4.3. Picture from the Test Control Panel

4.2. Experimental work for Mode I fracture tests

4.2.1. Mode I tests Set Up

The tensile tests are carried out to study the crack development in Mode I, in a bi-material junction. It measures the amount of external pressure necessary to break the ice block that formed over a series of exposed specimens, in tensile direction.

The test specimens are based on the ones described by Andrews (Andrews & Stevenson, 1978), placed inside the Tunnel in transversal bars. Some pictures from the test are showed in Figure 4.4.

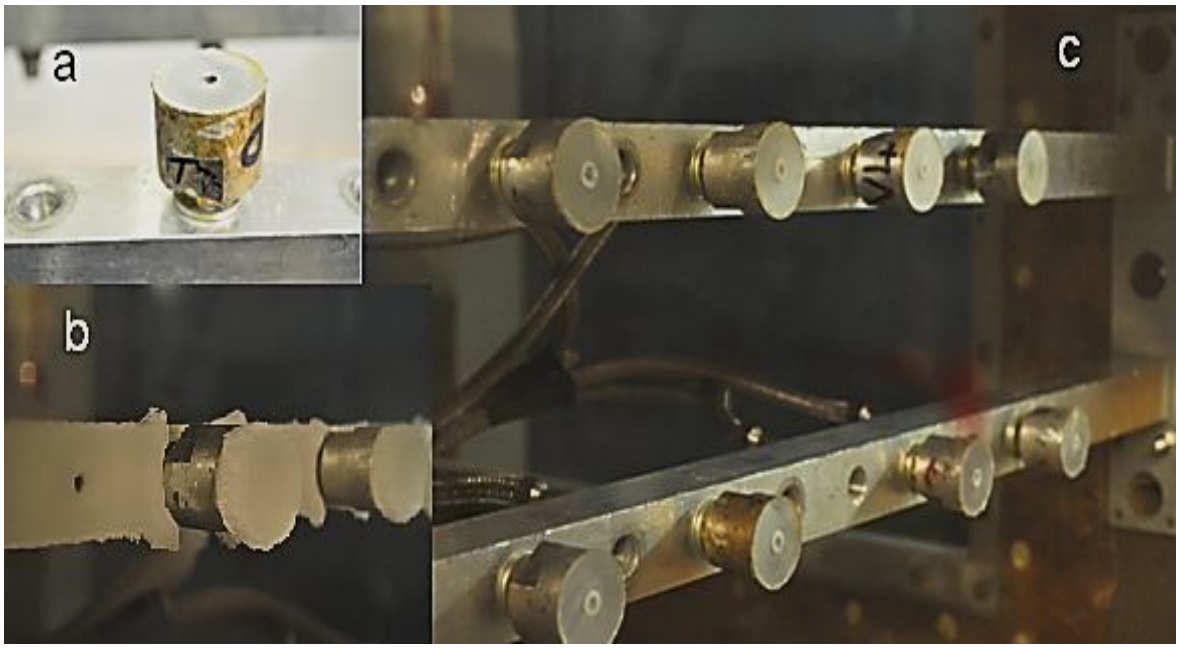

Fig 4.4. Aspect of a coated substrate (a), when ice grows on it (b) and the distribution inside the tunnel (c)

The specimens consist of Aluminium cylinders coated with polymeric coupons. The specimens have a hole (Figure 4.4-a) through which the external pressure is applied. The holes are covered with a PTFE disk. This disk has two duties. The main duty is to act like a crack-starter defect. The disk diameter is the defect size to be taken in account for further calculations. The other duty of the disk is to prevent the sprayed water from accumulating inside the pipes. The vacuum system is used only in tensile tests to hold the PTFE disk until the water begins to be sprayed and ice starts to form.

4.2.2. Mode I Routine and data acquisition

The specimens must be dry and clean before the PTFE disks are put in place and held by the vacuum system. This PTFE disks that will simulate a defect (crack starter) are prepared from a PTFE sheet, whose thickness is approximately 0.15 mm.

The test Temperature is targeted and, once it stabilizes inside the Tunnel, the water is sprayed from the nozzles grid. At that point, every element inside the Tunnel is assumed to be at the test Temperature (below zero). The cloud formed by the sprayed droplets is driven towards the testing area due to the air flow. The low temperatures of the elements inside the tunnel let the water to freeze when it gets in contact with the exposed surface, simulating the atmospheric icing conditions.

The moment to start the ice shedding process is set as the moment when the ice attached forms a block that is approximately 15 mm thick. This thickness is visually estimated (visually compared with the cylinders height, which is approximately 30 mm). The value of 15 mm is chosen so it is 2.5 times bigger than the defect diameter, which allows plane strain conditions within the ice; therefore, the stress field within the volume of ice is not affected by the thickness.

This value of 2.5 is taken after following the recommendations by Andrews and Lockington (Andrews & Lockington, 1983). The authors studied the Adhesion Level of ice through the calculation of the Fracture Energy 2τ (Adhesive Fracture Scenario). They developed an equation to obtain that value based on the Stiffness of the Ice E, the Critical Pressure recorded the break the ice σ_C, the defect size c and an *f-factor*. The equation is:

$$2\tau = \frac{{\sigma_c}^2 * c}{E * f} \qquad [4\text{-}1]$$

The Adhesion Level is proportional to 1/*f*. This f-factor depends on the relationship between ice thickness and defect size *f(c/h)*, the fracture mode and the Poison´s Modulus of the Ice. The f-factor is calculated through the equation 4-2:

$$f = \left(\frac{c}{h}\right)\left\{\frac{3}{32}\left[\left(\frac{c}{h}\right)^3 + \left(\frac{c}{h}\right) * \left(\frac{4}{1-v^2}\right)\right] + \frac{n}{\pi}\right\}^{-1} \qquad [4\text{-}2]$$

Where n=1 in Adhesive Fracture and n=2 in Cohesive Fracture

Through a variation of the values for ice thickness *h*, considering then defect size as 3 mm (defect radius), it is possible to observe which value of *c/h* makes 1/*f* (and, consequently, the Adhesion Level) not to vary significantly when the ice thickness increases. This case is observed in Figure 4.5:

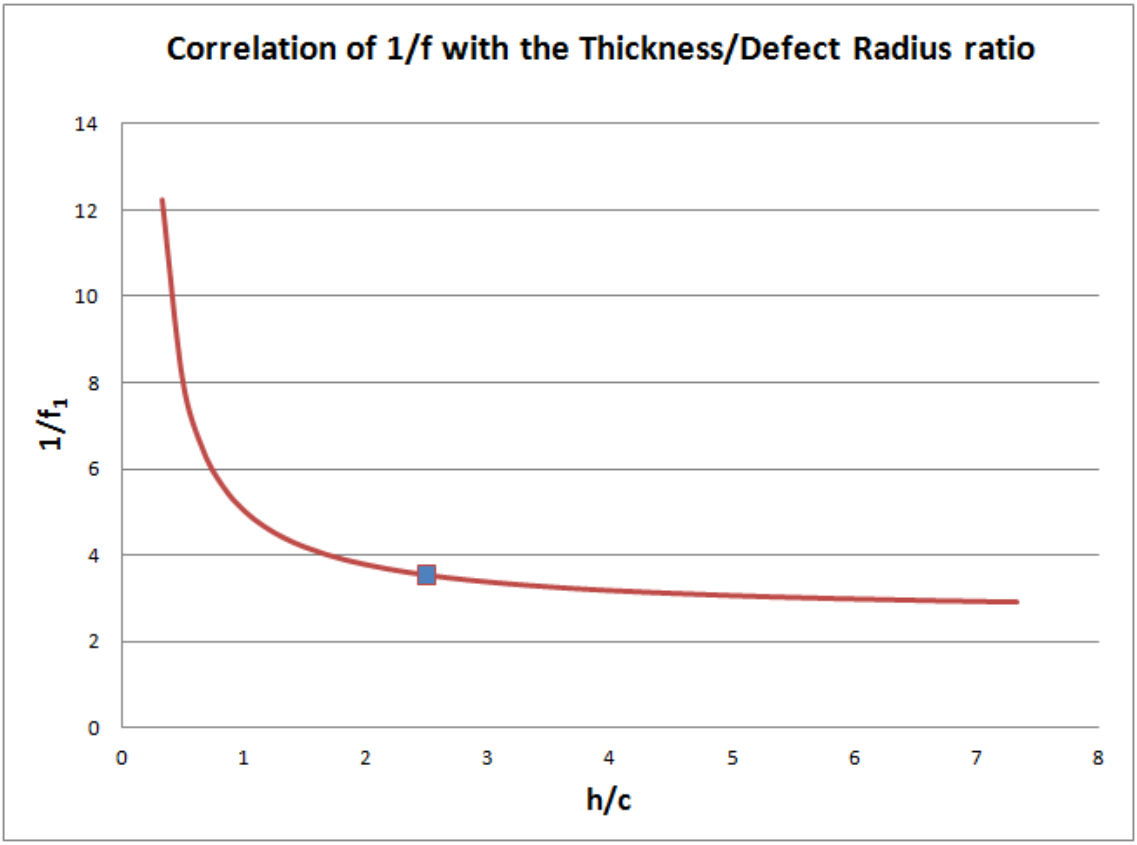

Fig 4.5. Estimation of c/h in order to ensure Plain Strain Conditions within the ice

Figure 4.5 shows the trend line of 1/*f*, proportional to the Fracture Energy (or Adhesion Level). The author has considered that 2.5 is a ratio where the variation of 1/*f* is not significant as the thickness increases. This ratio allows a block thickness of 15 mm. Notice that the most interesting ratio is the lowest possible one, since low ratios will involve lower ice block thickness, therefore, lower Icing Tunnel testing times. In order to get an ice thickness of 15 mm in the specimens, it was required an average of 40 minutes for the blocks of ice to reach that thickness (when the impact air speed was 50 m/s, the most common value employed in these tests for this parameter)

The step-by-step routine for a whole singular test itself are:

- Spray starts:
- Observe when the ice forming over the substrates has a thickness of approximately 15 mm (visually estimated)
- Switch off the vacuum pump

Ice block grows up to 15 mm:

- Switch the valve from the vacuum pump to pressure bottle.
- Open the valve of the first specimen to be tested.
- Switch on the pressurization system. Every tests carried out in this work is made for a Pressurization rate of 10 bar/sec.
- Wait for the ice to shed
- Switch off the pressurization system once the ice sheds
- Annotate the type of fracture (adhesive of cohesive) of the ice (second output)
- Annotate the critical pressure read, recorded in a scope (third output)
- The valve for the tested specimen is shut off and it is opened the valve for the next specimen to be tested

The output from this routine is the critical pressure and the fracture mode (adhesive, mixed or cohesive).

The Critical Pressure recorded is an electric signal read from the sensors placed inside the piping system (Figure 4.3). This electric signal is read in a scope and transferred into Pressure magnitude through the equation:

$$\sigma_C = 12{,}5 * \Delta V$$

The value of 12.5 is the constant to multiply the increment of Voltage read due to the coding procedure of the sensor. ΔV is the difference of Voltage transmitted to the scope, being $V_0 = 2V$ the voltage sent out to the scope when the piping system is at atmospheric pressure

4.3. Experimental work for Mode II fracture tests

4.3.1. Mode II Set Up

Mode II is an expression that refers to the Fracture Mechanics of materials when there is a defect embedded within the volume or interface of the bodies to separate. Mode I nomenclature, employed previously, applies according to the literature as there is a defect in the interface of both bodies (PTFE disk). On the other hand, in the shear Adhesion Level test rig, there is not any defect placed. However, in the shear Adhesion calculations procedure, the author has taken the liberty to assume the existence of a crack of the order of the ice grain size in the interface between ice and coating. From now on, the shear Adhesion experimental tests will be named as Mode II fracture tests.

The test rig consists of a six Ice Shedding Devices (ISD) placed on a couple of bars put transversally inside the Tunnel, in the positions named as SP# in Figure 4.2. The points to place the ISD are chosen by estimating which positions have similar values of LWC (See Appendix A). A sketch of one ISD is showed in Figure 4.6 and their placement inside the Tunnel in Figure 4.7. The must have a thickness of 4 mm to fit inside the ISD. These ISD also comprises a plunger that moves parallel to the ice accretion plane and creates a stress field within the block of ice grown over the sample in order to shed it. This piston is moved by a natural rubber balloon placed inside the device which is inflated by external gas supply. The Pressure inside the rubber balloon creates a load in the plunger-ice contact side. Once it is larger than the Critical Stress Intensity Factor in the Ice-Coating interface, the plunger moves suddenly, creating the Mode II fracture.

For the ice to accumulate in the designed zone, the device is designed to be mounted with an inclination of approximately 45^0. The ISD contains additionally a bottom and a top cover plate. These plates prevent the surrounding areas to accumulate ice to the extent possible. In case the ice grew in areas nearby the icing zone it could create bridges and attach to the ice grown in these areas and, therefore, record erroneous pressure data.

Small rubber guides are placed in the space between the piston and the case, above the piston. These rubber tubes have the duty to press the piston over the specimen, to ensure the fracture is occurring in the interface, not through the ice

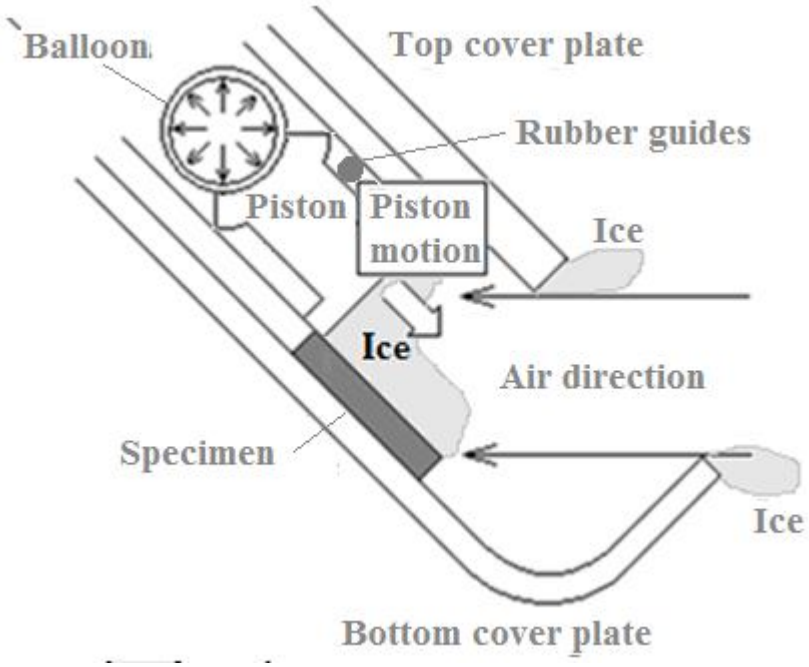

Fig 4.6. ISD sketch

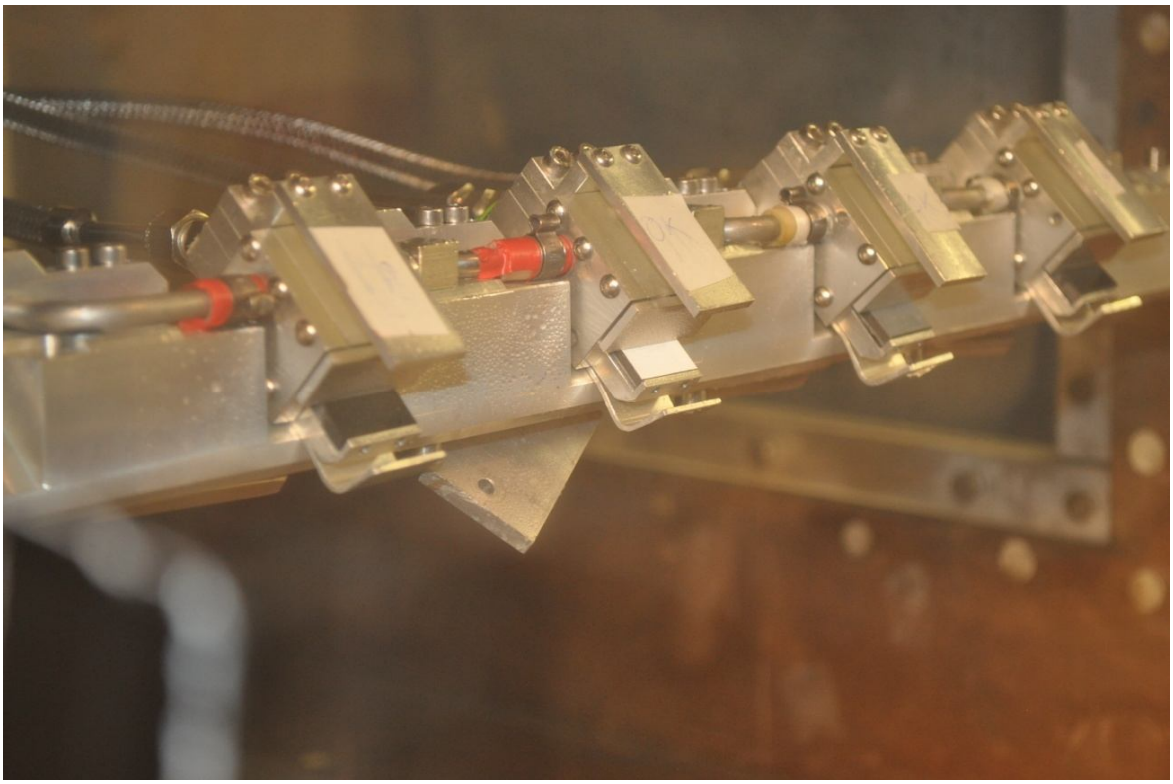

Fig 4.7. Picture of the real ISD placed in the Tunnel with specimens placed inside them

4.3.2. Mode II routine and data acquisition

The set up process is similar as in Mode I, being the source of Load a pressurization bottle, using the pneumatic map in Figure 4.2, with the exception that this mode does not need of the Vacuum system as no defect is placed.

The tests are ready to be done when the thickness in the ice accumulation zone is approximately 5 mm. According to Lou study (Lou, 2010), the shear stress field in the interface of a bi-material junction, for the geometry of these fixtures, is not affected by the thickness variation of the block ice for thickness values larger than 5 mm (Figure 4.8). This thickness is visually estimated, comparing the block of ice formed over the samples with its thickness (4 mm)

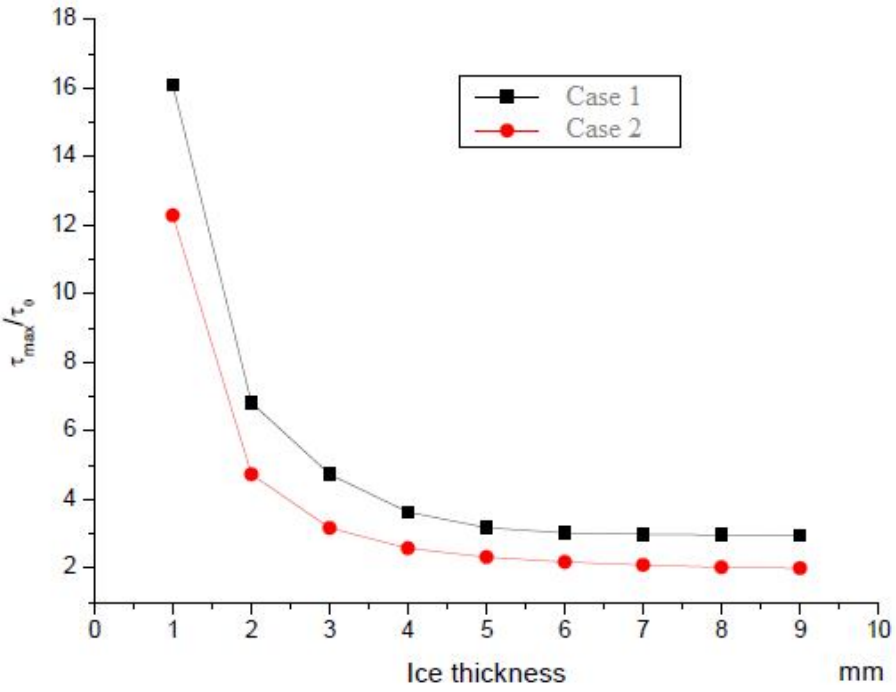

Fig 4.8. Stress concentration evolution as a function of ice thickness, as found at Lou´s work (Lou, 2010)

The routine is similar that the one in Mode I. However, the different geometry of both test fixtures makes some differences in the testing procedure. The pressurized gas is driven towards the specimens and, due to the design; the gas is trapped inside the rubber balloon. Consequently, there is no escape for the gas when the ice sheds.

Bearing this in mind, it is suggested a method to work with the shear test rig where two operators are required. First, the ice is left to grow until the ice block thickness grows up to the desired thickness. Second, the pass valve is opened. Third, the first operator turns on the individual pass valve that drives the gas to a single specimen. At this stage, the pressure in the piping increases progressively.

There is a point where the pressure moves the piston breaking the ice. At this point, the ice is out and no more pressure supply is needed. The second operator must warn that the ice is off. Once the signal is received, the first operator must the switch off the valve. It is very important to switch it off quickly, so the pressure inside the balloon is not increasing excessively.

There is a high probability for the rubber balloon to blow out is the gas pressure within is too large. The ISD designed has sharp metallic corners that can poke the rubber balloon once it is inflated. A quick response from the operators reduces considerably the risk of rubber blowing out.

Once the switch is off, it is opened the atmospheric valve to drop the remaining relative pressure inside the system to '0'. Finally, it is closed the pass valve and the process re-starts for the next ISD

The output from those tests is an electric signal suitable to be translated into the Critical Pressure inside the piping system necessary to break the ice. The value of that pressure is not the maximum point read from the scope as it was in Mode I, but must be considered that the inner pressure keeps on growing until the gas supply is switched off. The moment of the fracture causes the movement of the piston to shed the ice away. This process causes an increment of volume within the balloon, consequently, during that brief moment were the volume increase, the pressure has a decrement. The pressure recorded just before the decrement is the real critical pressure for the fracture.

Figure 4.9 shows and example of one of the data points fracture record. The trend line shows the increment of pressure inside the piping system at the moment the ice broke (marked with a circle, not corresponding to the pressure peak). This figure is extracted from Pervier´s work (Pervier, et al., 2012).

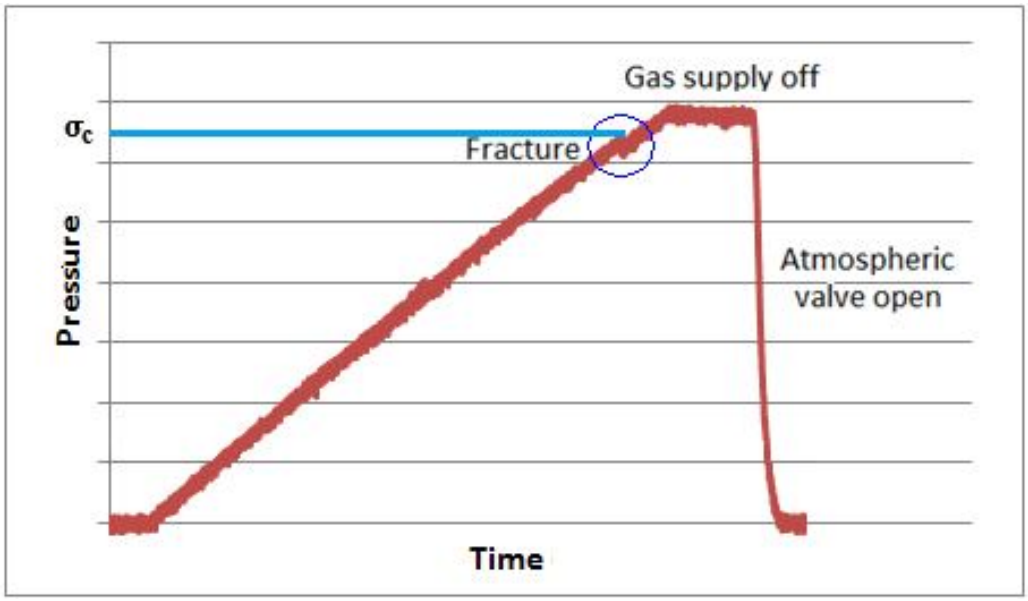

Fig 4.9. Pressure evolution and σ_C in a graph from Mode II tests

The values of the Critical Pressure extracted from the experiments must be applied a correction factor α. The correction factor employed is the one suggested by Pervier (Pervier, 2012). This factor corrects the change of geometry where the pressure is applied due to the rubber tube thickness. The gas inside the rubber tube is applied over the inner surface of the rubber tube, which is different from surface where the outer side of the rubber tube and the convex surface of the plunger are in contact. The correction for this ISD is described in equation 4-3

$$\alpha = \frac{D-2e}{D} = 0.667 \qquad [4\text{-}3]$$

Being *D* the diameter of the rubber tube and *e* the thickness of the tube.

CHAPTER 5. NUMERICAL WORK CARRIED OUT IN FINITE ELEMENTS

5.1. Motivation

The target of the numerical work is to obtain the stress field in the crack development plane (interface between ice and coating). The stress cosidered will be the maximum principal stresses for tensile tests and shear stresses for shear tests.

The Numerical work is carried out through Finite Elements Analysis (FEA), using the software Abaqus(C)[1]. The samples used in the Icing Tunnel test rig, for both tensile and shear tests, are modelled in FEA. The designed models are simplifications of the real specimens. The Boundary Conditions and Loads included in the FEA model are an adaptation of the real Boundary Conditions and Load points from the real test rigs for the FEA models.

The stress field obtained as a result in this Chapter will be employed to obtain the stress state in the vicinity of the crack: the Stress Intensity Factor in the interface between ice and coating per unit Remote Load, in the Mathematical Methodology (See Chapter 6)

[1] Abaqus 6.11-3. Original authors: Dassault Systems. Developed by Abaqus Inc. Cranfield University Licensed.

5.2. Tensile FEA model

5.2.1. Model Geometry

This model is an adaptation of one of the specimens used in the Mode I fracture tests carried out in the Tunnel. The numerical model consists of three parts tied together. One of the parts designed represents the block of ice, another one representing the soft coating and a third one represents the Aluminium substrate. Figure 5.1 shows a picture of a real sample compared to the Finite Elements first drafted model

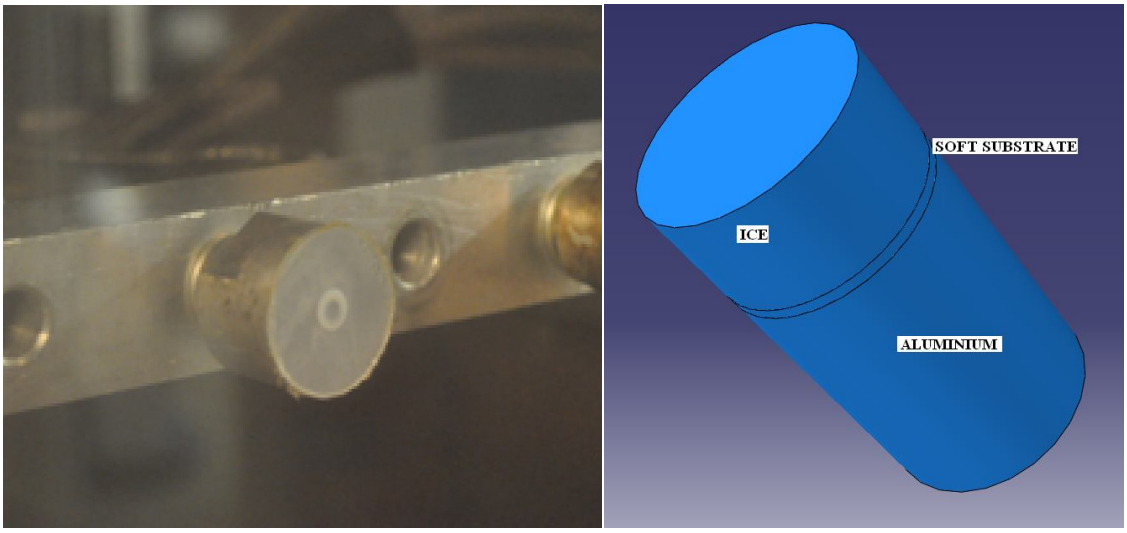

Fig 5.1. Real and designed test rig

This model showed is a fair representation of the real specimen, with an additional part tied representing the block of ice that forms in the Tunnel. The “Aluminium” part is not well scaled in comparison with the real specimen; however, this is not a concern since that geometry does not affect to the stress distribution is the areas of interest (coating and ice).

This work will require a wide range of scenarios to simulate in FEA, for different cases of Coating Stiffness and Thickness. This model is too numerically intensive and makes worth to attempt a simplification of it. Therefore, a simplification is carried out.

The simplification consists of a reduction in the geometry, in order to get shorter simulation times by reducing the number of elements. The geometry reduction consists of an adjustment the cylinder showed in Figure 5.1 into a slice (Figure 5.2). This adjustment incorporates an variation in the crack development area, this is, the fracture develops in a rectangular plane, rather than a triangular (sector of a circular area) plane from the centre, as it would happen in the non-simplified model. This geometry adaptation will be corrected through a geometric factor (disclosed in Chapter 6).

The simplification also comprises the reduction in the size of the parts composing the model in the two dimensions not corresponding to the slice thickness. The specimens used in the Icing Tunnel had a radius of 30 mm whereas the radius of the FEA model is reduced to 15 mm. The thickness of the sliced model is 0.25 mm. The block of ice had a height of 15 mm in the experimental tests and that value is kept in the FEA model, since it ensures Plane Strain conditions in the ice. These simplifications do not affect the stress distribution in the areas of interest. (Critical zone showed in Figure 5.3).

The complete simplification is a dimensionally-reduced slice of the first model showed in Figure 5.2. The model is designed in 3D so the stress intensity factor in the interface between ice and coating can be represented along a flat area.

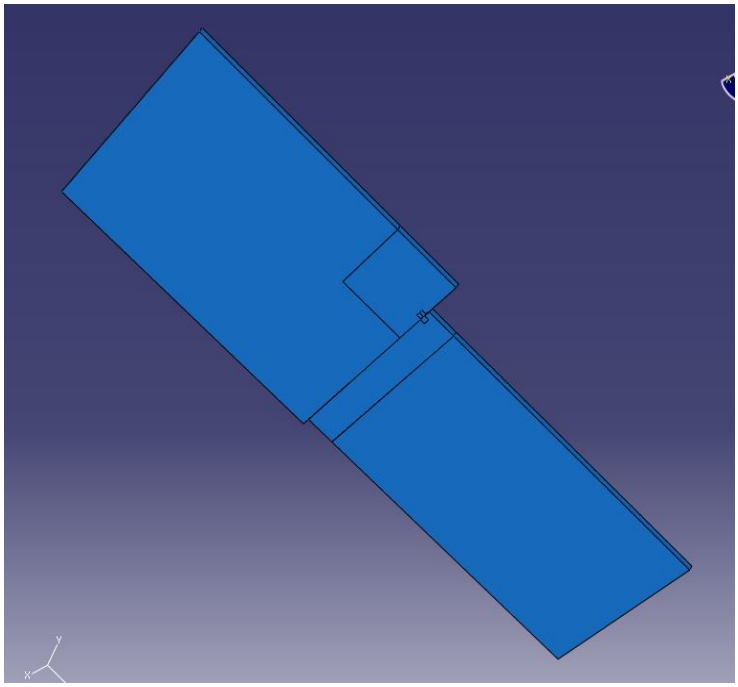

Fig 5.2. Simplification of the Mode I FEA model (geometrically-reduced slice)

The PTFE disk is represented in the FEA model through de-bonding area where ice and coating are in contact within the Load Application Area (Figure 5.6, deformed shape). The area where to Load is applied to has the same length as the PTFE disk radius employed in the experiments

The “Coating” part will change its thickness depending on the test. This variation will be employed in the work to study the effect of Thickness on the value of the Stress Intensity factor. The “Aluminium” part is the fixed bar in the tests.

Figure 5.3 shows a magnified picture of the simplified model where the Load Application Area and the Critical Zone (zone where the crack starts to grow) are emphasized. A remote Load is applied perpendicular to the Load Application Area. Load characteristics will be disclosed in epigraph 5.2.4.

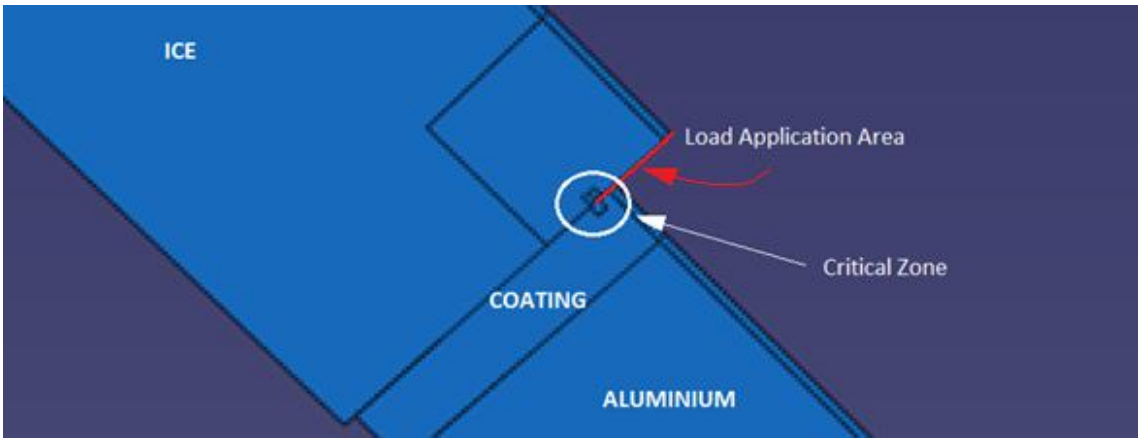

Fig 5.3. Representation of the Load Application Area and the Critical Zone in the Mode I model

5.2.2. Model Mesh

The FEA work is intended to be carried out over a large number of scenarios; therefore, there is interest in making simulation times as fast as possible, without jeopardizing the accuracy of the numerical results. It is suggested, by Finite Elements user manuals, that a mesh made of of brick elements, if the geometry allows it, since the stress distribution is more accurate. Also, the element distribution must be fine and rectangular grid-structured in the areas where the numerical results must be the most accurate. On the other hand, the mesh distribution in the areas separated from the critical area has a free mesh. Both mesh types are sketched in Figure 5.4. This figure also shows two partitions in the “Ice” part. These partitions are made in order to create in order to have a

progressive element size reduction from the edges of the “Ice” part and the Critical Area without compromising the aspect ratio of the elements. The Partition 1 is made in order to create a transition to concentrate a large number of elements towards the Critical Area. Partition 2 is the transition between the Free Mesh and the Structured Mesh (rectangular grid distribution)

A general view of the meshed model is showed in Figure 5.5. This figure represents the large element density around the critical area, whereas the elements on the “Ice”, “Coating” and “Aluminium” edges are the largest, having, for example, five nodes on a 15 mm sector, in the furthest edges from the Critical Area. This element size does not affect the Stress State extracted results from the FEA, this number of nodes is chosen as the minimum number where the aspect ratio of the Elements within the part mesh are not distorted.

The simplified model will have different meshes in the “Coating” part, depending on the Thickness of the coating. Thinner coatings require finer mesh to avoid excessive distortion of the elements. This element size reduction involves the element size of the contact parts to be reduced too to get similar size.

A sample of the mesh distribution in the deformed shape is showed in Figure 5.7. The figure also shows the defect radius (3 mm), the Load Application Surface and the stress concentration in the crack tip

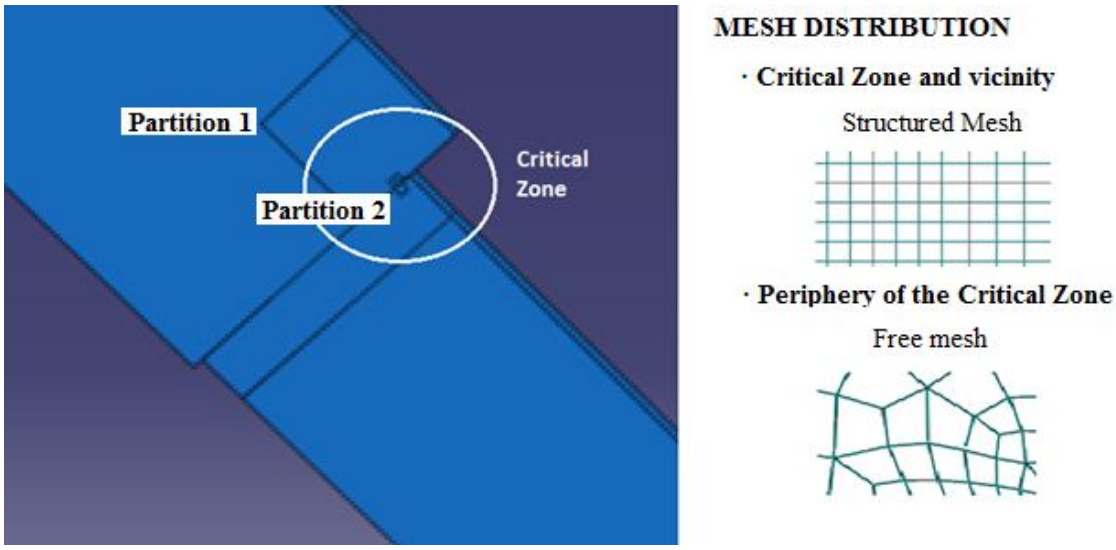

Fig 5.4. Mesh distribution in the model

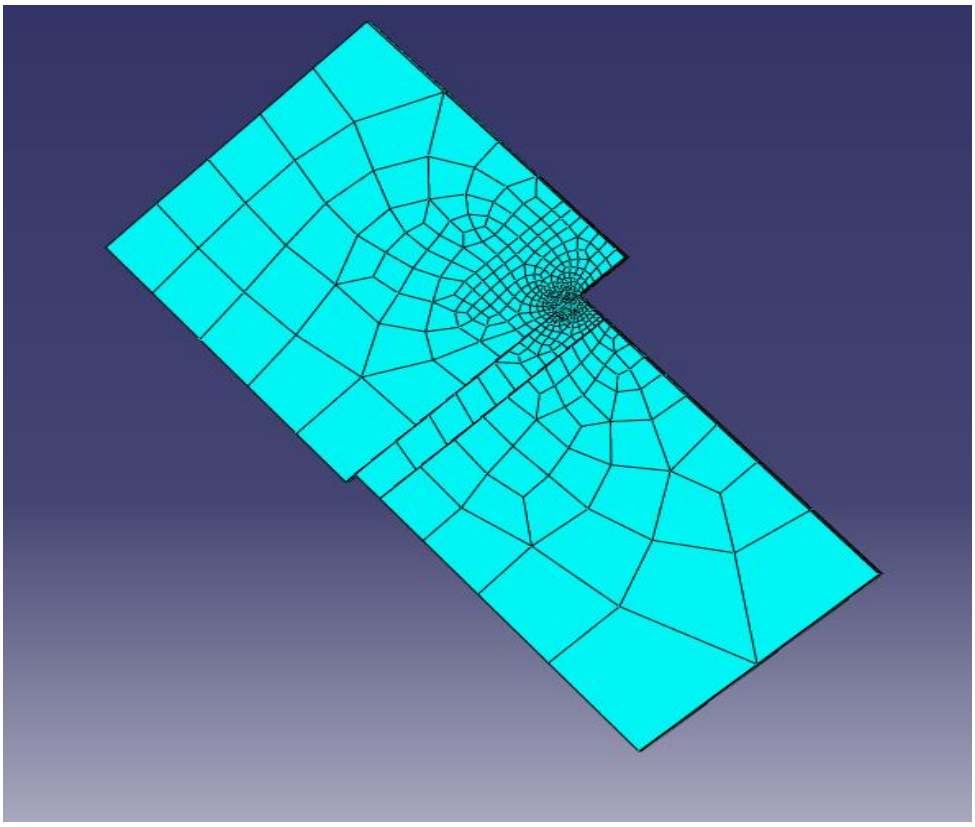

Fig 5.5. Meshed model for Mode I, in a case where coating Thickness is 1.5 mm

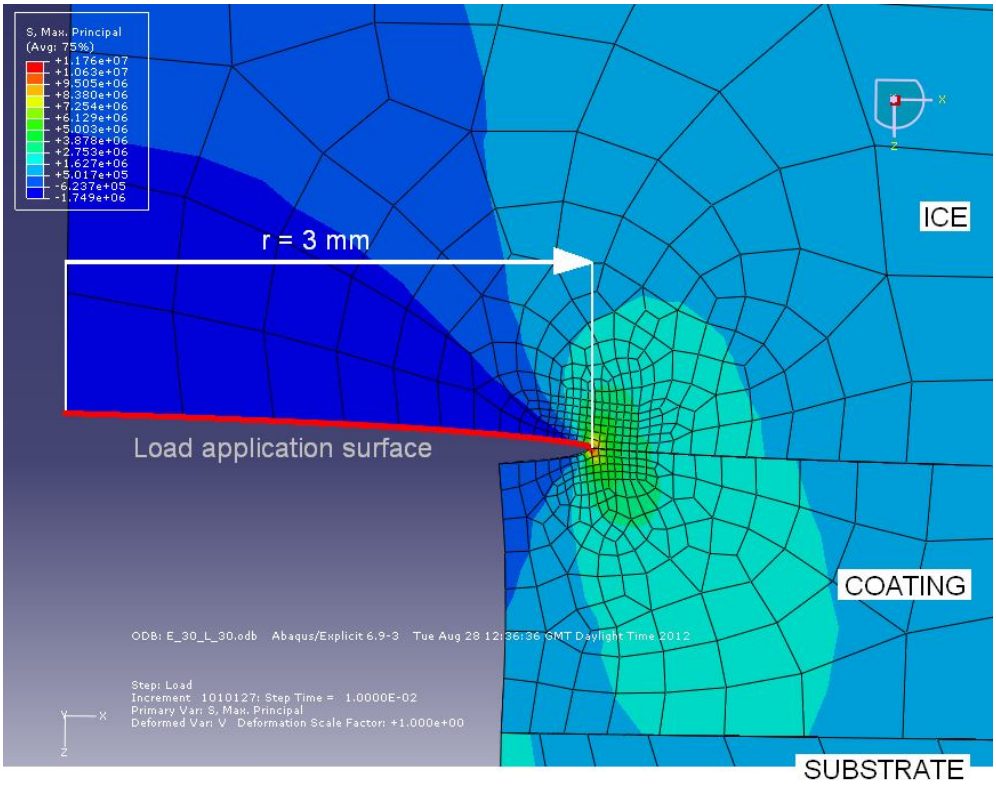

Fig 5.6. Critical area (deformed shape) showing the mesh distribution

5.2.3. Mesh Validation

The mesh pattern is recommended to be orthogonal and fine nearby concentrated points. On one hand; the mesh around this area must be as fine as possible, for accuracy reasons. On the other hand, the LEFM approach will give a singularity as a result at the geometric discontinuity. For such a situation, reducing the element size will just increase the value for maximum principal stress in a way that the local stress tends to an infinite value as the element size tends to zero.

A series of simulations reducing progressively the element size around the critical area has been carried out. The results are plotted in Figure 5.7. It is represented the maximum principal stress evolution in the crack plane. It is observed the asymptotic line as a result of the singularity.

The correct mesh will be that one that fits in the "LEFM applicable curve" showed in Figure 5.7. The simulation labelled as "JOB7" has the fastest simulation times of those curves sufficiently matching with the "LEFM application curve" and it is the mesh taken for further analysis (smallest element size = 0.05 - 0.1 mm)

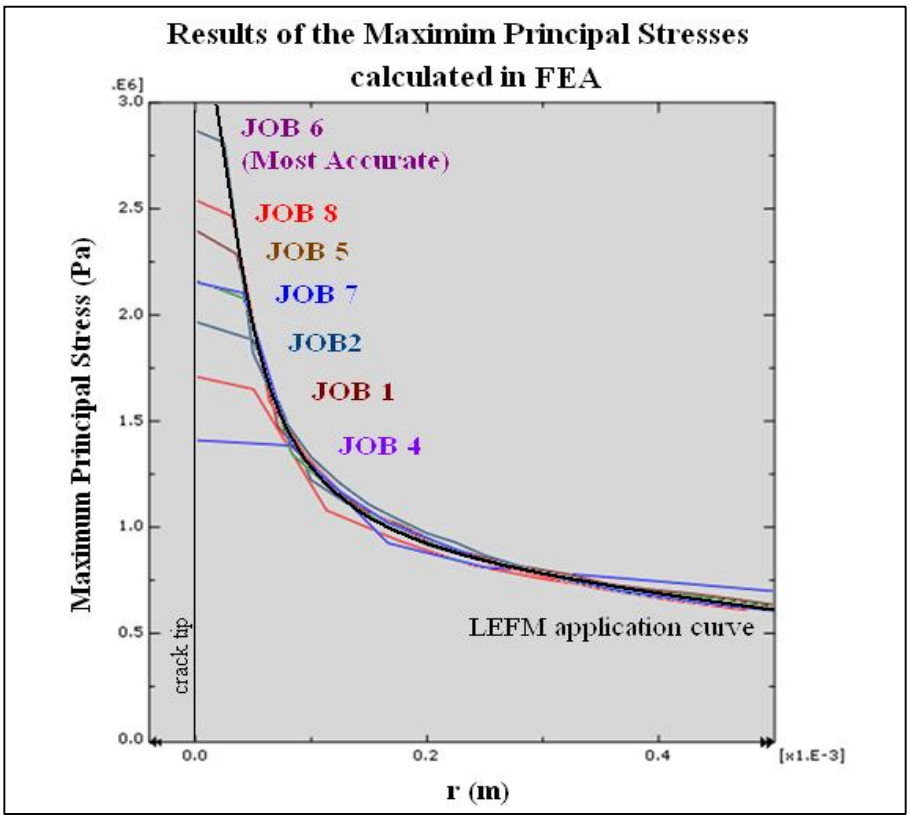

Fig 5.7. Abaqus screenshot. Max Principal stresses evolution for different meshes

5.2.4. Boundary Conditions and Load

The slice modelled must represent the stress state of the real cylinders accurately. The boundary conditions adapt this model to the real cylinders.

Figure 5.8 sketches the boundary conditions of the FEA model. The flat vertical sides of the slice (”Ice”, “Coating” and “Aluminium” parts) are applied symmetry boundary conditions in perpendicular direction (Y-symmetry or X-symmetry, depending on the plane, according to the coordinates in Figure 5.8). These boundary conditions allow the motion and stress state that a single layer might have in the real cylindrical sample. A flat vertical side on the “Ice” part is applied the boundary condition Symmetry in X-direction for the same reasons. The bottom side of the “Aluminium” part in applied the Boundary Condition “Encastre”, no displacement or rotation allowed).

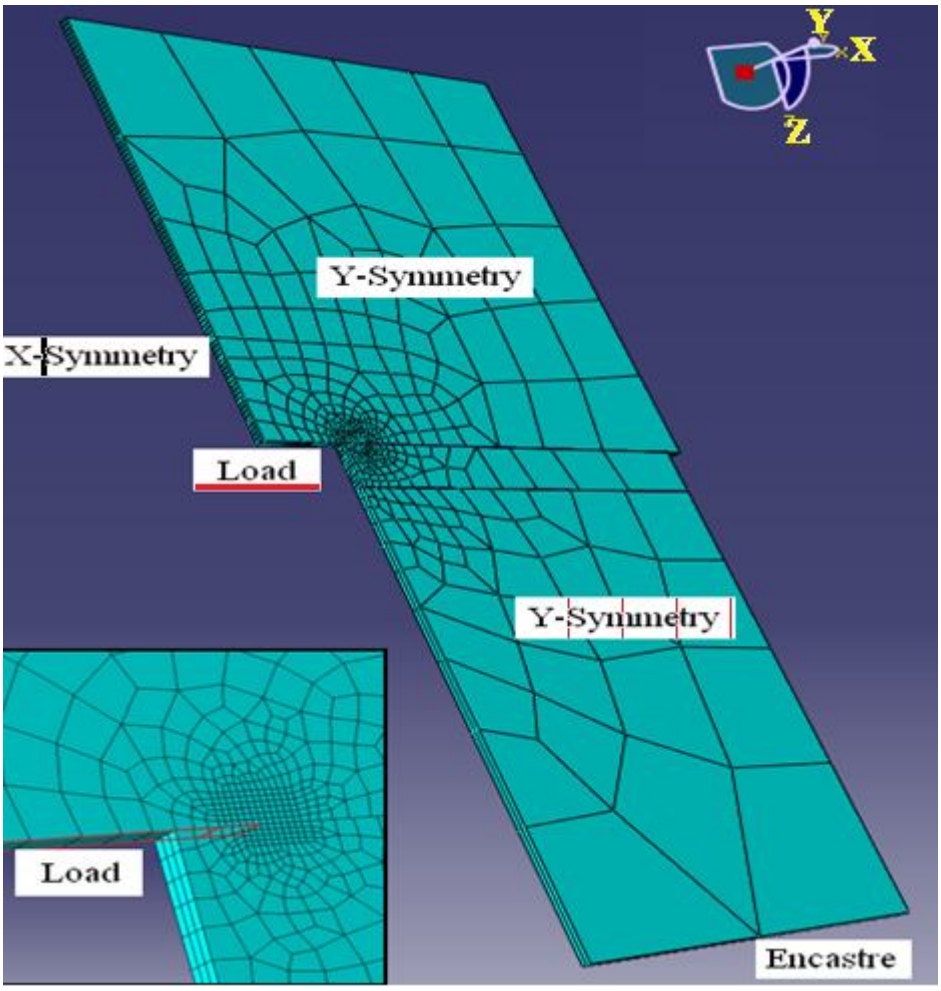

Fig 5.8. Sketch of the boundary Conditions and Load

The Remote Load σ is applied in the FEA model over the Load Application Surface, in perpendicular direction compressing the "Ice" part. The applied load is a pure tensile load, as it is aimed to represent tensile Stress Intensity Factor in a bi-material junction. The current bi-material junction is a modification of the well known Classic Mode I tensile tests. Both models, classic and current are sketched in Figure 5.9.

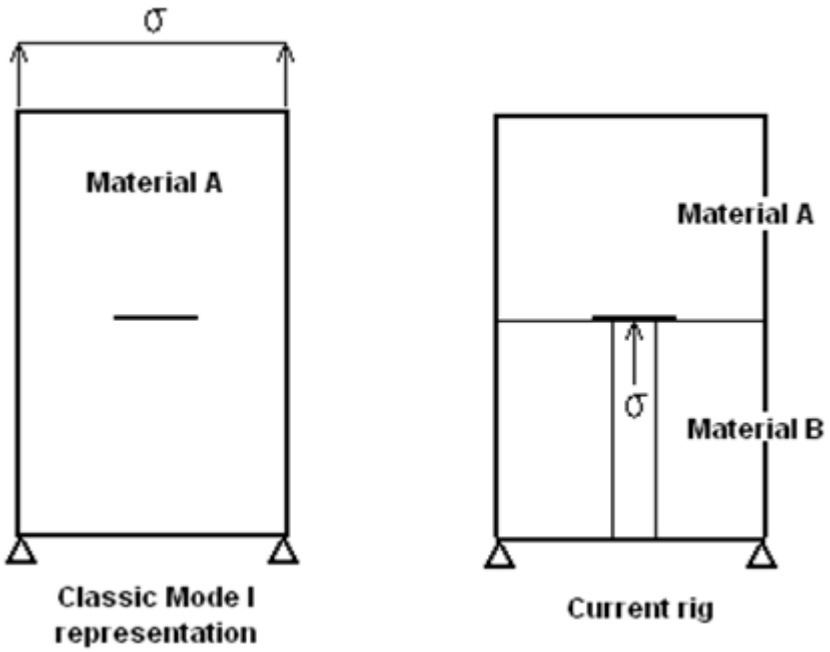

Fig 5.9. Classic Mode I test rig and current Mode I test rig for a bi-material junction

The output data extracted from the FEA simulations is the Maximum Principal Stress in tensile direction; therefore, it is preferred to apply a pure tensile Load although it is not going to be fully representative of the realistic Load condition in the Experimental work. The Load applied in the FEA simulations and the real load generated in the test rig due to the gas pressure is sketched in Figure 5.10.

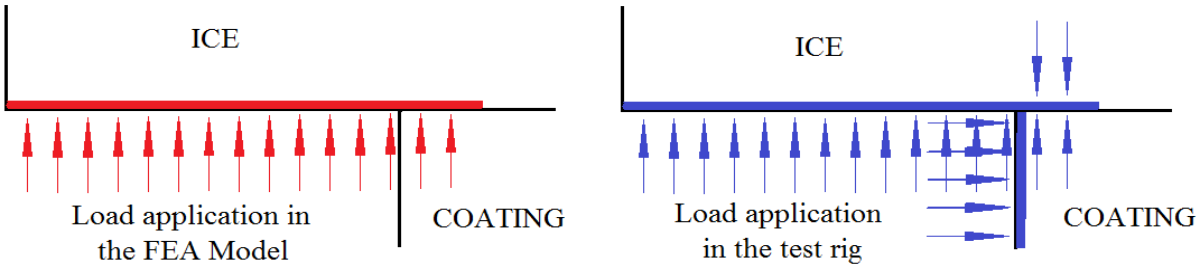

Fig 5.10. Comparison between Load application as designed for the FEA model and the realistic one due to the gas pressure in the Icing Tunnel

The designed mode omits the load that is perpendicular to the Coating side. That load is produced due to the gas pressure in the substrate hole. This Load is omitted in order to put aside the shear stress that this load will cause in the bi material interface. The existence of this shear stress field is going to have an influence in the Maximum Principal Stresses calculated, distorting the pure tensile state. It is neither designed the load that the gas pressure produces in the crack tip, in the first stage of the crack onset. This is represented in Figure 5.10 as the Load perpendicular to the Load Application surface, in the contrary direction. It is applied in the small area corresponding to the contact of the coating with the defect, in the test rig. The ice is assumed to break suddenly, but there is a deformation in the ice on the previous stages of the fracture. This allows the gas pressure to enter in that cavity (sketched in Figure 5.6, in the deformed shape). However, this cavity created before the fracture exists for few fractions of a second and the friction of the walls for the pressure to penetrate might reduce the real magnitude of it.

There is no instrumentation to measure how long the cavity will exist before the sudden fracture. It is estimated to be fractions of a second. The pressurization rate employed in the test rig in 1 MPa/sec and the experimental results give Critical Pressure values from 0.5 – 1 MPa. Moreover, it is not likely that there will be pressure enough for the ice to deform in the earliest stages of pressurization growth inside the substrate hole. Assuming that the ice will start to deform at 20% of the Critical Pressure, it can be supposed that the cavity will exist for 0.3-0.5 seconds. In this short time period, gas is allowed to penetrate the cavity and create a Load over the. This short time, together with the existence of friction losses in the cavity walls makes reasonable to neglect this Load in the FEA Model

5.2.5. Conditions of the Simulation

With this geometry, the FEA conditions are:

- Dynamic-Explicit Load: The simulations are carried out through the Explicit package in Abaqus. The reason to choose this is the fact that the load is applied through Amplitude in an intention to reproduce the experimental pressure rate when the switches from the pressure bottle are opened. The pressure rate employed in the Tunnel is constant along every test and it is 1 MPa/sec. The Amplitude chosen is a tabular type, this is, the Relative Load Amplitude, which simulates the evolution of the Pressure in the piping network in the Tunnel rig is '0' at zero seconds and '1' at the first second.

The amplitude is having only the increment until the first second. The FEA model assumes that 1 MPa is enough to produce the fracture of the ice. This is an approximation, since most of the tests resulted in the ice breaking at lower Critical Pressure than 1 MPa. However, that difference is not going to be major and will not have an important influence in the data extracted from the simulations.

The amplitude employed is described in Figure 5.11

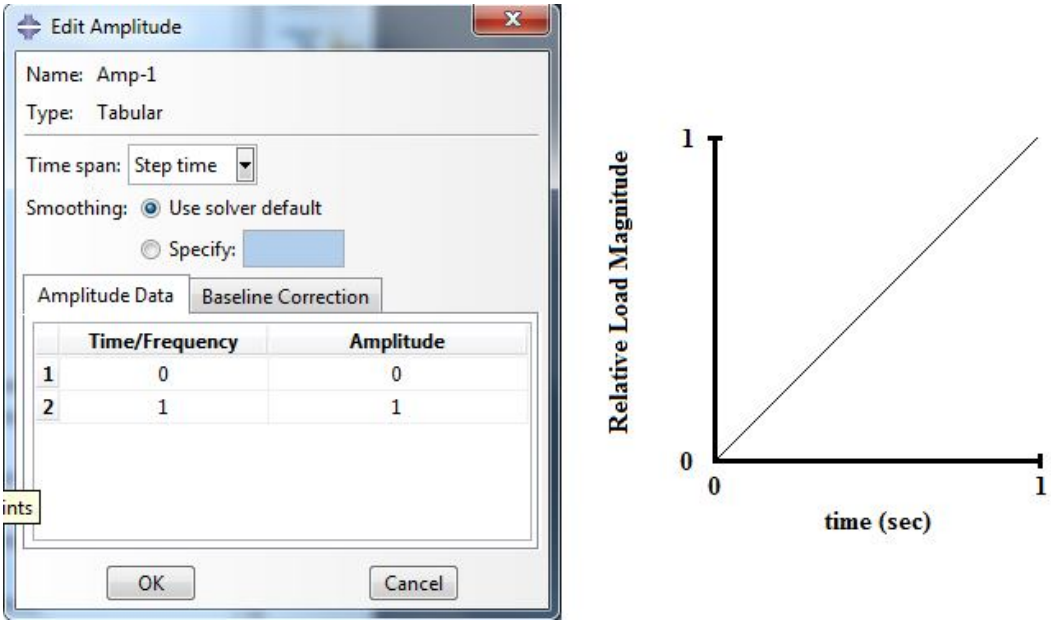

Fig 5.11. Amplitude chosen to reproduce the Pressure Rate and sketch of the behaviour

- Linear Elements: The elements employed are Linear (8-node) hexahedral (brick) elements C3D8. A screen shot from the Element Type window from Abaqus is showed in Figure 5.12 for more detail. Brick elements are the most commonly employed and the ones recommended in the FEA Literature and, C3D8 in particular, is the most cost-effective choice (Reddy & Gartling, 2010). The geometry of the parts employed in the FEA model is not complex; therefore, these elements can be employed in order to mesh this geometry in both Structured (crack tip and vicinity) and Free (periphery) mesh styles without compromising aspect ratio.

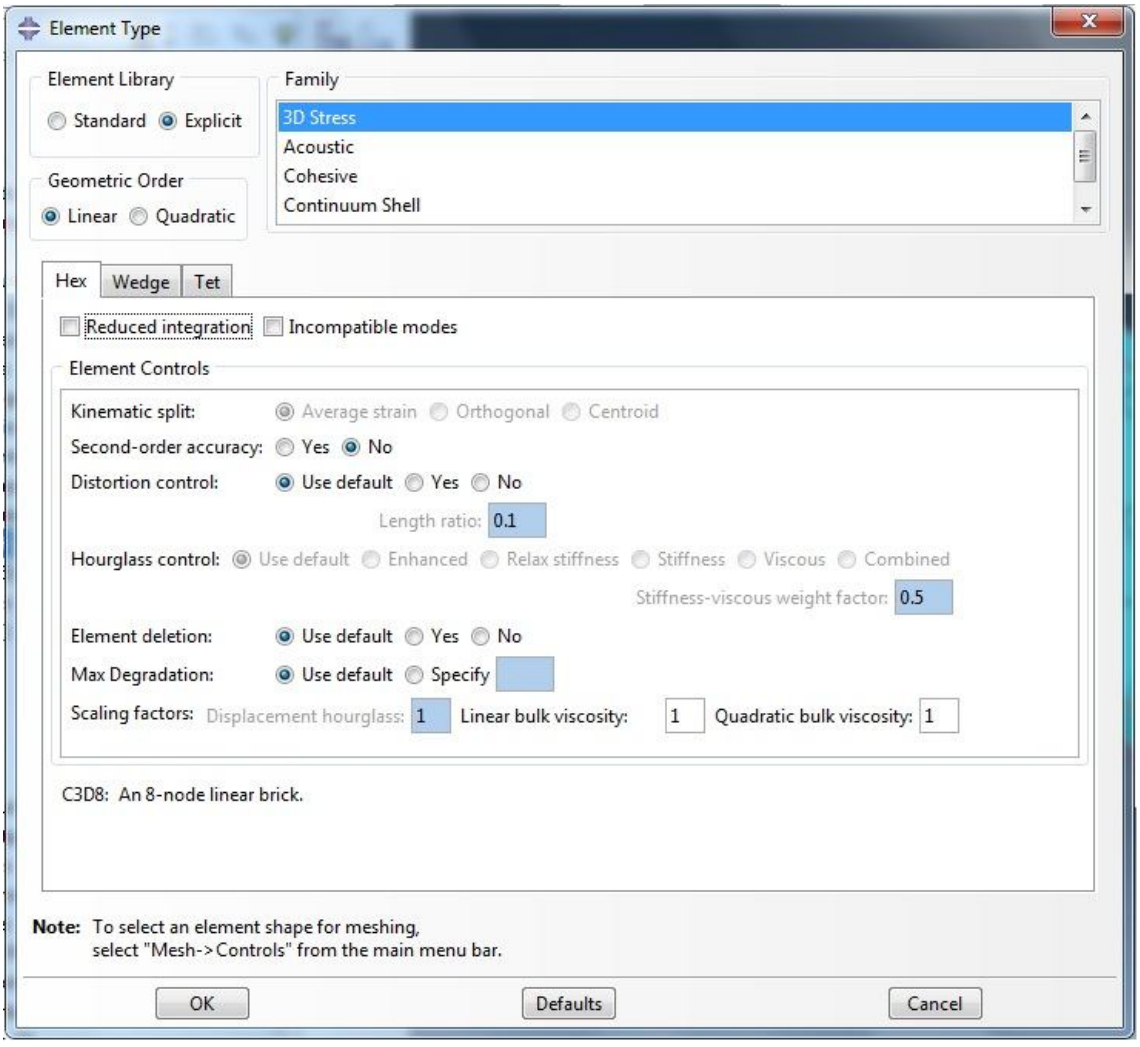

Fig 5.12. Element type information

5.2.6. Post process

The output extracted from the numerical simulation is the Maximum Principal Stress field along the crack plane. In the Testing Facilities, the fracture was observed to occur in brittle way and under simple tensile conditions, through small deformations on the polymeric coating. That is the reason to prefer Maximum Principal Stress rather than Von Misees. A sketch for this situation is showed in Figure 5.13.

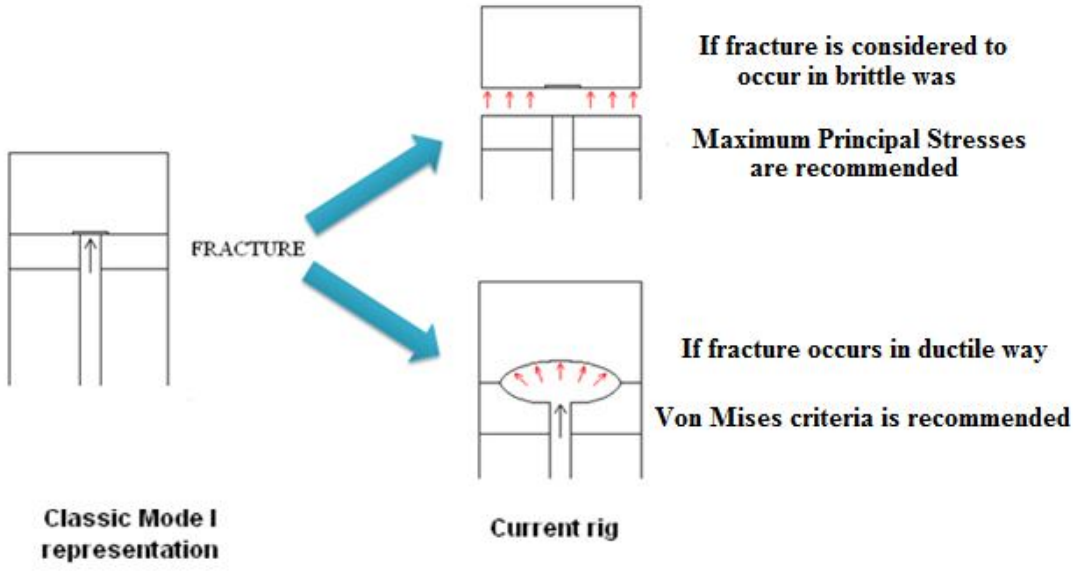

Fig 5.13. Reasoning for using Maximum Principal Stresses as FEA output

.

5.3. Mode II FEA model

5.3.1. Model Geometry, Load and Boundary Conditions

This model is an adaptation of the ISD used in the laboratory for the Mode II fracture tests. This model comprises of four parts: An “Ice” part, a “Coating” part, an “Aluminium” part and another part named as “Plunger” that represents the piston in the real test where the remote load is applied. This part cannot be neglected since the load applied to the piston in the test rig is not unidirectional but applied over a convex surface. The contact between parts is a Surface-to-surface tie.

Figure 5.14 shows a picture of a real ISD and the Finite Elements model. More information about the ISD can be consulted in Chapter 4. This model consists of a slice of the FEA adaptation of the real ISD, as it was done for the Mode I Finite Elements model. The geometry of the FEA parts is exactly the geometry of the real test rig (except the fact that this model is a slice whose thickness is 0.25 mm). The “Ice” part is designed to have a height of 5 mm, which corresponds to the minimum thickness allowed for the ice blocks in the real test rig. The reason for choosing this thickness is the independence of the shear stress fields in the interface from the ice block thickness when this value is larger than 5 mm. This was explained Chapter 4.3.2, according to Lou´s work (Lou, 2010).

The Remote Load is applied in the convex surface of the “Plunger” part. Every part in the model: “Plunger”, “Ice”, “Coating” and “Aluminium” have their movement restricted only to the plane X-Z, according to figure 5.14 coordinates. The bottom surface of the “Aluminium” part has a Boundary Condition: Encastre, no displacement or rotation allowed. The Remote Load is applied through the same Amplitude described in Mode II model, as the pressurization rate was the same in Mode I and Mode II tests.

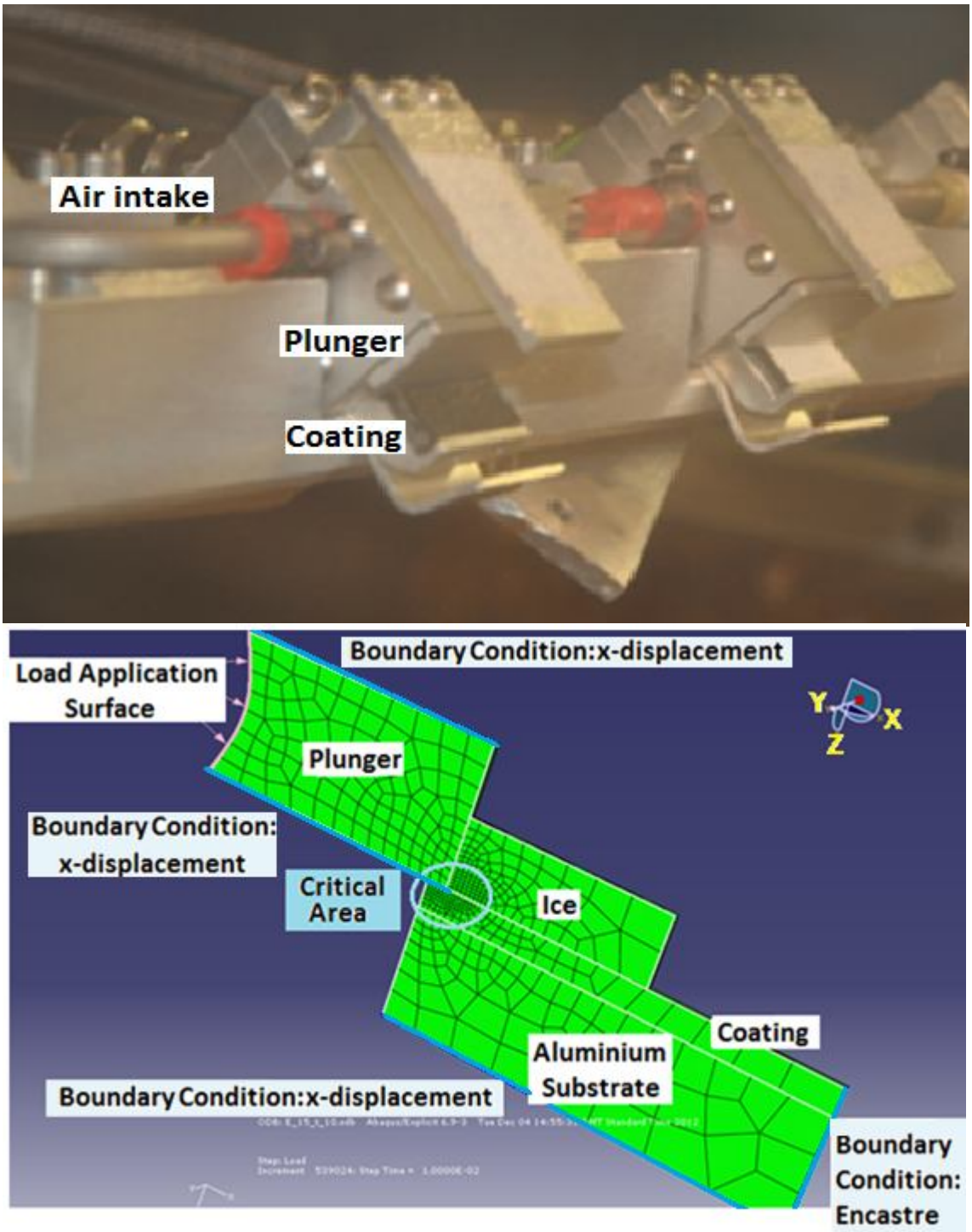

Fig 5.14. Comparison between a real picture of the Mode II ISD and a numerical model

5.3.2. Model Mesh and Validation

The process to generate the mesh is the same as the one employed for Mode I. There is singularity in the crack tip due to the use of LEFM equations (Stress as a function of $1/\sqrt{\pi r}$) as it occurred in Mode I. Notice that there is not a defect that works as a crack starts in the shear adhesion tests; however, it is going to be considered that a crack exists in the point where the "Ice", the "Coating" and the "Plunger" parts coincide. That crack is considered to have a size the order of the grain size.

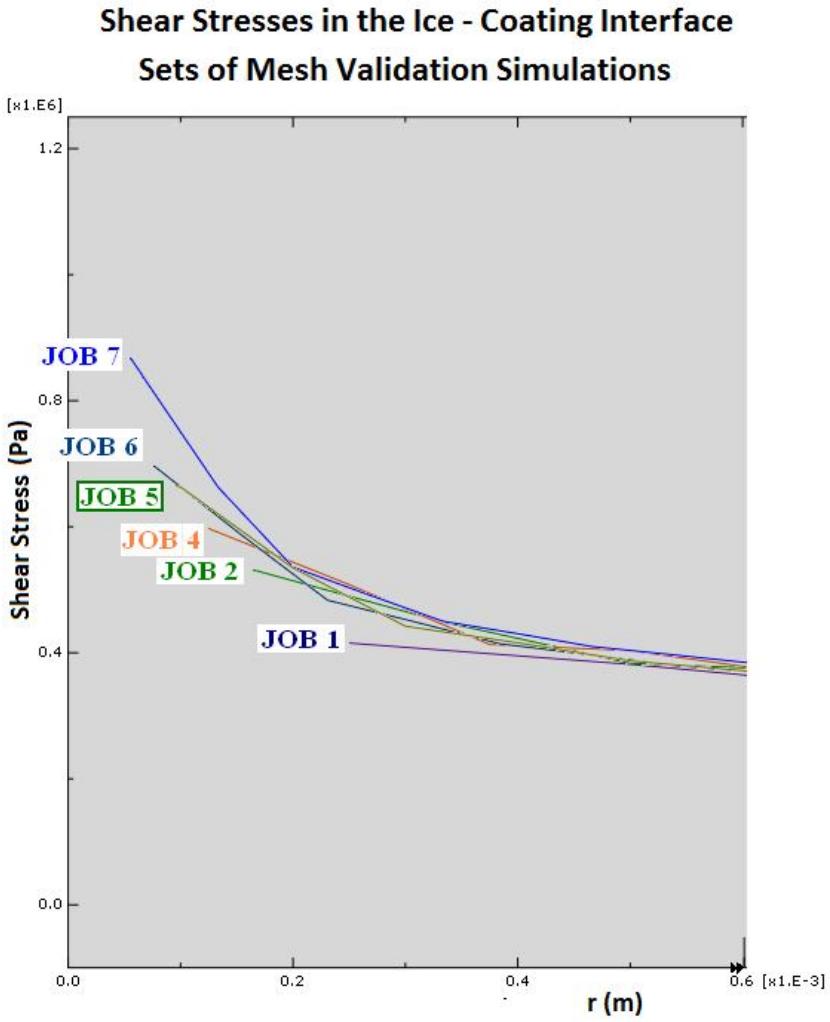

Fig 5.15. Results of the Validation Simulations

The set of simulations to establish an adequate mesh is carried out following the same procedure as the one employed in Mode I FEA model mesh validation. The mesh size is gradually reduced in every simulation until the trend line of Shear Stresses in the interface fit fairly in the LEFM applicable asymptotic curve. The results for the validation jobs in Finite Elements are plotted in Figure 5.15. “JOB 5” is the chosen distribution for Mode II. This mesh is found to match acceptably with the LEFM application curve for Mode I, having as a reference for this curve the one described by “JOB7”, the most accurate and the one requiring larger simulation times. “JOB 5” simulation times were an average of 30-35’ whereas the JOB simulating the finest mesh took around 1h 45’ – 2h

The elements employed are brick elements, distributed orthogonally around the critical areas (vicinity of the crack onset) and swept in the areas outside that area of influence (see Figure 5.14 picture on bottom). This element type was chosen for the same reasons it was chosen for the Mode I model. A sample of one of the results obtained in one of this set of simulations is showed in Figure 5.15.

The output from the Mode II simulations, for different values of Stiffness and Thickness of the “Coating” part is the Shear Stress field in the plane of the interface between ice and coating. Those values of stress along the crack plane will be employed in a methodology to calculate the values of Stress Intensity Factor in Shear Direction in the interface between Ice and Coating and the relationship between the stress intensity factor and remote load applied. See Chapter 6

CHAPTER 6. MATHEMATICAL METHODOLOGY TO POST-PROCESS THE NUMERICAL RESULTS

6.1. Objectives of the Methodology

This Methodology is developed in order to obtain the stress state in the vicinity of the crack tip from the stress field results in the FEA model. This Stress State is the Stress Intensity Factor per unit of Remote Load, in tensile or shear direction. Therefore, the Mathematical Methodology will be different for tensile and shear direction.

6.2. Methodology for tensile load simulations

The Maximum Principal Stresses obtained in the FEA are used as starting point in this methodology. The first step is to calculate the stress intensity factor, K_{I_i}, for isotropic and homogeneous bodies, in every point in the crack plane. It is calculated through the Irwin approach, modified for a plane strain conditions scenario (Anderson, 2005).

$$K_{I\_i} = \sigma_{Y\_i} * Y * \sqrt{2\pi r_i} \qquad [6\text{-}1]$$

Where σ_{Y_i} is the Maximum Principal Stress obtained in FEA, at every i-point along the crack plane. '*Y*' is a geometric factor and 'r_i' is the distance along the axis of the crack plane.

In this study, the values for 'r_i' are linked to the element size in the Finite Elements model. Each r_i-point is the distance between the crack tip and an element edge.

The geometric factor "*Y*" adapts the results for different geometries of the crack development area. The reason is that, in the crack development, *dA/dr* has an effect on the level of Stress Intensity Factor. In this case, the geometry of crack development employed numerically (A_{FEA}) is rectangular, *dA/dr = 0*, whereas the geometry of the crack development in a slice of the real rig (A_{REAL}) has a triangular shape, *dA/dr = constant*. Both geometries are sketched superimposed in Figure 6.1. Both surfaces must be coincident on the crack tip width in order to make both geometries comparable and suitable to be adapted through a factor "*Y*"

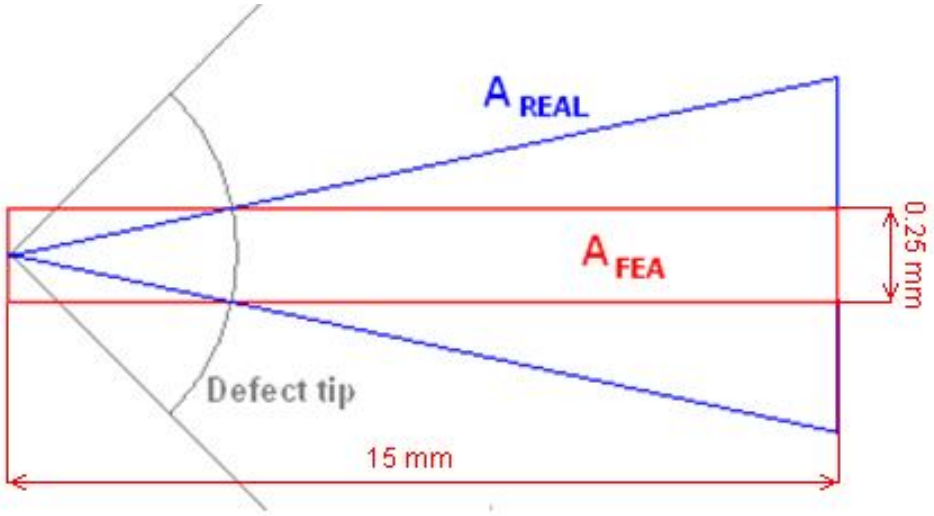

Fig 6.1. Sketch of the crack development geometries for Finite Elements A_{FEA} (dimensions used in the FEA included) and real test rig A_{REAL}

In order to estimate *"Y"*, a set of simulations have been carried out over two FEA models representing two bi-material junctions whose crack development surfaces are A_{REAL} and A_{FEA} respectively. The simulations are run in different scenarios of Load and Coating Stiffness (Table 6.1).

The rectangular geometry (A_{FEA}) is preferred in the numerical routine to the triangular geometry (A_{REAL}), as this one requires either the use of Tetrahedral elements or a very fine mesh in certain sharp areas (in the tips of the triangle that forms the crack development area). Tetrahedral elements in Abaqus$^{(C)}$ are stiffer elements and are subjected to algorithms that make them more inaccurate than the brick elements and carry larger relative error (Jochel, et al., 2006). The other option, a very fine mesh in abrupt areas resulted in excessive simulation times (up to 300% longer simulation times). Therefore, the realistic shape (triangular crack development area) is only employed for this comparison purpose. K_{I_i} values from these simulations are:

	K_I (A_{FEA} case) $Pam^{1/2}$	K_I (A_{REAL} case) $Pam^{1/2}$	Ratio (Y)
Load = 0.7 MPa $E_{coating}$ = 1.5 GPa	17705 (Time: 45')	11594 (Time: 2h 48')	0.654
Load = 1.6 MPa $E_{coating}$ = 1.5 GPa	40495 (Time: 40')	26510 (Time: 2h 30')	0.653
Load = 1.6 MPa $E_{coating}$ = 3.0 GPa	72068 (Time: 40')	48016 (Time: 2h 30')	0.623

Table 6.1. Comparison between K_{IB} obtained numerically with two different geometries

The results for K_I are found to be dissimilar when the contact areas are different. However; the ratio between both results can be assumed to be a constant. Besides, that geometric constant, for two different geometries coincident in the defect width, is found to be close to the square root of the areas ratio:

$$Y \cong \sqrt{\frac{A_{FEA}}{A_{REAL}}} = \sqrt{\frac{3.75}{9.375}} = 0.63 \qquad [6\text{-}2]$$

The Geometric Factor employed in the numerical simulations, for Mode I, to adapt the effect of *dA/dr* in the calculations of K_{I_i} is *"0.63"* for the particular geometries employed in this work

This K_{I_i} is valid for bulk material scenarios. In this work, the crack grows in the interface of a bi-material junction, so that, those values for K_{I_i} must have a correction to be valid. For bi-material junctions, the Equation 6-1 was discussed to be incorrect by Stone et al (Stone, et al., 1975). The stress field obtained in the FEA simulation are stresses that include the effect of the different layers and, therefore, cannot be employed in an equation that refers to a bulk material. To obtain the stress intensity factor in the interface between two materials of different stiffness, the theory for adhesive joints developed by Spinks et al (Spinks, et al., 1993) is adapted for this situation. This was support by FEA simulations by the authors. They named the Stress Intensity Factor in the joint as K_{IJ}. The Factor is re-named as K_{IB} in this work ("B" for "bond"). The equation 6-3 is taken to obtain the K_{IB} along the interface of two bonded bodies.

$$K_{IB\_i}(r_i) = K_{I\_i}\sqrt{\left(\frac{E_{coating}}{E_{ice}}\right)} \qquad [6\text{-}3]$$

K_{IB_i} values at very r_i-point are the evolution of the Stress Intensity Factor in the interface of a bi-material junction along the crack plane. However, the existence of the singularity nearby the crack plane, due to the use of LEFM, makes this value to be "0" in the crack tip (non realistic). In order to obtain realistic values, the trend line of K_{IB_i} is extrapolated from an zone where the LEFM apply to the vertical axis.

This extrapolation is plotted in Figure 6.2 (for one of the particular simulations). A dashed line is added to show the extrapolation function of the K_{IB_i} curve.

$$K_{IB} = lim_{r\to 0}\, K_{IB\_i}(r) \qquad [6\text{-}4]$$

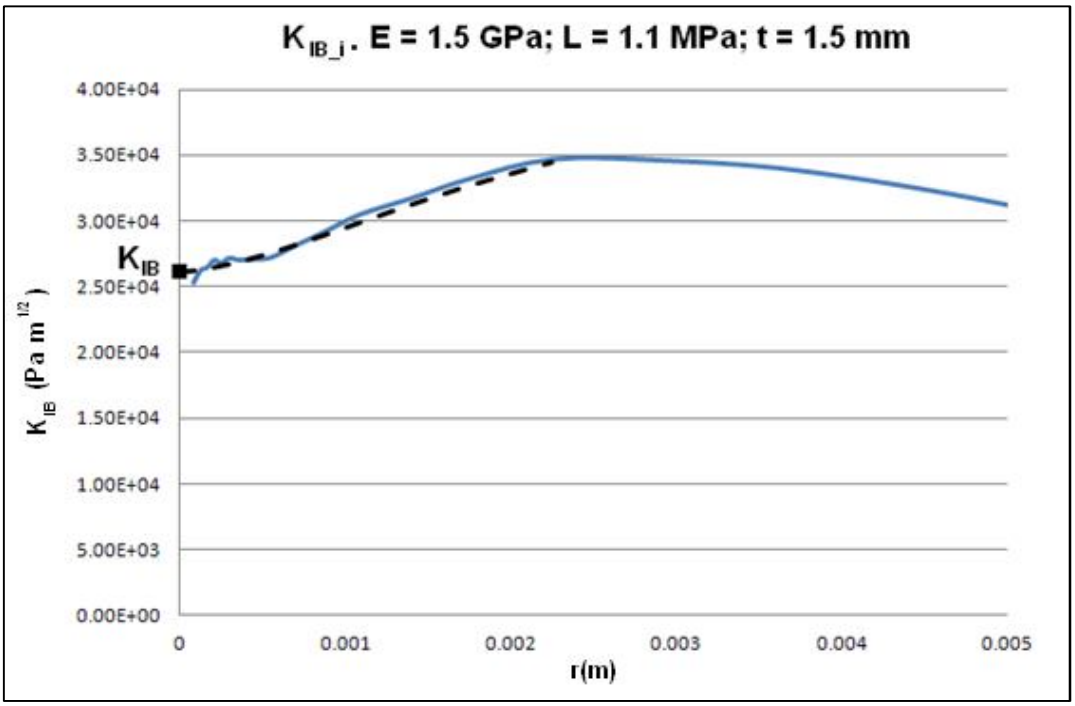

Fig 6.2. K_{IB_i} curve (whole) and extrapolation to the crack tip (dashed)

The relationship between the remote Load σ and the Stress Intensity generated at the crack tip is linear since this is a LEFM case study and the fracture is considered to occur in elastic conditions. Therefore, $K_{IB} = A * \sigma$, where the slope 'A' is a constant that depends on the coating properties.

Figure 6.3 is a graph showing the linear relationship between Remote Load σ and K_{IB} generated, comparing the constant $A = K_{IB}/\sigma$ for two different Coating Stiffness values E. This linearity is considered to be a validation of the methodology to obtain K_{IB}/σ

The slope that describes the relationship between K_{IB} and σ can be plotted as a function of the Coating Stiffness. Figure 6.4 shows that relationship for the particular case where the Coating Thickness is 1.5 mm, the value of K_{IB}/σ for every Stiffness simulated, in a range between 0.8 and 8 GPa.

The Figures showed in this Chapter are used as an explanation purpose. Effect of Thickness and Stiffness on the Stress State will be studied in Chapters 8 and 9

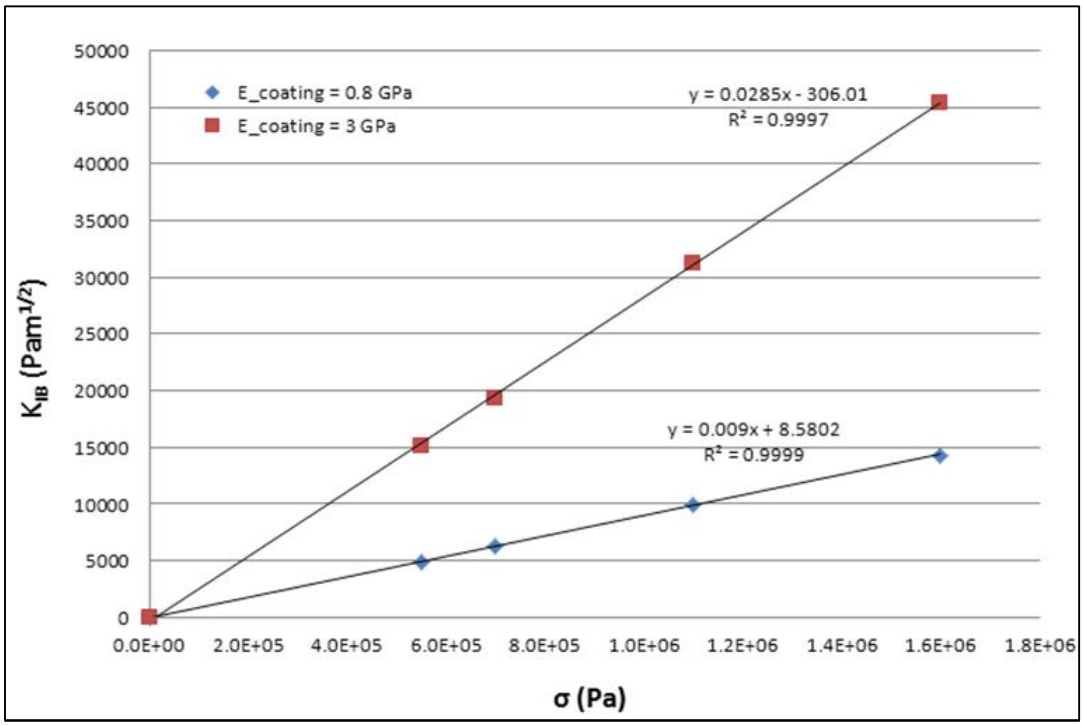

Fig 6.3. Linearity in the FEA Simulations between K_{IB} and σ

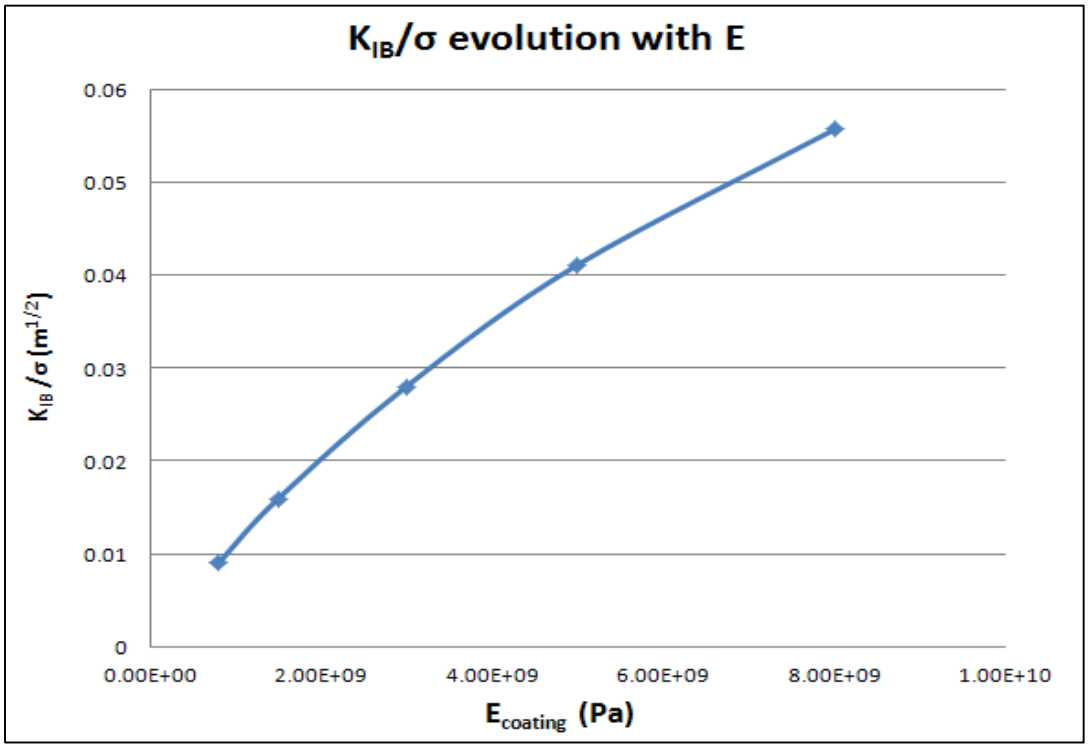

Fig 6.4. Mechanical relationship between stress magnitudes and coating stiffness

6.3. Methodology for shear simulations

The Methodology in the shear simulations transfers the Remote Load applied over the convex surface of the plunger into Stress Intensity factor in shear direction, in a bi-material junction interface, saving the singularity effect.

Figure 6.5 shows the sketch of the path that the numerical work and this methodology has to follow to calculate the Stress Intensity Factor in shear direction, in the bi-material interface. A remote Load in the convex surface of the plunger makes this part to move parallel to the ice-coating interface. This motion aims to move the part "Ice" in the same direction, generating a shear stress field in the interface. This stress field results in stress intensity in the vicinity of the geometric discontinuity in the "Ice" and "Coating" contact part. The experimental work is assumed to contain a crack whose size is the order of the grain size of the ice, which is (around 50 µm according to Pervier work, (Pervier, 2012). Due to the reduced dimensions of the crack, it was not modelled for the FEA.

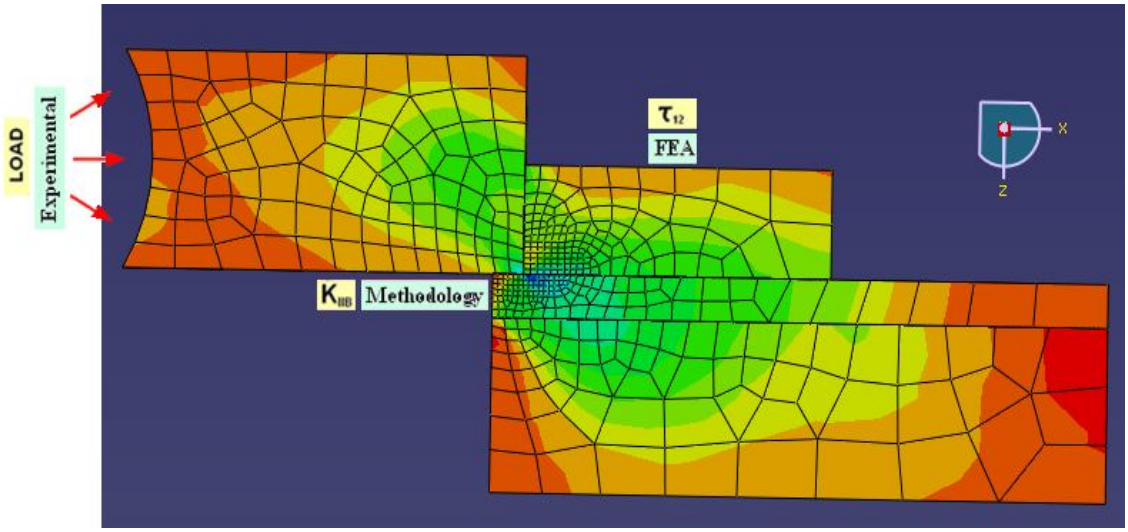

Fig 6.5. Representation of the slice of mode II test (τ_{13} represented).

In shear direction, the system does not follow the Hooke´s Law "spring model", like the system that tested the tensile load, but a more complex one. The spring analogy systems for tensile and shear load are compared in Figure 6.6. As a result, the Methodology to obtain the Stress State in shear direction is different.

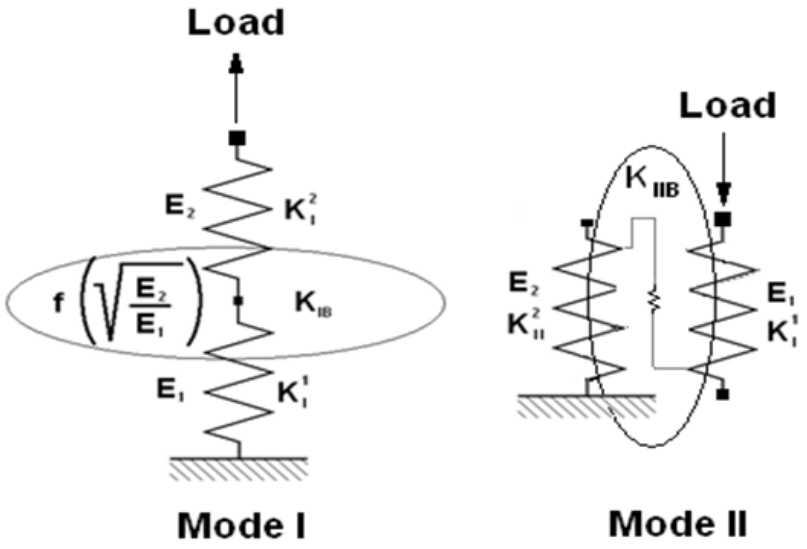

Fig 6.6. Stiffness and Stress Intensity Factor in an interface of a biomaterial joint for tensile and shear loads (spring analogy)

The Methodology to calculate the K_{IIB} in the interface is based on the suggestions by Ahmad and Majumdar (Ahmad & Majumdar, 1992) for a ceramic/ceramic joint. This methodology is capable to be adapted to this scenario, since the fracture in the model developed by the authors is understood to occur in brittle way (no plastic deformation observed visually in the experimental coupons after the tests).

In their work, a disk was loaded with separation loads at different angles, so that; there was a combination of Mode I and Mode II loading.

$$\tau_{13}(r) = \frac{1}{\sqrt{2\pi r}}(K_I\, sin(\eta) - K_{II} cos(\eta)) \qquad [6\text{-}6]$$

Where:

$$\eta(r) = \varepsilon * ln\left(\frac{r}{2c}\right) \qquad [6\text{-}7]$$

$$\varepsilon = \frac{1}{2\pi} ln\left(\frac{G_{SOFT}+(3+\upsilon_{SOFT})*G_{HARD}}{G_{HARD}+(3+\upsilon_{HARD})*G_{SOFT}}\right) \qquad [6\text{-}8]$$

Being *G* the Shear Modulus, υ the Poisson ratio, *2c* the defect size (length in the crack propagation plane, taken in this work as the edge element size) and *r* is the distance in the crack plane.

In this particular case of pure shear loading, the equations suggested can be simplified since $K_I = 0$ (pure shear). Re-writing equation [6-6]:

$$K_{IIB_i}(r) = \frac{\tau_{13}(r) * \sqrt{2\pi r} * Y}{cos(\eta(r))} \qquad [6\text{-}9]$$

Following a similar extrapolation to the r=0 axis, as it was done for tensile load case:

$$K_{IIB} = lim_{r \to 0} K_{IIB_i}(r) \qquad [6\text{-}10]$$

τ_{13} *are* the shear stresses observed in the bi-material interface, extracted from the FEA model for Mode II (shear stresses generated due to the Remote load applied on the convex face of the plunger). The "*Y*" factor has the value of *1.0*, since the *dA/dr = 0* in the crack propagation surface, in both the experimental and the numerical model (rectangular crack development area in both models, no geometric adaptation needed)

Mode II Methodology, as it happened in Mode I method, obtained the value of K_{IIB} through an extrapolation of a K_{IIB_i} function, saving the singularity found in the crack vicinity. Figure 6.7 shows, for a particular case, the evolution of the K_{IIB_i} and shear stresses in the interface trend lines and the extrapolation to the axis where r = 0 in order to obtain K_{IIB}

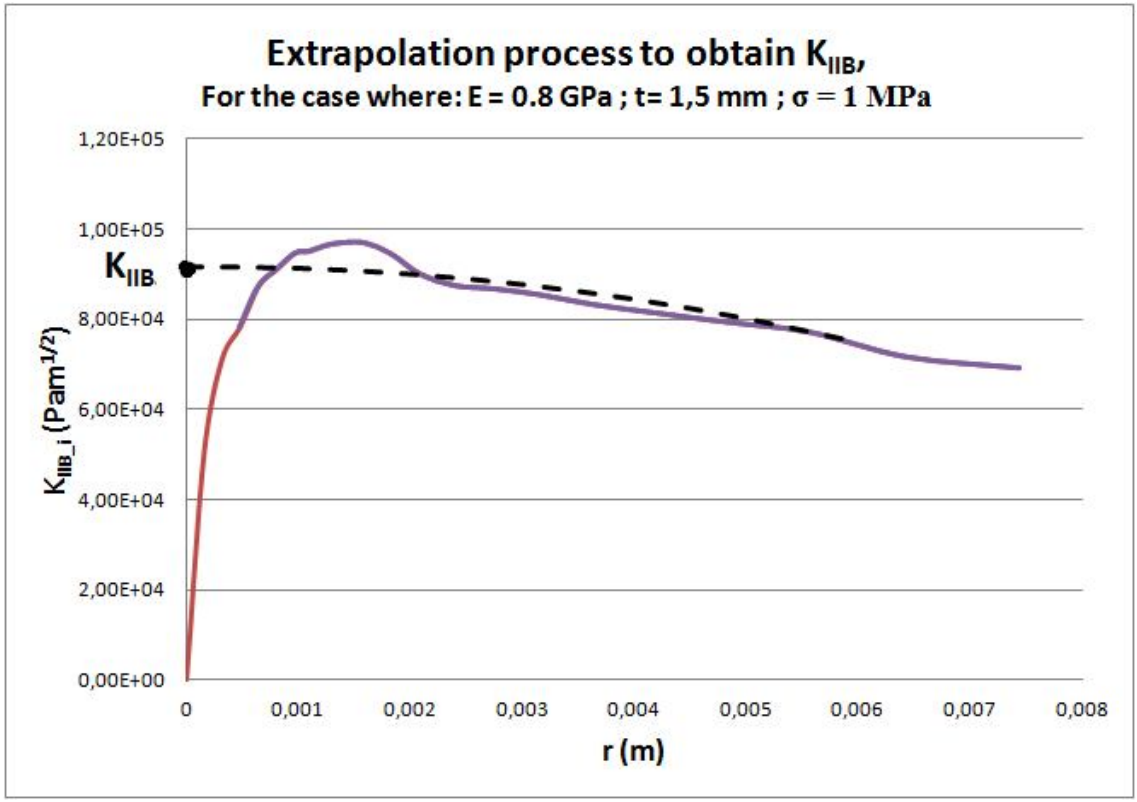

Fig 6.7. K_{IIB} obtained through extrapolation of a K_{IIB_i} function

CHAPTER 7. EFFECT OF AMBIENT CONDITIONS ON ICE ADHESION

7.1. Introduction

This part of the work is carried out to study the effect of two icing parameters on the Ice adhesion strength: Impact air speed and temperature. The sets of tests (one for each parameter) are carried out in the Icing Tunnel varying one of these parameters to observe the evolution of the Critical Pressure to break due to that parameter.

These tests were carried out as a contract work for two companies. The interest of these tests was a material, however, some conclusions from the experimental work can be employed in this Project to start to understand non-metals behave under different ambient conditions, comparing the results to those ones obtained by Pervier to metals (Titanium alloys) using the same facilities (Pervier, 2012)

The composition of the materials was not revealed by the supplying companies as the materials were subjected to confidentiality so that, they are not disclosed in this chapter. As a brief description, the materials are composite-based materials coated or not with different types of polymers, painted on top or not.

7.2. Effect of impact air speed on Ice Adhesion

7.2.1. Tests Motivation and Set Up

A set of tests were carried out in the Tunnel to evaluate the effect of impact air speed on the Critical Pressure to break the ice off. The speed variation is an important aspect in the adhesion when working with rotating elements. The speed at which the super-cooled droplets impact over the exposed surfaces varies with the atmospheric wind speed and with the rotating speed, the impact speed in this case is larger in the tip of the blades than in the hub.

The effect of the impact speed in the Critical Pressure is a factor that makes possible to evaluate the differences in the adhesion level along the blade. The variation of the speed is sketched in Figure 7.1**.**

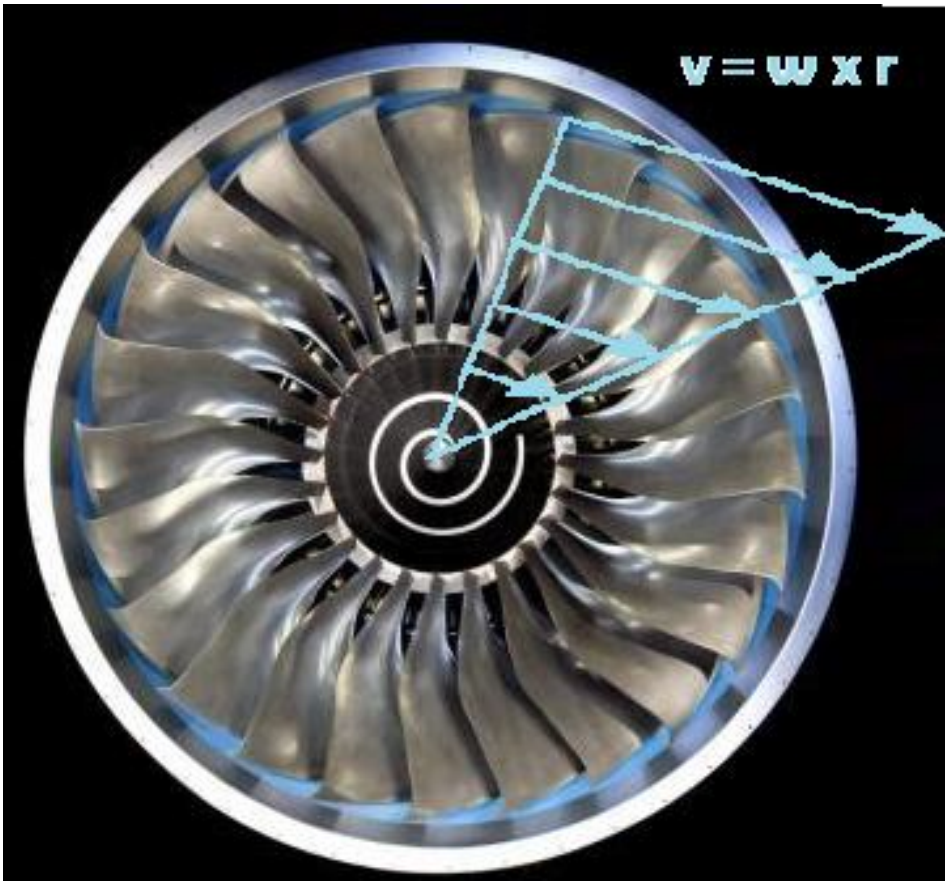

Fig 7.1. Speed distribution along a blade (Trent 900, front, Rolls-Royce)

7.2.2. Tests Results

The impact speed effect tests were carried out as a contract work for a wind turbine manufacturer. This is an exception in this work, where all the work is focused towards gas turbines. However, the author considered that some of the conclusions extracted from this piece of work can be employed in this project, since both systems have similarities and the results for one of them can be useful for the other. The LWC, for instance, is similar in the high risk icing scenarios in both cases.

The constant parameters of these tests are set up so as they are rational when simulating wind turbine operational conditions, due to the company demands. The temperature for the tests is fixed at -5^0C. The LWC is set at 0.3 g/m^3, which represents the freezing fog conditions. The impact air speeds chosen for the tests are 30, 40, 50 and 60 m/s. The speed values are taken according to the limitations of the Tunnel (Hammond, et al., 2003)

Table 7.1 shows the results for Mode I. This table shows the Critical Pressure recorded inside the piping system necessary to break the block of ice formed. The table also shows the Growth Rate of ice on the exposed samples as the speed increases and the Fracture Mode. The Evolution of Critical Pressure with the impact speed is plotted in Figure 7.2 and the accretion rate of ice is showed in Figure 7.3.

The same procedure has been carried out for Mode II. The results for Mode II are showed in Table 7.2. Figure 7.4 shows the evolution of Critical Pressure to break the ice in Mode II, after the correction (Equation 4-3). Mode II fracture is always in adhesive mode

The results of Critical Pressure are extracted from the average of at least six data points, a number that is considered by the author enough to obtain realistic values.

	Critical Pressure		Growth Rate		Fracture mode
	Mpa		mm/min		
speed (m/s)	average	st dev	average	st dev	
30	1,179	0,071	0,424	0,053	Cohesive
40	1,282	0,158	0,467	0,158	Mixed
50	1,243	0,237	0,543	0,141	Mixed
60	1,207	0,184	0,671	0,192	Cohesive

Table 7.1. σ_C in tensile direction, Growth Rate and Fracture Mode at different speeds.

	Critical Pressure	
	Mpa	
speed (m/s)	average	st dev
30	1,360	0,333
40	1,475	0,268
50	1,320	0,097
60	1,458	0,256

Table 7.2. σ_C recorded in the piping system in Mode II tests at different speeds.

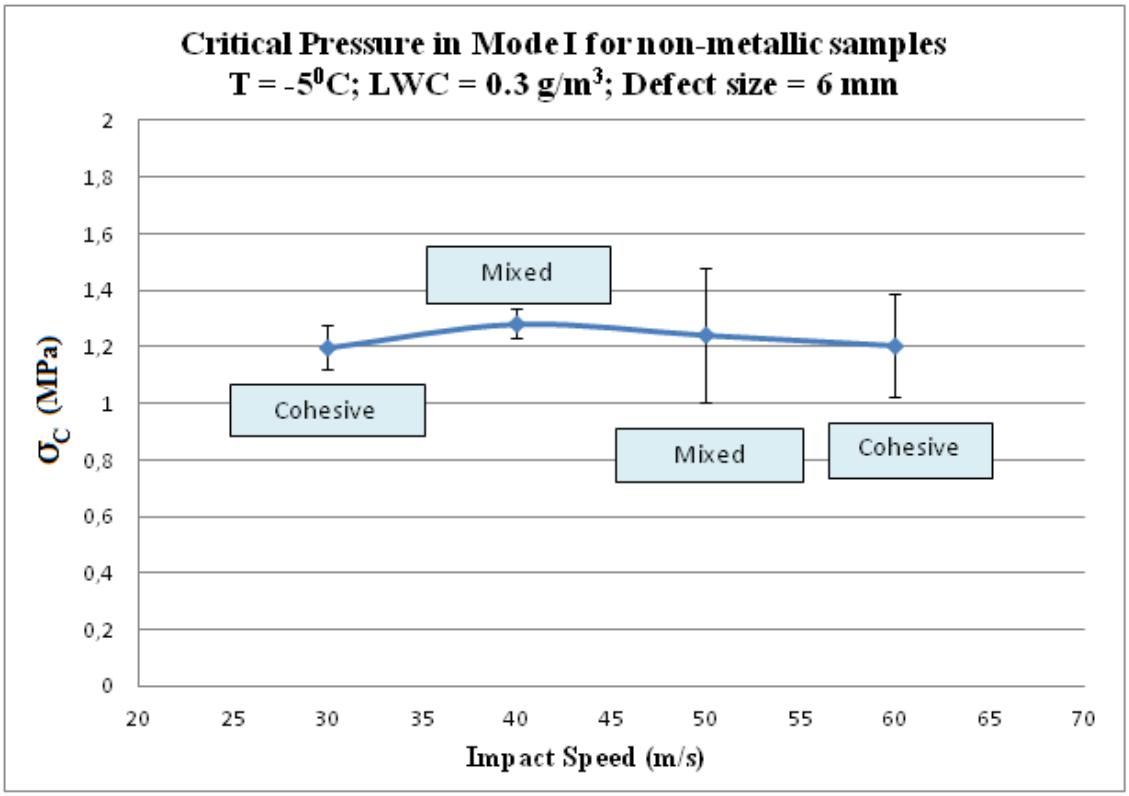

Fig 7.2. σ_C evolution as the Impact Wind peed changes. Results for Mode I

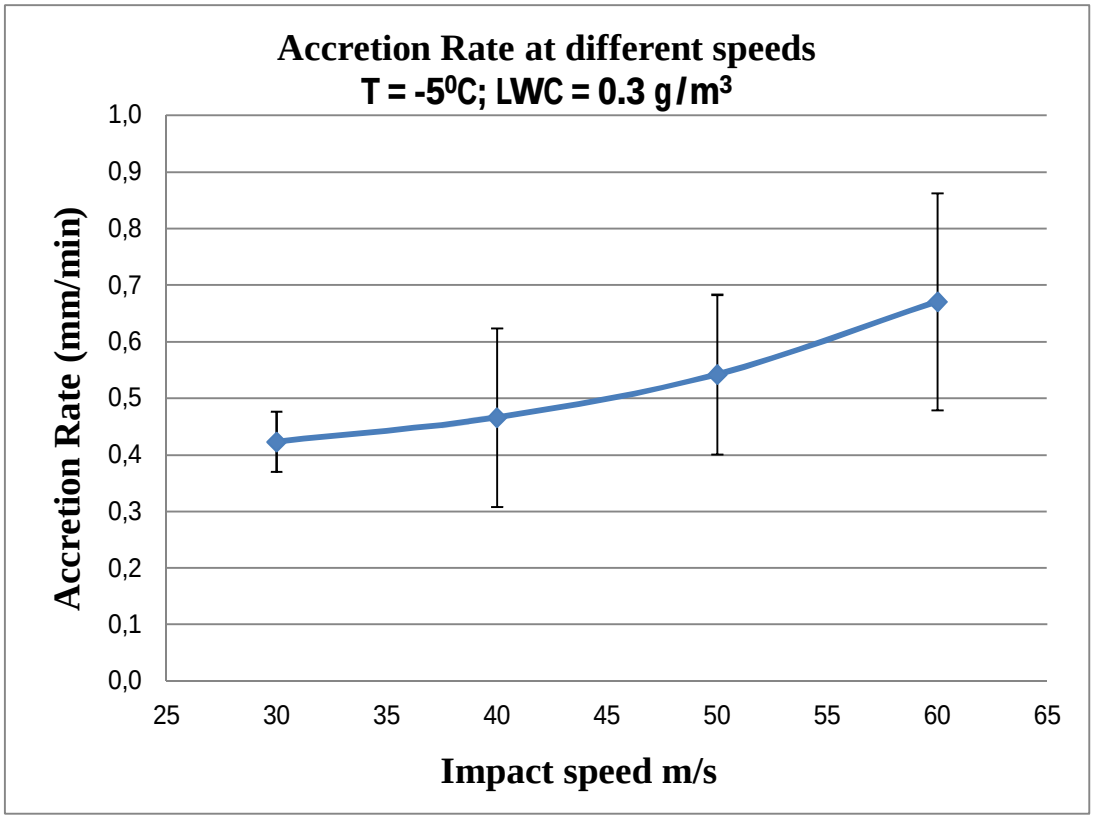

Fig 7.3. Accretion Rate at different speeds

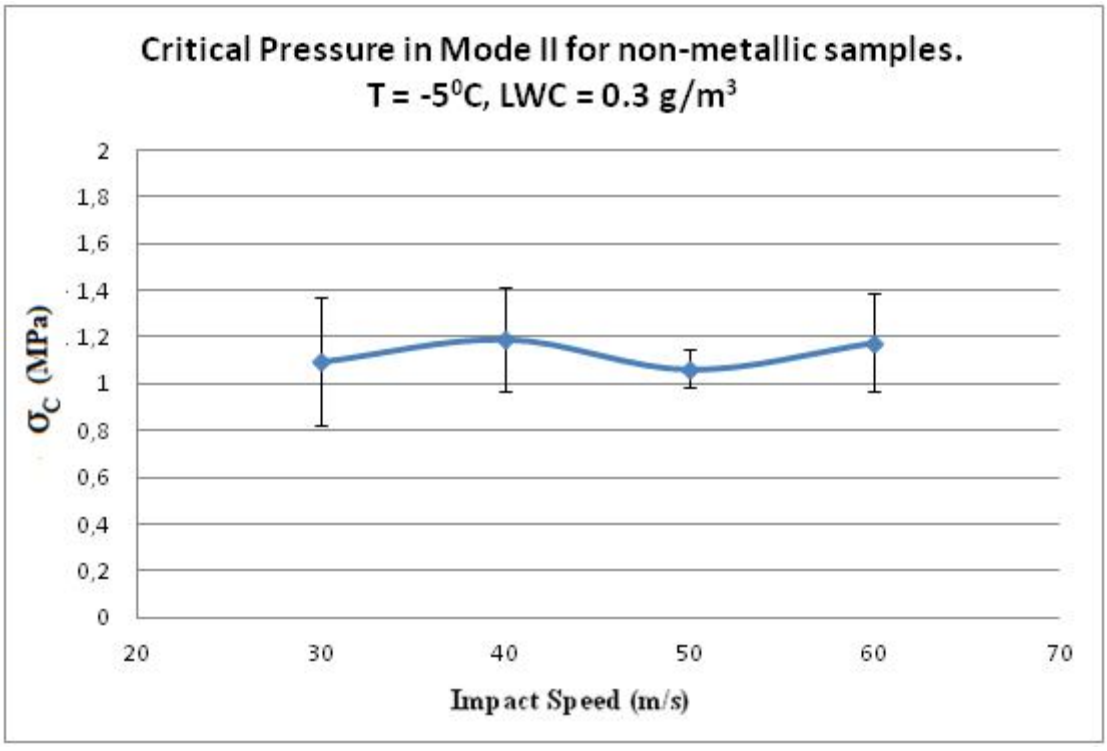

Fig 7.4. σ_C evolution as the Impact Wind Speed changes. Results for Mode II tests

7.2.3. Conclusions

According to the graphs, the impact air speed had no effect on ice adhesion, nor tensile or shear. In rotating elements, this means that ice attachment has the same strength in the tip than in the hub. This affirmation is valid for the range of impact speeds tested: 30 – 60 m/s.

This situation can be extrapolated to gas turbines fan blades. The conditions of LWC employed in the tests can be assumed to be the conditions that a fan can face in stratus clouds, when the ambient temperature is -5^0C. The impact speed range employed in the Tunnel is more realistic for wind turbines rather than gas turbines, due to of the limitations of the driving fan of the Tunnel.

Based on these results, the Adhesion Level is the same at any point along the blade length, and based on what has been seen in videos and pictures from icing-tested engines, the ice sheds from the fan blades exclusively due to the centrifugal forces, either in tensile or shear direction. The fact that the ice will shed in one or the other direction depends on the conditions of regimen, humidity, motion of the blades, vibrations, collection factor that might accumulate more quantity of ice at certain points, etc. These factors can cause the Adhesion Level to be overcome in certain areas and cause the ice to shed. As an example, Figure 7.5 shows a case of a fan blade after ice shedding in the area nearby the tip.

According to Figure 7.3, the accretion rate is not linear, as it would have been expected theoretically (doubling Impact Wind Speed up, under the same temperature and LWC conditions, will imply double water collected and therefore, double growth rate). The reason for that is the splash and run-back of the impacting super cooled droplets. In the testing conditions, ice is more prone to form in glaze type, this means slower solidification times. Consequently, large percentage of the impacting droplets will splash away and do not freeze in the exposed surface

Fig 7.5. Aspect of a fan after icing event (Rolls-Royce property)

The tensile and shear stresses are similar for the temperature tested. More precisely, the tensile strength is found to be slightly larger in average, although it can be considered that both forces are the same order. This fact should not drive to erroneous conclusions, since the temperature the tests were undertaken at was -5^0C. Under such conditions, the ice forms as glaze and the adhesion is low, therefore the ice fractures in smaller pieces. At this temperature the client was satisfied with the results in order to extract its own conclusions; however, this thesis needs some more tests, changing the Temperature, to understand how ice attaches to surfaces and which fracture mechanisms occur within the material.

This results lead to the next experiment within this project, the effect of the Temperature on tensile and shear adhesion

7.3. Effect of Temperature on Ice Adhesion

7.3.1. Tests Motivation and Set Up

The tests to study the effect of Temperature on Ice adhesion were motivated by Rolls-Royce. The target was to test how strong ice attaches to a set of materials that the company had in mind as suitable candidates to be used as coatings for blades. The materials tested are samples composed by a composite material developed by the company, coated (some specimens were not) with different Polyurethanes manufactured by external suppliers. The results will show how different the Temperature evolution is when the nature of the coatings is different.

The tests performed are both Mode I and Mode II, being extracted the same output than in the "Effect of Impact Speed" study

The tests are carried out in the following conditions, for Mode I and Mode II. The cloud had an average LWC of 0.3 g/m^3. The tests were performed at 50 m/s. The droplet size was 20 μm. The range of temperatures varied between -5 and -20^0C. The tests have been carried out, measuring the critical pressure for the ice to break from the test rig. These conditions cover the range of temperatures where icing event is possible to occur for a value of LWC likely to be found in cumulus clouds.

7.3.2. Materials overview

The specimens supplied by Rolls-Royce for these tests consist of polyurethane coatings attached to a composite. The underneath composite substrate is common for every sample. The materials employed in these tests are proprietary and were not revealed. However, some assumptions of these materials are made:

- The coatings are Polyurethanes. The elastic and thermal properties of all the coatings tested are considered to be the same. The specimens will be coded as PU1, PU2 and PU3. The specimens are tested on its bare form and painted.
- The typical Stiffness value for the Polyurethane is around 0.7 GPa. The substrate is a composite material whose Stiffness is estimated to be around $E_1 \approx 275$ GPa in fibbers direction and $E_2 \approx 20$ GPa in transversal direction. These values are estimated through the Rule of Mixtures for Stiffness Prediction in Composites
- PU1 coating is painted over the core composite. PU2 and PU3 are sprayed. The Thickness estimation for every coating is showed in Table 7.3. These values are estimated through a set of measurements with a calliper.

Individual Layer Thickness (mm)			
PU1	PU2	PU3	Paint
0.25	0.70	0.60	0.05

Table 7.3 Estimated thickness of the supplied material layers

7.3.3. Results and graphs

The results obtained experimentally are showed in Table 7.4 and Table 7.5 for Mode I and Mode II respectively. The results are obtained from an average of at least 6 data points. The evolution of the Adhesion Level with Temperature, for the different materials, in both modes is showed in Figure 7.6 and Figure 7.7

	σ_C (MPa)							
	T = - 5 C		T = - 10 C		T = - 15 C		T = - 20 C	
Material	σ_C	fracture	σ_C	fracture	σ_C	fracture	σ_C	fracture
Bare	1,372	mixed	1,605	adhesive	1,891	mixed		
PU1	0,920	adhesive	1,321	adhesive	1,364	adhesive	1,504	mixed
PU2	0,794	adhesive	1,985	mixed	1,762	adhesive	0,840	adhesive
PU3	1,423	mixed	1,723	mixed	2,439	mixed		
PU1 + Paint	0,851	adhesive	0,989	adhesive	1,101	adhesive	1,430	mixed
PU2 + Paint	1,326	adhesive	1,963	adhesive	2,025	cohesive	2,032	cohesive
PU3 + Paint	1,206	adhesive	1,937	adhesive	2,082	mixed		

Table 7.4. σ_C in Mode I and fracture mode for different materials

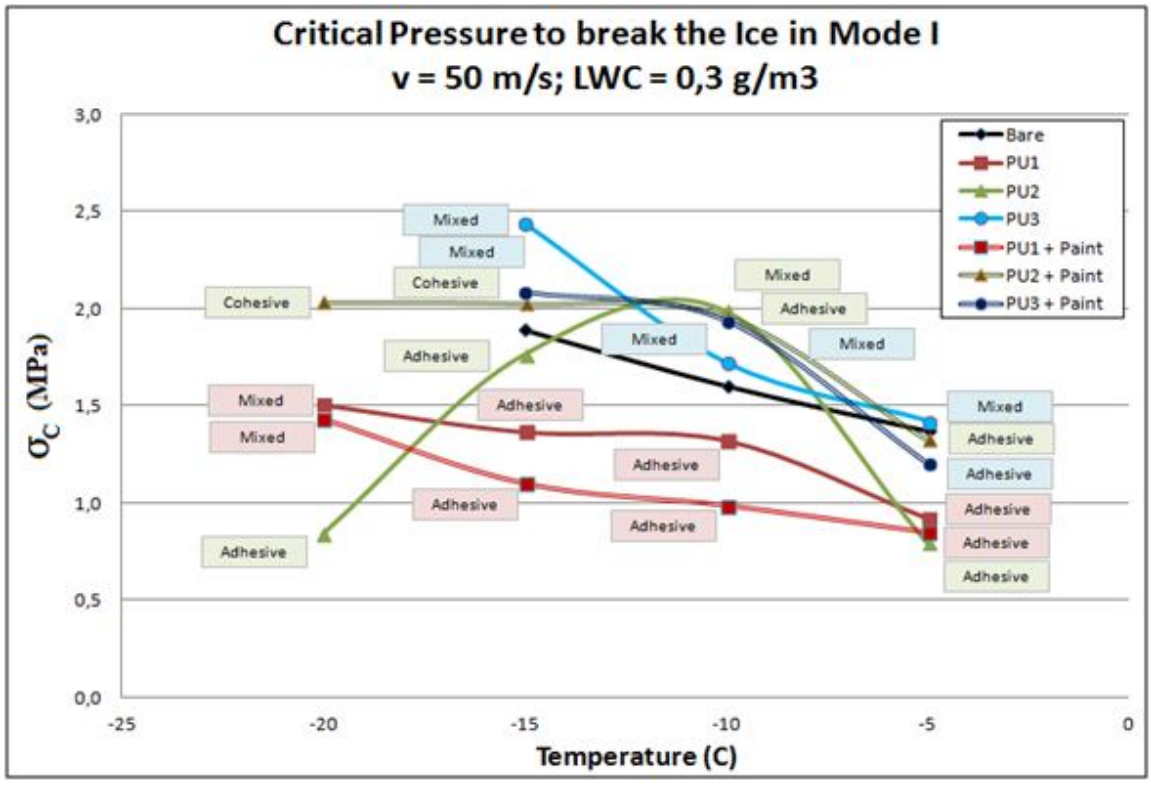

Fig 7.6. Evolution of σ_C, in tensile direction, as Temperature changes for different materials

The σ_C represented in the graph is the pressure recorded inside the rubber tube that pushed the plunger to cause the ice to break after the geometric correction (See Equation 4-1). The results are obtained from an average of at least 6 data points.

	σ_C (MPa)					
Material	–5^{0}C	– 7.5 ^{0}C	– 10^{0}C	–12.5^{0}C	– 15^{0}C	– 20^{0}C
Bare	0.908	1.071	-	1.136	-	1.403
PU1	0.698	0.780	0.715	0.816	1.030	1.134
PU2	0.704	0.847	0.725	0.854	0.901	1.077
PU3	0.542	0.684	0.871	0.905	0.938	1.057
PU1 + Paint	0.840	0.868	0.840	0.918	0.969	1.008
PU2 + Paint	0.759	1.049	0.881	0.952	1.071	1.040
PU3 + Paint	0.494	0.704	0.830	0.871	0.979	1.098

Table 7.5. Results for σ_C to break the ice in Mode II

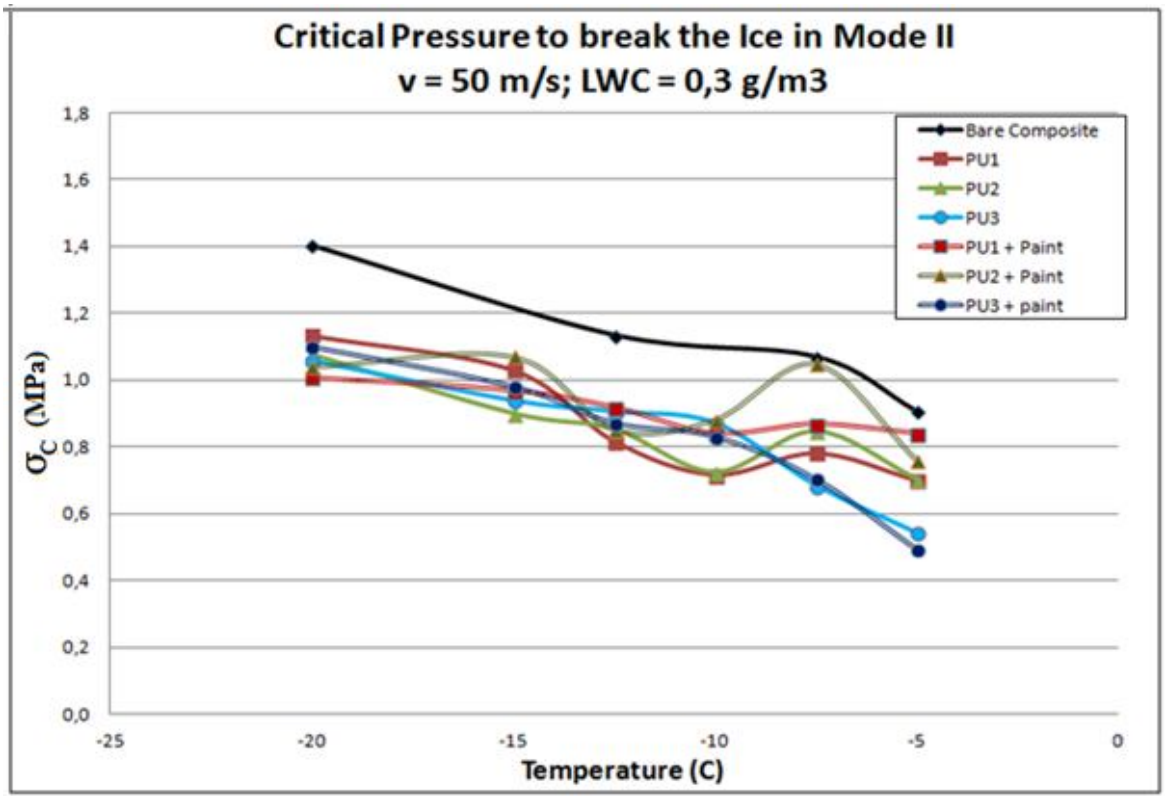

Fig 7.7. Evolution of σ_C for Mode II tests, as Temperature changes for different materials

7.3.4. Discussion of results for Mode I

In general, the Critical Pressure σ_C tends to increase as the temperature decreases but it is not observed a common tendency. The materials behave in different ways (Figure 7.6). The most common trend it to require larger quantity of pressure to break the ice as the temperature decreases. In the range from -5 to -10^{0}C the σ_C required increased as temperature decreased for every specimen. The σ_C in the range of temperatures from -10 to -15^{0}C tended to have a steady value, except in the case of the material labelled as PU3, which showed an augment of σ_C as the temperature decreases. There are less data points for tests carried out at -20^{0}C. The σ_C at these temperatures showed that one of the materials had a reduction in the required σ_C, whereas the other three materials tested showed a steady value or a minor increment. It is expected that the cases where the σ_C has steady values are in the transition between adhesive and cohesive fracture, therefore, the σ_C reaches the Fracture Toughness of the ice. The reduction in the σ_C as the temperature decreases, in the material PU2, might happen due to the increment of the residual stresses in the volume of the ice. This thermal residual stresses can be an extra aid to reduce the amount of pressure required to break the ice.

From the point of view of this Project, that studies the effect of Stiffness and Thickness of a coating on the ice Adhesion Level, the materials employed in this chapter are complex (heterogeneous, orthotropic), therefore, it is not possible to know accurately how the strain fields distribute within the volumes of both ice and coating. The specimens tested are not homogeneous, but have a soft coating over a relatively stiff substrate. This Thickness of the exposed material is likely to have an effect on the adhesion level, since larger volumes might allow larger strain fields within.

The evolution of the tensile Critical Pressure is plotted for the materials tested and these ones can be benchmarked according to their Stiffness / Thickness. However, the effect of the Temperature on the ice adhesion to non-metallic coatings cannot be generalized to other scenarios, neither the fracture mode. For example, it is found Adhesive fracture for the material named as “PU2” at 2.0 MPa (at T = -10^{0}C), whereas, the fracture mode in the sample coded as “PU3 + Paint”, in the same conditions, is found to be mixed.

7.3.5. Discussion of results for Mode II

The results in Figure 7.7 show that the coatings caused a reduction in the Critical Pressure required to break the ice off, compared to the bare composite. The adhesion has a growing tendency for every sample tested and can be assumed that it is quasi-linear. This is expected as the fracture is caused to occur in shear direction in the interface (no cohesive fracture found in Mode II tests). As it was observed by other authors, the decrement of the Temperature strengthens the chemical bonds that tie the ice and the coating. The values for the Critical Pressure of the ice to coatings are scattered for the highest Temperatures and are convergent to a common trend line at the lowest ones. In any case, the σ_C recorded is lower than that one required in order to the ice from the bare composite cases.

The existence of a paint layer as an exposed surface does not seem to have a remarkable effect on the adhesion level in the materials testes, neither in Mode I or Mode II (except in the case of PU2, in Mode I, where the tendency for the unpainted and painted samples is to decrease and to remain steady respectively). However, in general, the paint is very thin and can be assumed not to have an effect on the Adhesion level. The paint layer was estimated, after some measurements with a calliper, to be around 0.05 mm (Table 7.3). It is likely that such a thin layer (therefore, small volume) is not having an effect on the ice adhesion.

The magnitude represented in the graphs is the pressure that moves the plunger of the ISD, not the shear stresses in the interface. This magnitude is obtained through a FEA. This analysis is not made due to its complexity of the material tested and the fact that the value of the elastic properties is estimated, but unknown.

Chapter 8 will evaluate the effect of Stiffness and Thickness on ice adhesion from more simplistic materials, which will be isotropic and homogeneous. This chapter will help to explain how the Stiffness and Thickness of an exposed material has an effect on the Ice Adhesion Level.

CHAPTER 8. EFFECT OF COATING STIFFNESS AND THICKNESS ON ICE ADHESION IN TENSILE DIRECTION

8.1. Motivation and Procedure

This chapter studies the role of Stiffness and top coating Thickness on ice Adhesion Level to polymeric coatings, in tensile direction. The criterion used in this work to evaluate the Ice Adhesion Level is the Critical Stress Intensity in the bi-material junction interface, K_{IB_C}. It is named after the nomenclature of Stress Intensity factor in the interface, K_{IB}. The suffix "B" distinguishes this magnitude calculated in a bi-material junction, from K_I, found in the Literature for bulk materials.

The results observed in Chapter 7, in the study of the effect of temperature in σ_C in Mode I (Figure 7.6), showed that the materials tested were not having a common trend on its behaviour. The different evolution of σ_C, for the specimens tested, made the results obtained not appropriate to extract a general model about the effect of the Stiffness and Thickness on the Adhesion behaviour. The reason is that the specimens employed were anisotropic (orthotropic, core made of composite) and heterogeneous (some were coated with Polyurethane and/or painted on top). That complexity was obstructive to estimate the material properties and to establish a pattern to evaluate a general tendency in the Ice Adhesion with the material properties. Therefore, the experiments in this Chapter will be carried out over less complex specimens in order to understand the effects of Stiffness and Thickness on the K_{IB_C}.

In order to obtain the K_{IB_C} and its evolution with the coating Stiffness and Thickness, this chapter is going to follow the four steps described in Chapter 3: Experimental tests in the icing tunnel (routine explained in Chapter 4.2) using isotropic and homogeneous materials, whose properties are well known; Numerical work in FEA (Explained in Chapter 5) adapting the FEA model geometry and material properties to the ones of the real cases; adaptation of the stress field obtained from the FEA into Stress State in the crack tip through the Mathematical Methodology (explained in Chapter 6) and; finally, merging these results in order to obtain the Adhesion Level (this will be explained at the end of this chapter)

8.2. Materials

A set of materials was purchased to be tested in the Icing Tunnel to study the Effect of Stiffness and Thickness. Three materials are employed in these tests: High-Density Polyethylene, (HDPE, E = 0.8 GPa); Polypropylene, (PP, E = 1.5 GPa), and Polyvinyl chloride, (PVC, E = 3.0 GPa).

Additionally, four different sheets of Polypropylene, with different Thickness values, have been purchased. This set of sheets will be employed to study the Effect of Thickness. The values for Coating Thickness tested are 0.05, 0.2, 0.5, 1.0 and 1.5 mm

These samples are considered to cover acceptably the range of Stiffness and Thickness that most of the polymeric coatings might have. The nomenclature employed for the samples, used from now on, is described in Table 8.1. Stiffness and Thickness of the samples are stated. The table includes other properties of the materials that might have an effect on the adhesion level but are not considered in this Project. It is also included the properties of the ice employed in the tests, based on the results in Pervier´s Research (Pervier, 2012).

Code	Material	Stiffness (GPa)	Thickness (mm)	Relative Permittivity ε_r (@1Mhz)	Thermal Conductivity k (W/mK)	Expansion coefficient α (m/mK)(x10^6)
HDPE	High Density Polyethylene	0.8	1.5	2.26	0.5	200
PP005	Polypropylene	1.5	0.05	2.2-2.36	0.22	100-200
PP02	“		0.2	“	“	“
PP05	“	“	0.5	“	“	“
PP10	“	“	1.0	“	“	“
PP15	“	“	1.5	“	“	“
PVC	Poly-vynil-chloride	3.0	1.5	3	0.2	50
Ice	Impact Ice	8.5	-	-	2.30	51

Table 8.1. Properties of the polymers purchased and the Ice formed in the Tunnel

The coupons named as HDPE, PP02, PP05, PP10, PP15 and PVC are glued to an Aluminium substrate. The specimen named as PP005 is a Polypropylene tape stuck to Aluminium substrates.

Permittivity, Thermal Conductivity and Thermal contraction are not considered in the evaluation of the Effect of Material Properties on Ice Adhesion. In general, the molecules whose relative permittivity is "3" or lower are considered as non-polar (Zeus Industrial Products, 2005). Polyethylene and Polypropylene are non-polar as their molecules are formed by Hydrocarbons. PVC has a slightly larger value of relative permittivity, although non polar, because of the Halogen-Carbon (Chloride – Carbon) covalent bond on its molecule. Therefore, no one of the materials is considered to be polar, so no remarkable effect on the moisture absorption / Ice Adhesion strength is expected due to polarity. Thermal conductivity is in the same range for every material tested (0.2-0.4 W/mK) and it is not expected to have a differentiating effect.

The Thermal Expansion Coefficient α is different for each material and might have an influence in the generation of residual shear stresses parallel to the bi-material interface. When super cooled droplets freeze over a sub-zero surface, the solidification of the water produces the release of the Latent Heat of Solidification. This energy release makes the temperature to reach 0^0C (theoretically) in the surfaces where the solidification is happening. On the other hand, the other surfaces are below zero. This difference of temperatures within the volume of ice generates residual thermal stresses. The existence of these residual stresses might have a real effect in those cases where the Thermal Expansion Coefficients of the materials forming the bi-material junction are different. For the materials tested, this situation would be noticeable in HDPE and, in lower scale, the Polypropylene sheets. However, the tests in Mode I are carried out when the block of ice has a thickness of 15-20 mm (See Chapter 4). Having the block of ice that volume before the fracture, it is going to be assumed that there is a relaxation of the Residual Thermal Stresses in the vicinity of the Ice-Polymer junction and, consequently, Thermal Stresses can be considered not to have a differentiating effect on the Ice Adhesion Level to these polymers.

8.3. Effect of Coating Stiffness on Ice Adhesion in Mode I

8.3.1. Experimental Results to different coating materials

The Experimental Work consists of a set of Mode I fracture tests in the Icing Tunnel. The materials properties well known, showed in Table 8.1 and their values of Stiffness and Thickness can be considered to be representative of that range suitable to be employed as coatings in practical cases.

The tests have been carried out in the Tunnel at -5^0C and -10^0C, LWC = 0.4 g/m^3. Impact Wind speed is 50 m/s and MVD is 20 μm. The specimens are tested at two different temperatures, as there is an interest in knowing whether the temperature will have the same effect in polymers as it had in metals.

The σ_C results are plotted in Figure 8.1 and Table 8.2. Fracture occurred in adhesive way in every scenario.

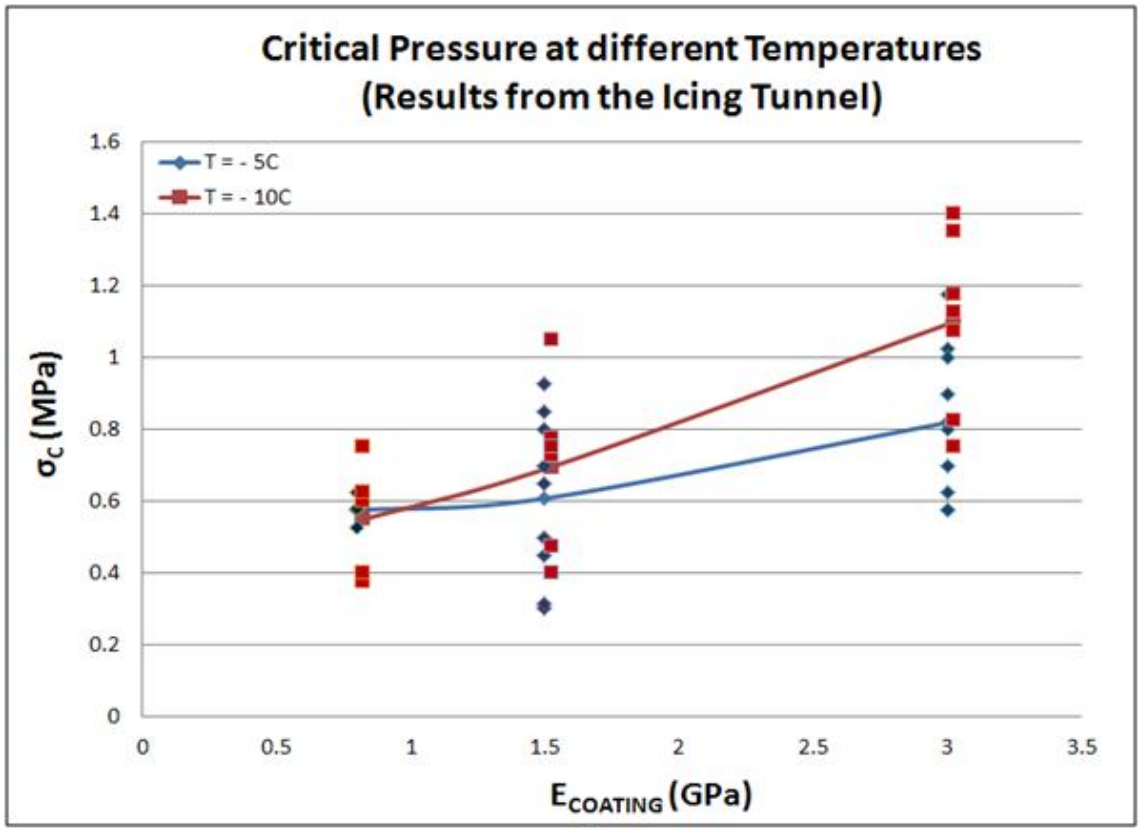

Fig 8.1. Experimental Results for σ_C values for different coatings

		T = - 5 C		T = - 10 C	
Material	$E_{coating}$ (GPa)	σ_c (MPa)	stdev	σ_c (MPa)	stdev
HDPE	0.8	0.575	0.21	0.55	0.16
PP15	1.5	0.608	0.23	0.696	0.23
PVC	3	0.819	0.22	1.1	0.23

Table 8.2. Experimental Results for the σ_c, in Mode I, recorded in coatings with different Stiffness

8.3.2. Numerical Results and Stress State

The numerical Simulations are carried out in FEA, using the model described in Chapter 5, for tensile load in order is to obtain the stress field in the bi-material junction interface. The parts in the FEA are modelled so they have the similar properties as the elements of the real test they represent. The properties inserted in for the FEA are the density and the elastic properties *E* and *v*.

The stress field obtained, processed with the Mathematical Methodology described in Chapter 6, will provide the values for the Stress Intensity Factor in a bi-material interface as a function of the remote Load, along the crack plane: the Stress State or K_{IB}/σ. This evolution was discussed in Chapter 6 and can be assumed to follow a quadratic relationship, represented through Equation 8-1 and Figure 8.2. The Figure shows the numerical results for the particular case where the coating thickness was t = 1.5 mm.

$$\frac{K_{IB}}{\sigma}(E) = C_1 * E^2 + C_2 * E \qquad [8\text{-}1]$$

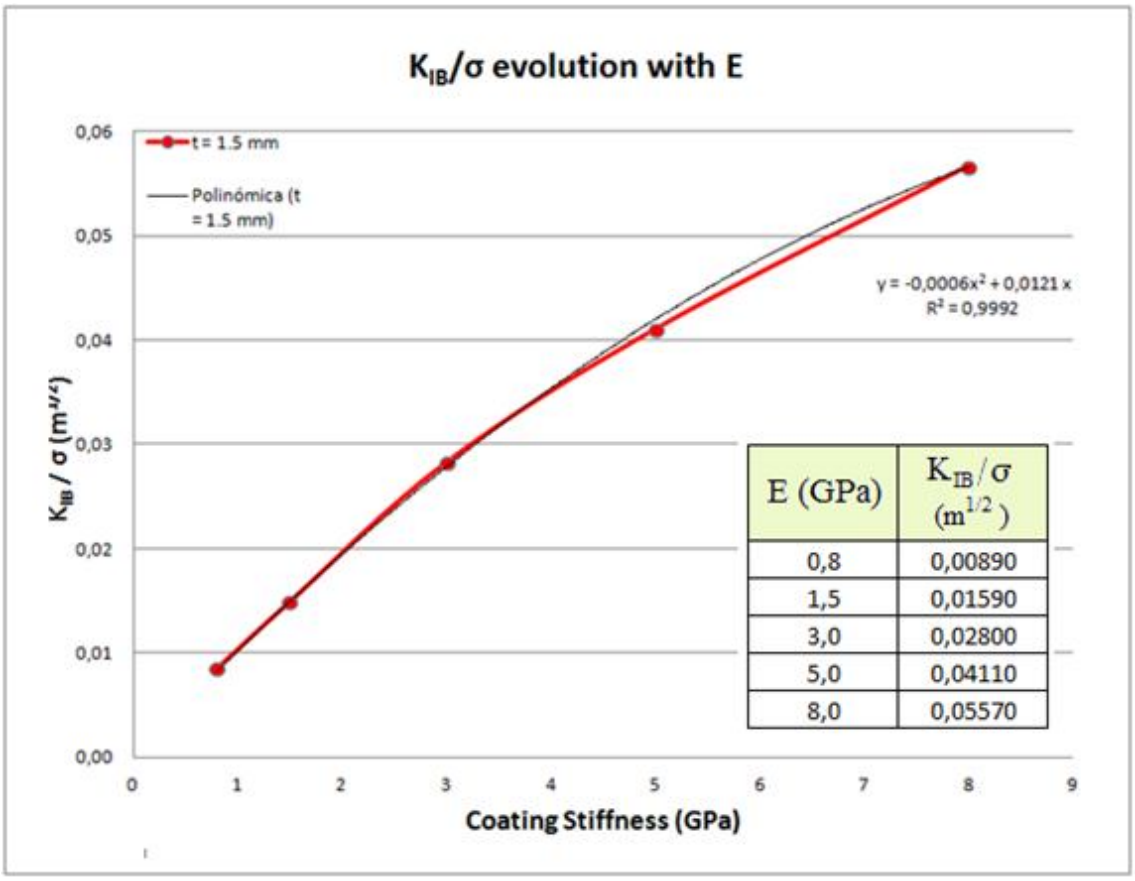

Fig 8.2. Effect of the Stiffness on the Stress State

8.3.3. Calculation of K_{IB_C}. Effect of Stiffness on Ice Adhesion

$K_{IB\_C,}$ the metric that represent the Adhesion Level of ice used in this work, is the critical value of the stress intensity factor K_{IB}, for a given Load, which causes the crack evolution. This K_{IB_C} is reached when the fracture occurs; this is, when the Remote Load in the Stress State K_{IB}/σ relationship reaches the value of the Critical Pressure σ_C. Figure 8.3 sketches this situation:

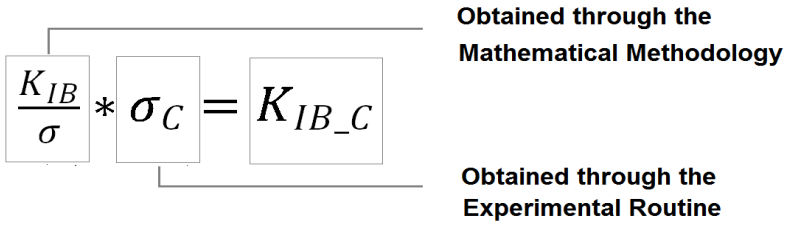

Fig 8.3. Sketch explaining the calculation of K_{IB_C} by combining experimental and mathematical work

K_{IB_C} comes from the combination of the numerical value for K_{IB}/σ, which depends on Stiffness and Thickness (properties varied in the FEA) and the experimental value σ_C, which puts in the equation which Remote Load caused the fracture. This equation assumes that it is viable to combine real tests with a numerical model where only three properties of these tests are inserted (density, stiffness and thickness), in order to isolate the parameters Stiffness and Thickness to observe their effect on the K_{IB_C}

For the particular case showed in Figure 8.2, the values for the C-Constants are C_1 = -0.0006 and C_2 = 0.0121. These values are going to be employed to obtain the evolution of the K_{IB_C} as a function of the coating Stiffness and the two temperatures tested.

The C-Constant values are inserted in Equation 8-1 with the σ_C results from Table 8.2 for each coating Stiffness case, resulting in:

$$K_{IB\_C} = (-0.0006 * E^2 + 0.0121 * E) * \sigma_C$$

		T = - 5 C		T = - 10 C	
Code	E (GPa)	σ_c (MPa)	K_{IB_C} (Pa $m^{1/2}$)	σ_c (MPa)	K_{IB_C} (Pa $m^{1/2}$)
HDPE	0.8	0.575	4580	0.55	4259.2
PP15	1.5	0.608	8572.8	0.696	9813.6
PVC	3	0.819	21621.6	1.1	29040
Titanium (Pervier)	120	1.900	85509,94	2.387	97748,5

Table 8.3. Results for σ_C (experimental) and K_{IB_C}

These results are plotted in Figure 8.4. The graph also includes the ice adhesion to Titanium results obtained by Pervier (Pervier, 2012), obtained using the same facilities, testing fixtures and strain rate than this work.

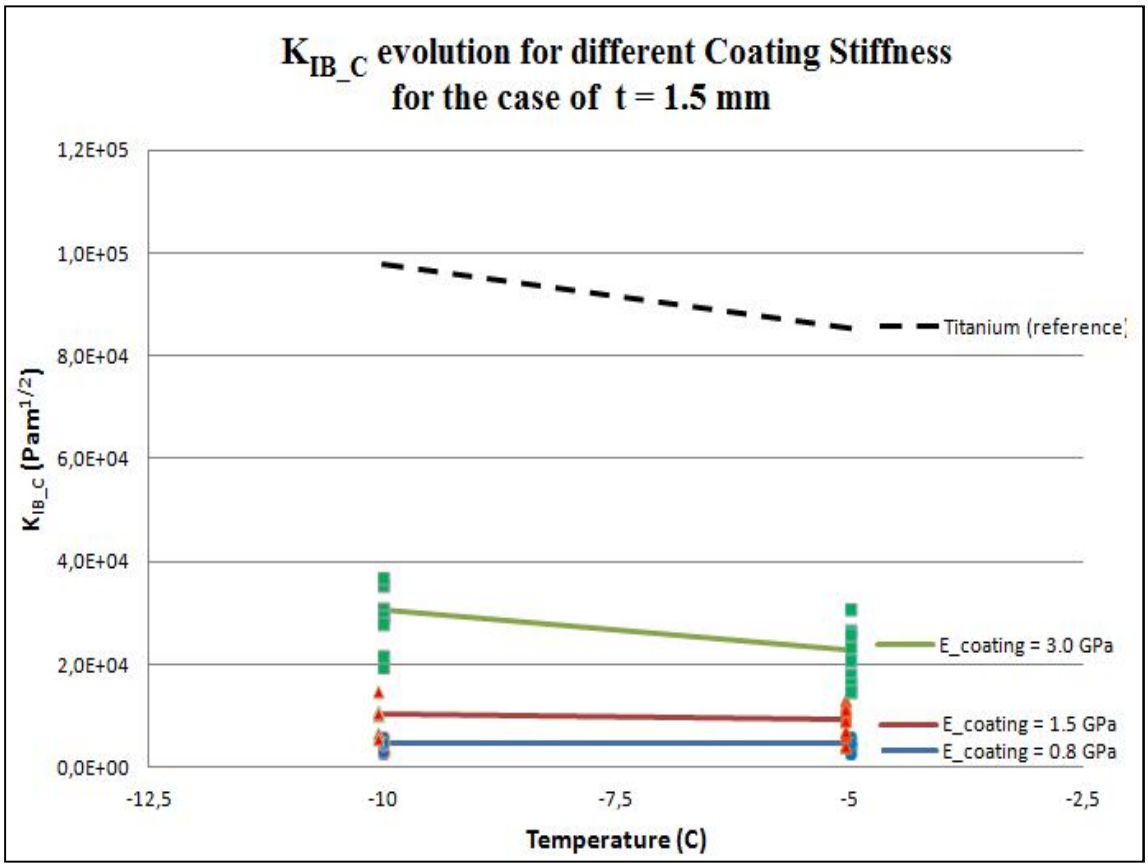

Fig 8.4. Ice adhesion level comparison for different Coating Stiffness at different Temperatures

The graph in Figure 8.4 shows that the K_{IB_C} of ice attached the polymers is lower than the one resulting when it attached to Titanium alloys. The Stiffness is not the only factor that has an effect in the reduction of the Adhesion Level, as the Titanium is a material that is much polar than the polymers tested. However, among the polymers, it is found that the Adhesion Level is lower when ice attaches to the least stiff polymer (HDPE). When comparing polymers to each other, some properties that might affect the Adhesion level such as the polarity, permittivity and contraction coefficient were assumed to be the same order, therefore the Stiffness does have an effect on the K_{IB_C}.

The Temperature has an effect on the Ice Adhesion Level for the Stiffest polymer tested (E = 3 GPa) as it had for much stiffer materials. However, the K_{IB_C} is not affected by temperature when the coatings are much softer than the ice.

All the observations will be more widely discussed in epigraph 8.3.5

8.3.4. Comparison of K_{IB_C} when ice attaches to polymers and metals

One of the main targets addressed by the sponsor is a comparison between the Adhesion Level found in the ice-polymeric (less stiff material) bi-material junction compared to that in the ice-metallic junctions. The results obtained are compared to the results obtained by other authors

Results in Adhesion Level might differ depending on the experimental rig and procedure, so that, the results chosen from the Literature to compare with the current ones are the ones obtained from an Icing Tunnel (Hammond, 1996), (Pervier, 2012) or from distilled freezing water using similar test rig (Andrews & Lockington, 1983)

The process to calculate K_{IB_C} is different whether the other material in the bi-material junction is stiffer than ice (metals) or not (polymers). Other authors have referred the Adhesion Level to the Fracture Energy; the values they obtained are transformed into K_{IB_C} through the Equation 8-1:

$$K_{IC} = \sqrt{\frac{FE*E}{(1-\nu^2)}} \qquad [8\text{-}2]$$

Notice that K_{IC} refers to the general Critical Stress Intensity Factor in either a bi-material junction or a bulk material (Fracture Toughness). In order to compare the results from other authors with the ones obtained in this work, the Fracture Energy must be the one calculated in those cases where the ice shed 100% adhesive. In those cases, K_{IC} refers to the Stress Intensity Factor in the Interface and, so, to K_{IB_C}.

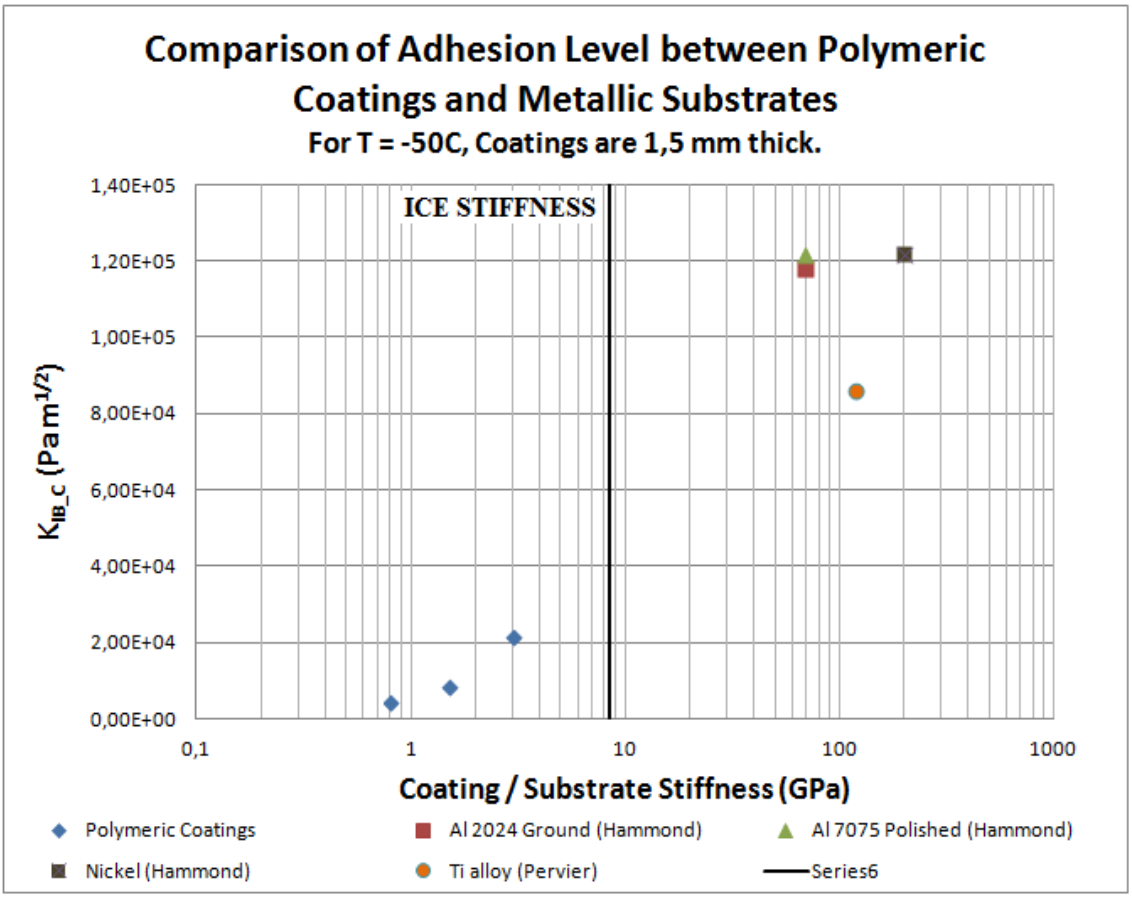

Fig 8.5. Comparison of the Adhesion Level of ice to Polymeric coatings and Metallic substrates

Material	E (GPa)	K_{IB_C} (Pa $m^{1/2}$)	Comments
HDPE	0,8	4580.00	
PP	1,5	8572,80	
PVC	3	21621,60	
Al 2014 Ground	69	118019,37	Hammond. FE = 1,5 J/m^2
Al7075 Polished	69	121889,88	Hammond. FE = 1,6 J/m^2
Titanium	120	86189,16	Pervier. FE = 0,8 J/m^2
Nickel	200	121889,88	Hammond. FE = 1,6 J/m^2
Titanium	120	75000	Andrews, FE=0.6 J/m^2

Table 8.4 Comparable Adhesion Level to some Materials

8.3.5. Observations

It is observed the effect of the Coating Stiffness on the σ_C (Figure 8.1) and so in the K_{IB_C} (Figure 8.4 and Figure 8.5). The least stiff materials required lower pressure to break the ice (in the experiments) or lower stress intensity was required to start the crack and cause the fracture (after the calculations of K_{IB_C}).

The key to explain this might be the generation of larger strain within the volume of the less stiff body. A graph extracted from three FEA simulations (Figure 8.6) shows the strain field in the ice-coating interface for a softer coating (E = 1.5 GPa), for a coating as hard as the ice (E = 10 GPa) and for a stiffer substrate (Aluminium, 69 GPa). It is observed that the strain field generated in the crack development plane of the exposed coating, is very large for a soft material, approximately the same order for a coating the same level of Stiffness of the ice and insignificant when ice attaches to a much harder material.

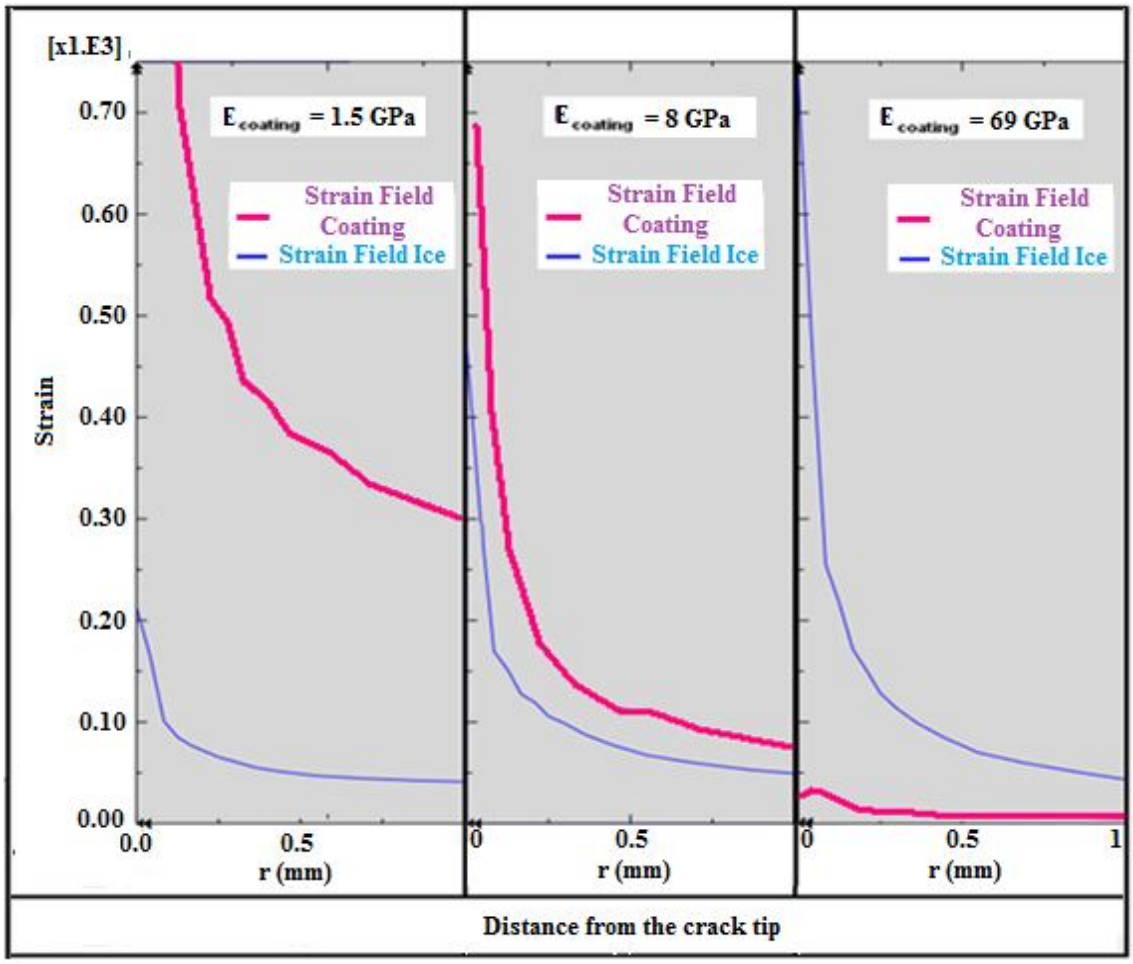

Fig 8.6. Strain rates for different coatings/substrate.

All the materials are on its glassy state when tested, since their Glass Transition Temperatures are T_{G_HDPE} = 0 - 30^{0}C, and T_{G_PP} = 0^{0}C, T_{G_PVC} = 80^{0}C this is, above the testing temperatures. The σ_C recorded from the experimental work is much lower than the values of the Yield Strength of the tested materials on glassy state: σ_{Y_HDPE} = 26-33 MPa, σ_{Y_PP} = 12-43 MPa and $\sigma_{Y\_PVC} \approx$ 50 MPa. Therefore, it is going to be assumed that the stress – strain behaviour of the polymers is linear elastic, with no creep effect

The work carried out in the linear elastic zone make the strain fields to generate retraction forces as a result due to Hooke´s Law. A body subjected to an external load in pure elastic behaviour generates a restoring (retraction) force, in the opposite direction, as a response of the external load, tending to get back its original shape. The retraction force in the coating under tensile load is analogous to the Hooke´s Law applied to springs, where the system follows the equation (Spring Analogy):

$$F = -k * X$$

Where F is the retraction force, k is the Stiffness of the spring (analogous to the Coating Stiffness in this work) and X is the deformation (Strain field in this work).

In this case study, the larger strains (Figure 8.6, left side picture), within the elastic zone, will result in larger retraction stresses. This retraction stresses might cause the fracture of the ice by peeling it off from the coating. This situation is inverse to the one observed by the authors that tested ice adhesion to metals (much stiffer materials); in those cases, the strain fields were larger within the volume of the ice, the least stiff material in an ice-metal junction (Figure 8.6, right side picture), and fracture was caused either adhesively (provided the H-bonds strength was lower than Ice Fracture Toughness), either cohesively (lower Fracture Toughness).

The fact that every fracture mode found was adhesive in every case tested in this work supports this assumption.

The effect of the temperature strengthening the H-bonds was discussed by other authors when testing metals, such as Titanium alloys (Pervier, 2012) or brass (Andrews & Lockington, 1983) in the range of Temperatures from -5 to -10^0C.

In the results obtained for the polymers, the Temperature was not found to have a remarkable effect in the Adhesion Level when the ice was attaching to much less stiff materials (E = 0.8 and E = 1.5 GPa). In these scenarios, the coating Stiffness has a large contribution in the reduction of the K_{IB_C} by peeling the ice off. This capacity to generate larger retraction forces hid completely any effect that the temperature might have in strengthening the H-bonds between ice and coating.

The temperature, on the other hand, did have an effect on the K_{IB_C} for the case of the PVC (E = 3 GPa). This material was the stiffest among the polymers and, therefore, it is expected that the strain fields generated were not as large as the ones generated in the other polymers. This material reduced the Adhesion Level considerably if compared with the Titanium (Figure 8.4), but the retraction forces generated due to the strain are not large enough to hide the effects of the temperature.

8.4. Effect of Coating Thickness on Ice Adhesion in Mode I

8.4.1. Experimental Results to coatings with different thickness

The procedure to study the effect of coating Thickness on the Adhesion Level is similar to the one employed in the study of the effect of Stiffness: An experimental routine in the Icing Tunnel with different specimens, numerical work in FEA adapting the designed model to the specimens tested, a Mathematical Methodology to obtain the Stress State from the numerical results and, ultimately, the combination of these results to obtain the Critical Stress Intensity factor and its evolution with the coating thickness.

The experimental work is carried out to a set of tests at one single temperature (-10^0C). The tested material is the polypropylene (E = 1.5 GPa) in different Thickness (different sheets and one tape employed).

A first set of tests carried out to PP02, PP05, PP10 and PP15 (Specimens description in Table 8.1). The results from this first set of tests showed that the σ_C had a peak at an intermediate thickness value. This situation was unpredicted and led the author to think that there were two competing factors in the adhesion strength of ice. Increasing the thickness will result in a decrement of the σ_C due to the capacity of a larger volume to store more energy and generate retraction forces to peel the ice off. On the other hand, the adhesion strength to thin coatings was affected by the underneath material, since the top coating was so thin that was not able to cope with the larger strain fields generated within. In this particular case the underneath material was glue (up to 100 times softer than the polymers), therefore, the σ_C was reduced. The glue layer was estimated to be 0.5 mm thick in average.

A second set of tests was carried out with the same coupons; but they were squeezed after being glued. The glue layer thickness was estimated to be reduced to 0.3 mm, in average. This set was carried out to observe if a reduction of the underneath soft volume will have an effect on the Adhesion Level.

Last, a third set of tests has been carried out to find a scenario where the underneath glue layer thickness is the low and there is no glue underneath. In order to achieve this, a Polypropylene tape is stuck to the substrate. The thickness of the PP tape was

estimated to be 50 µm, being the glue layer estimated to be around 10 µm (measured after removing the glue by rubbing the finger over it and measured with a calliper). In the same set of tests, the Ice Adhesion level was tested also over bare Aluminium substrate

Table 8.5 and Figure 8.7 show the σ_C results for every set of tests and the trend line of the critical pressure as a function of the top coating and underneath material thickness.. The graph also includes the σ_C registered for the uncoated Aluminium

		$t_{glue} \approx 0$ mm	$t_{glue} = 0.3$ mm	$t_{glue} = 0.5$ mm
Material Code	$t_{coating}$ (mm)	σ_c (MPa)	σ_c (MPa)	σ_c (MPa)
PP005	0.05	1.682	-	-
PP02	0.2	-	0.93	0.35
PP05	0.5	-	1.01	0.57
PP10	1.0	-	1.03	1.02
PP15	1.5	-	0.88	0.70
Al (bare metal)	-	1.718		

Table 8.5. σ_C results for different coating and glue (underneath material) Thickness

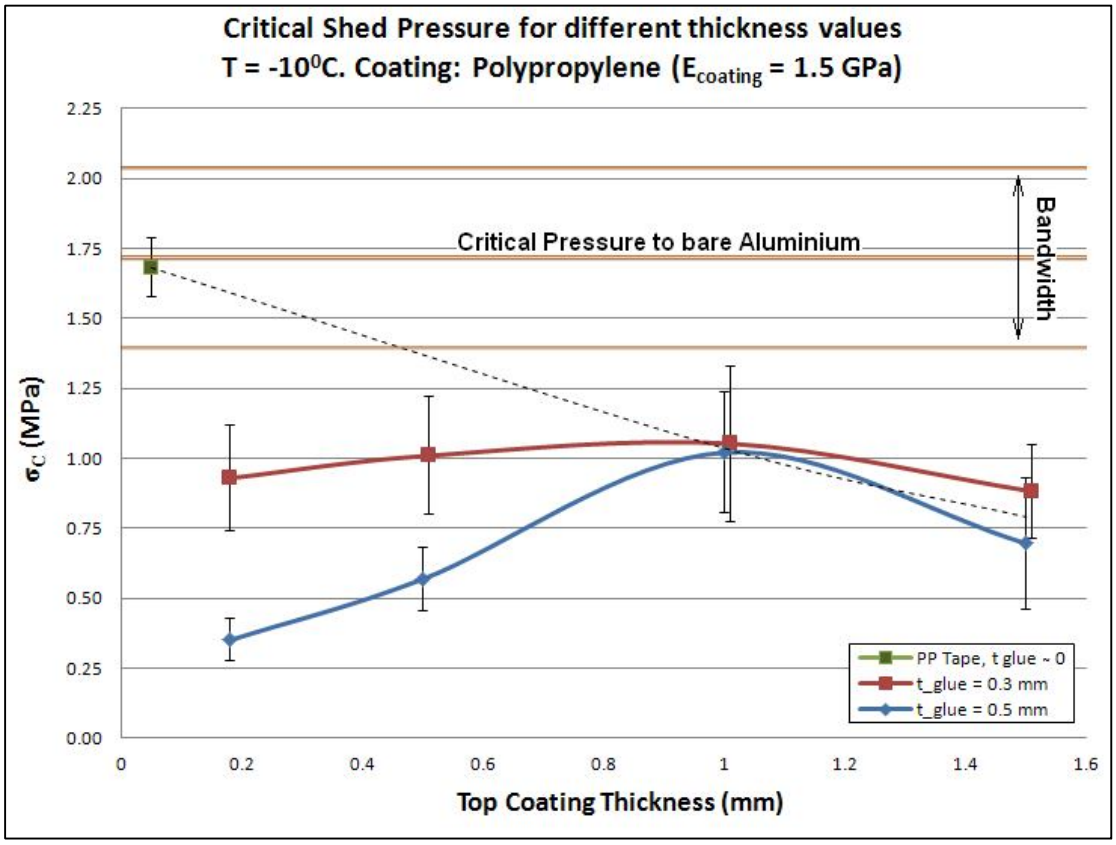

Fig 8.7. σ_C for different coating and glue thickness

8.4.2. Discussion of the Experimental results.

The results in Figure 8.7 support the idea that the underneath materials affect the adhesion level as long as the exposed material volume cannot cope with all the stress fields generated within. This happened when the top coating had a thickness of 0.2 and 0.5 mm, having a Stiffness of 1.5 GPa.

The decrement of the σ_C in the thicker coating case is due to the larger capacity of larger volumes to store energy. This storage capacity is deducted from the capacity of a volume to generate strain fields within. A simulation in FEA is carried out to show the capacity of a coating to have a displacement of his side in contact with the ice, depending in its thickness in Figure 8.8. Within the elastic zone, these larger displacements provide an extra aid for the ice to be peeled off.

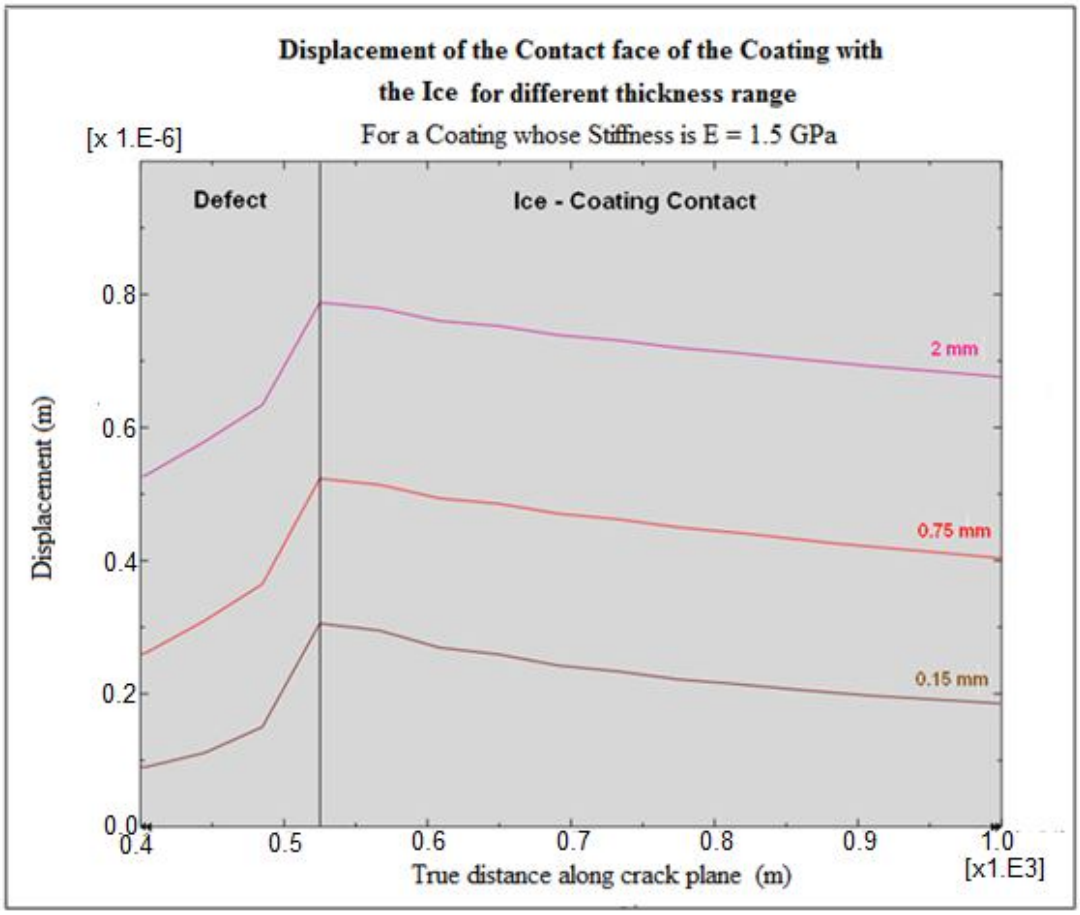

Fig 8.8. Displacement of the coating side exposed to ice accretion, for coatings with different Thickness

On the other hand, when the thinner materials were tested, the σ_C required decreased too. The reason might derive from the attachment method of the coatings to the substrate: glued. The glue underneath is much softer than the exposed and, in those cases where the volume of the coating is low, the Ice Adhesion Level is affected by the effect of the underneath material.

In the first set of tests (t_{glue} = 0.5 mm), the trend line of the σ_C had a peak when the coating thickness is 1.0 mm. For thicker coatings, as Andrews mentioned (Andrews, et al., 1984), σ_C is reduced since larger volumes have larger capacity to generate retraction forces. For thinner coatings, the underneath material affects the adhesion level.

In the second set (t_{glue} = 0.3 mm), the Critical Pressure – Thickness trend line shows a less sharp peak at the same point (t = 1.0 mm). For thicker coatings than 1.0 mm, the adhesion level is similar to the one observed in the first set. Therefore, the σ_C is independent from the underneath material properties for coatings that are thicker than 1 mm. In the thinner coating cases, the σ_C is larger than the one recorded in the first set since the underneath volume has been reduced, but it still has an effect on the σ_C. The reduction of the volume results in lower capability of generating strain fields within and, therefore, lower capability in generating retraction forces that aid the interfacial fracture of the ice.

A third set of tests ($t_{glue} \approx 0$ mm) recorded the σ_C to break the ice formed in very thin coatings (Polypropylene tape, approximately 50 μm thick) and uncoated Aluminium specimens. These tests are carried out in order to observe the influence of a very thin coatings on the ice adhesion, provided the underneath material is much harder (no soft material underneath). The results showed that the adhesion level is very similar for both uncoated and coated cases. The Polypropylene coating (tape) is the only different fixture between both situations, and, according to the results, its existence did not have a remarkable influence in the Critical Pressure recorded. It is reasonable to consider that a coating does not have any influence on the ice adhesion in tensile direction, no matter what the Stiffness or Surface properties are, as long as its volume is not large enough to generate retraction forces to peel the ice off.

The observation of the results, especially the ones in the third set, makes reasonable to consider that Thickness has an important effect on the Ice Adhesion Level.

It is possible to distinguish two cases when studying the effect of coating thickness on the ice adhesion, depending on whether there is an effect of the underneath material on the adhesion level or not: The Single-Layered Case and the Multi-Layered Case

- The Single-Layered case is the case where only the top coating has an effect on the Adhesion Level, hiding the effect that any other underneath material might have. Ultimately, the values obtained for K_{IB_C} will depend only on the material properties of the top coating. The K_{IB_C} calculations and conclusions developed in this work will be applicable for the Single-layered case
- The Multi-layered case is that one where the top coating is so thin that cannot cope with the strain fields generated within and the K_{IB_C} is affected by the effect of the underneath materials. This situation was observed in this work (Figure 8.7) for the cases where the thickness was 0.2 and 0.5 mm. The σ_C decreases because of the effect of the soft underneath material. The K_{IB_C} case in the Multi-layered cases will depend on the properties of the underneath material too. K_{IB_C} is not disclosed in this work for multi-layered cases, however, the effect of underneath material will be explained in epigraph 8.4.6

The dashed line in Figure 8.7 connects the data points belonging to the Single-layered cases. The cases where σ_C is not affected by the glue layer underneath are the specimen PP005, PP10 and PP15. These three σ_C values will be employed to calculate the K_{IB_C} following the explanation in Figure 8.3.

8.4.3. Stress State as a function of Thickness for the Single-Layered case

Observing the evolution of the σ_C, a number of Finite Elements simulations have been run in order to observe the evolution of the Stress Intensity Factor for coatings with different Thickness. The FEA work will be carried out for the Single-Layered cases, therefore, there will not be designed the glue layer that acts like an underneath material in the experiments.

A set of simulations has been run for two different Stiffness values in order to observe the evolution of K_{IB}/σ when the thickness of the Coating varies (Figure 8.9). A change in the trend line is observed in the Stress State evolution for the thinnest coatings

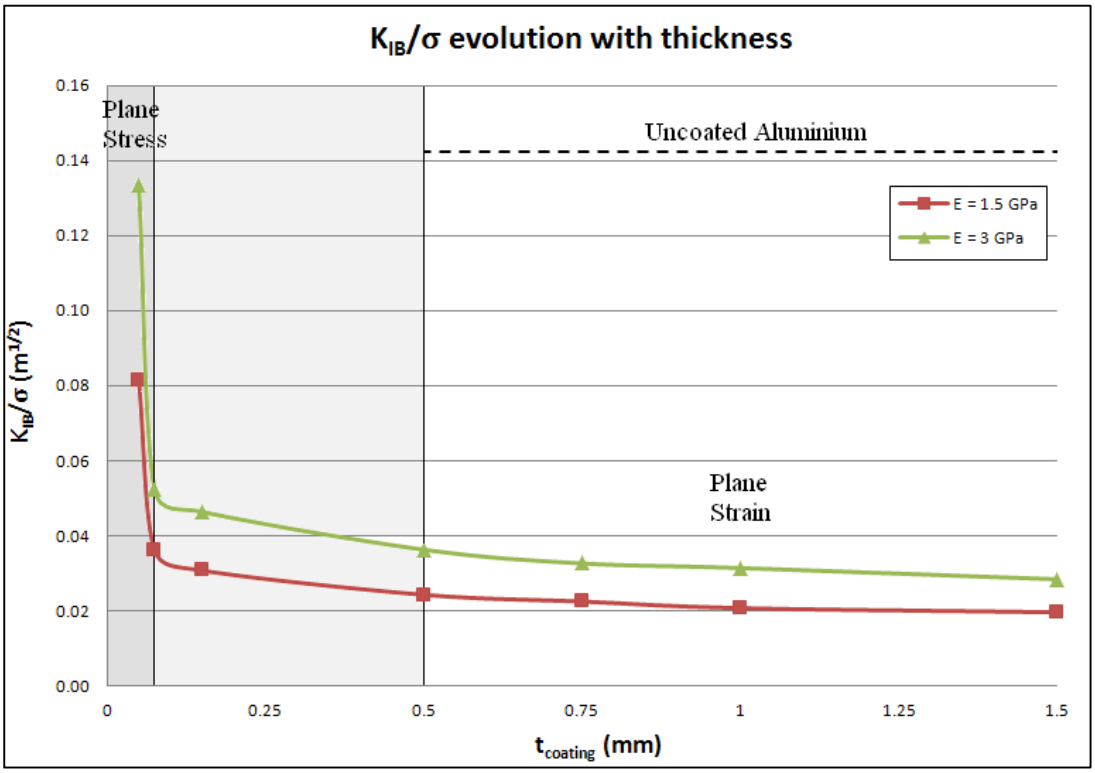

Fig 8.9. K_{IB}/σ trend line with Coating Thickness for different Coating Stiffness

The Plane Stress and Plane Strain dominated zones are distinguished in Figure 8.9. The literature describes “Plane-Stress conditions” when one of the dimensions of the loaded body is much lower than the other two (z <<< x, y), whereas the “Plane Strain conditions” happen when one of the dimensions is much larger than the other two (thickness “z” >>> in-plane dimensions “x”, “y”) so the z-dimension has no effect on the load distribution in that body.

The Stress Intensity Factor *K* for bulk bodies varies in Plane Stress Conditions and remains steady in Plane Strain Conditions. However, K_{IB}/σ has a gradual decrement gradient when the coating is in Plane Strain conditions.

The thickness has an effect on the Stress State in a bi-material junction, resulting in an abrupt change of the Stress State for the thinnest cases and a more gradual decrement for the thicker. This is observed in Figure 8.9 and sketched in Figure 8.10.

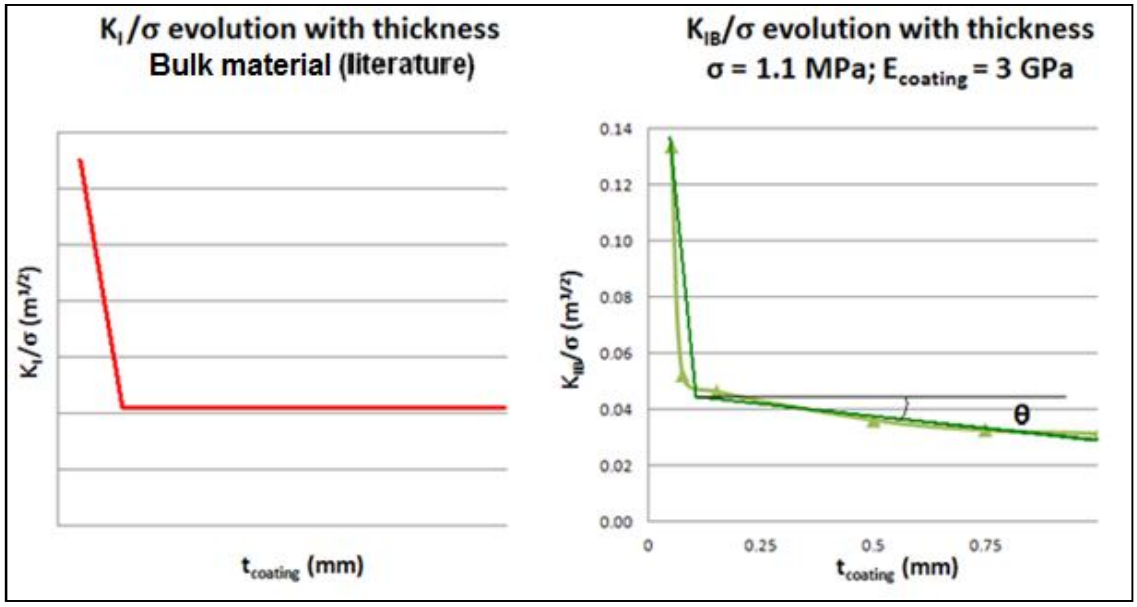

Fig 8.10. Comparison between K_I/σ described in the literature for bulk materials and K_{IB}/σ obtained in this study for bi-material junctions

Applied to the results obtained after the Mathematical Methodology of K_{IB}/σ in Figure 8.9, the coating can be assumed to work under plane strain conditions when its thickness is larger than 0.5 – 1 mm, for a defect radius of 3 mm,

8.4.4. Stress State as a function of Stiffness and Thickness

The results that correlate the Stress State with the thickness can be used to develop similar trend lines to the one showed in Figure 8.2

A set of numerical simulations is carried out to relate the Stress State K_{IB}/σ as a function of E for different thickness values. The results are plotted in Figure 8.11. The trend lines show the differentiation between Plane Stress and Plane Strain conditions: large variation with K_{IB}/σ in Plane Stress and small reduction of K_{IB}/σ when the coating thickness increases in Plane Strain conditions.

Those trend lines can be considered to follow a quadratic function where the quadratic constants C_1 and C_2 vary with the coating Thickness. Table 8.6 shows the C-Constants for the range of Thickness simulated and the Coefficient of Determination R^2. These constants are valid for the Single Layered cases.

It is aimed to calculate the C-Constants as a function of the thickness. K_{IB}/σ is observed to depend on the Coating Thickness both in Plane Stress and Plane Strain conditions for bi-material junctions, as observed in Figure 8.10. Therefore, Equation 8-1 will be re-written as a function of *t* and *E*

t (mm)	C_1	C_2	R^2
0,05	-0,0029	0,053	0,9915
0,15	-0,0011	0,0188	0,9828
0,5	-0,0008	0,0145	0,9709
1	-0,0006	0,0121	0,9971
1,5	-0,0004	0,0102	0,9992

Table 8.6. Quadratic Constants of the K_{IB}/σ (E) equation

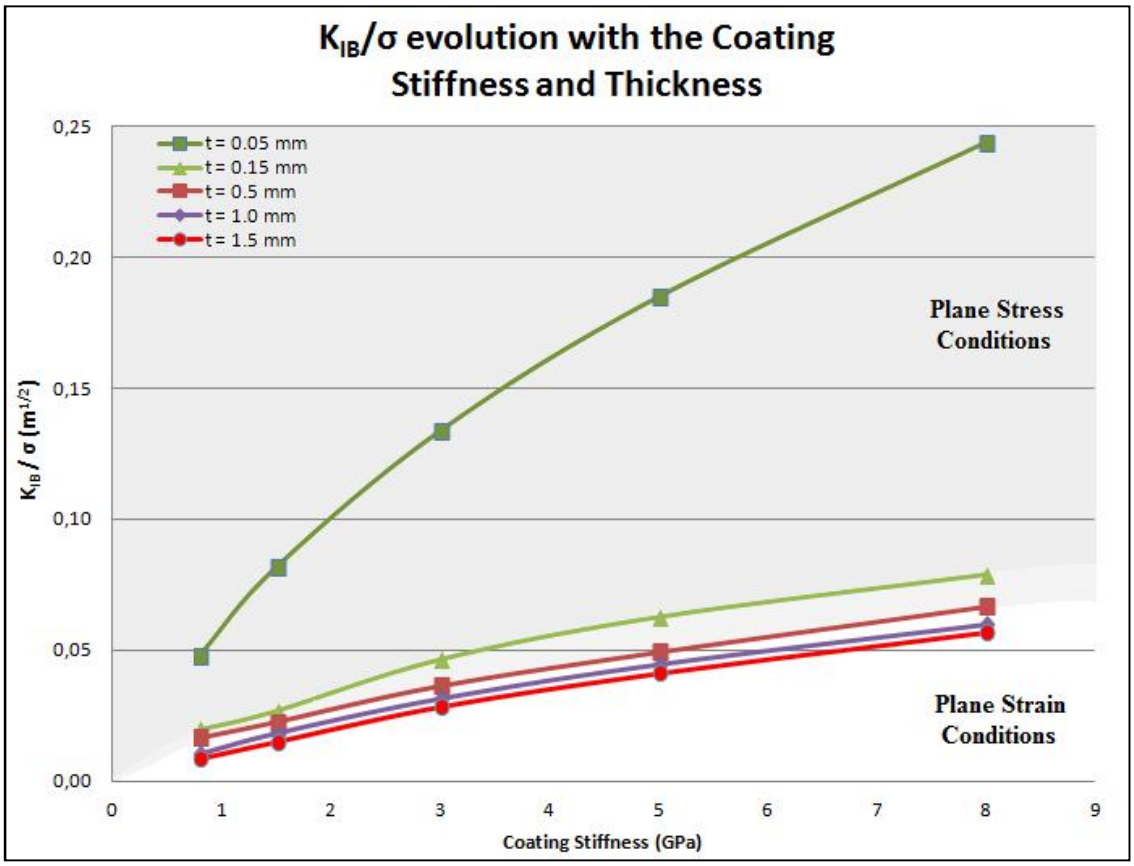

Fig 8.11. K_{IB}/σ evolution depending on the Stiffness and Thickness of the coating

The C-constant must be re-written as a function of Thickness. The relationship between C_1/t and C_2/t is:

t (mm)	C_1/t	C_2/t
0,05	0,0580	1,0600
0,15	0,0073	0,1253
0,5	0,0016	0,0290
0,75	0,0011	0,0183
1	0,0006	0,0121
1,5	0,0003	0,0068

Table 8.7. C_1/t and C_2/t relationships

These relationships have a power relationship as showed in Figure 8.12.

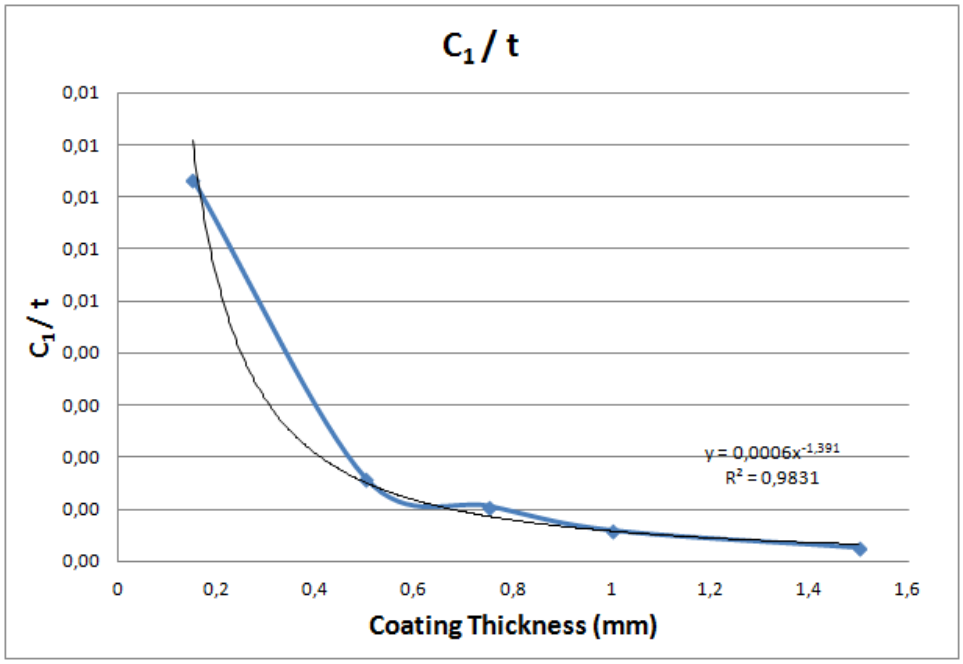

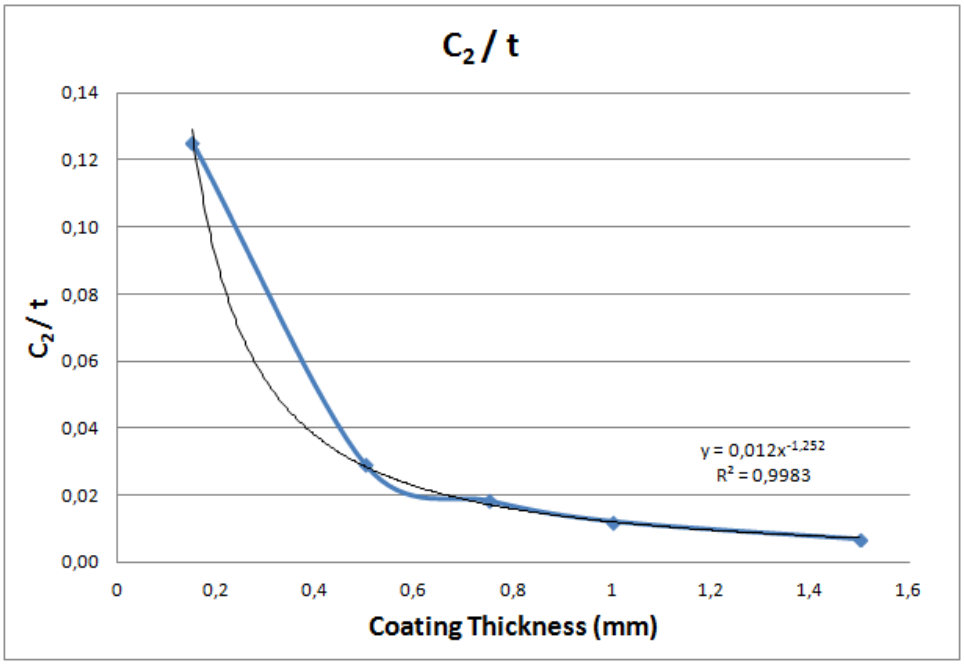

Fig 8.12. C_1/t and C_2/t graphs

The graphs follow the equations:

$$\frac{C_1}{t} = 0.0006 * t^{-1.391}$$

$$\frac{C_2}{t} = 0.012 * t^{-1.252}$$

So that, clearing C_1 and C_2 up:

$$C_1 = 0.0006 * t^{-0.391}$$

$$C_2 = 0.012 * t^{-0.252}$$

This relates C_1 and C_2 with the coating Thickness. These values are placed in equation 8-1 as:

$$\frac{K_{IB}}{\sigma} = -0.0006 * t^{-0.4} * E^2 + 0.012 * t^{-0.25} * E$$

Re-written in a general equation:

$$\frac{K_{IB}}{\sigma} = {K_1}^I * t^{-0.4} * E^2 + {K_2}^I * t^{-0.25} * E \qquad [8\text{-}3]$$

"t" and "E" represent, respectively, the Thickness (in mm for the Equation 8-3) and Stiffness (in GPa) of the coating. Figure 8.13 shows a comparison between the numerical results obtained in the Finite Elements package and the results obtained from Equaton 8-3.

This equation is valid for a bi-material junction loaded in tensile direction, where the ice attaches to coatings that are less stiff than it (E < 10 GPa) and whose thickness is larger than 0.5 mm (Plane Strain conditions). The equation is found to have lower exactitude for Coating Stiffness values lower than 0.8 GPa. However, the most of the materials appropriate to be employed as coatings are within the range of Stiffness where the Equation 8-3 matches (from 0.5 – 10 GPA). The Equation 8-3 has two K^I-constants (superscript "I" as they refer to Mode I case study), in this particular case "-0.0006" and "0.012".

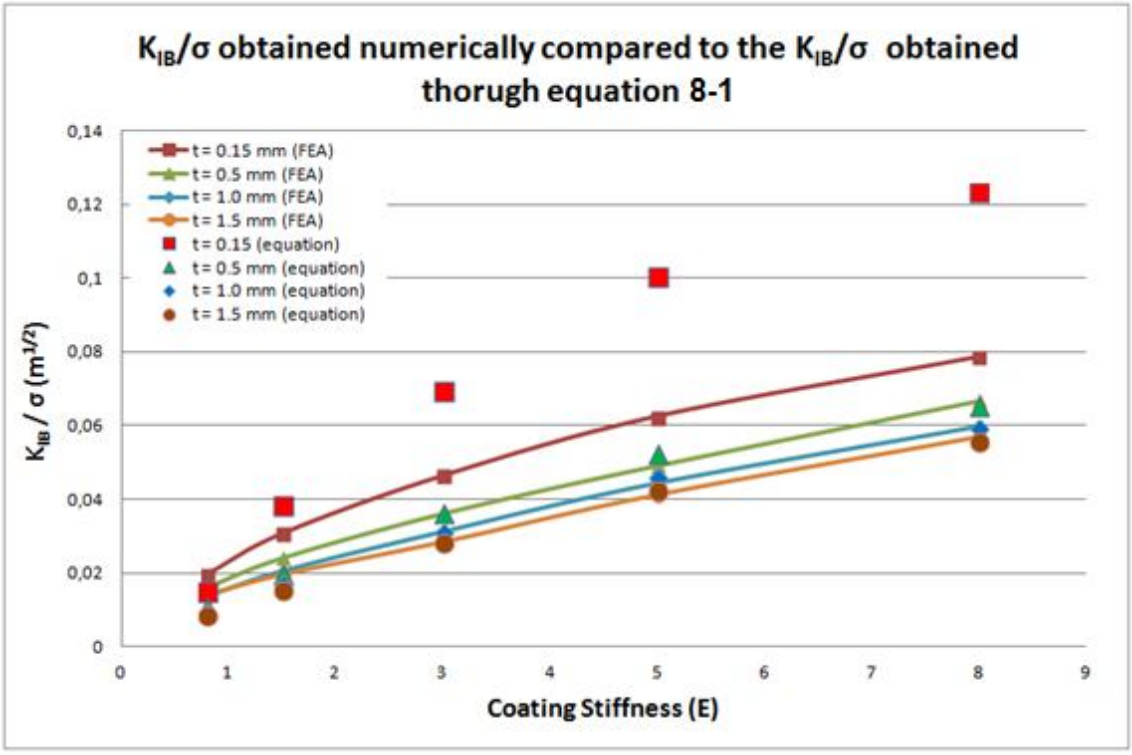

Fig 8.13. Results of K_{IB}/σ obtained numerically (line) compared to the ones obtained through the developed equation (dots)

8.4.5. Effect of Coating Thickness on K_{IB_C} for the Single-layered cases

The K_{IB_C} can be calculated as a function of coating Stiffness and Thickness at this point. The values for K_{IB_C} are calculated by inserting the experimental results of σ_C and the values of Stiffness and Thickness of every test scenario in Equation 8-3. The results are showed in Table 8.8. Equation 8-3 does not apply accurately enough to the scenario where t = 0.05 mm, so that, the K_{IB_C} value is calculated from the K_{IB}/σ value obtained from the FEA work..

Code	E (GPa)	t (mm)	σ_c (MPa)	K_1^I	K_2^I	K_{IB}/σ ($m^{1/2}$)	K_{IB_C} (Pa $m^{1/2}$)
PP005	1.5	0.05	1.875	-	-	0.0575	107850
PP10	1.5	1.0	1.02	$-6*10^{-4}$	0.012	0.0133	13500
PP15	1.5	1.5	0.79	$-6*10^{-4}$	0.012	0.0143	11300
Titanium (Pervier)	120	-	1.90	-	-	-	89509.94

Table 8.8. C-Constants and K_{IB_C} for the case studies

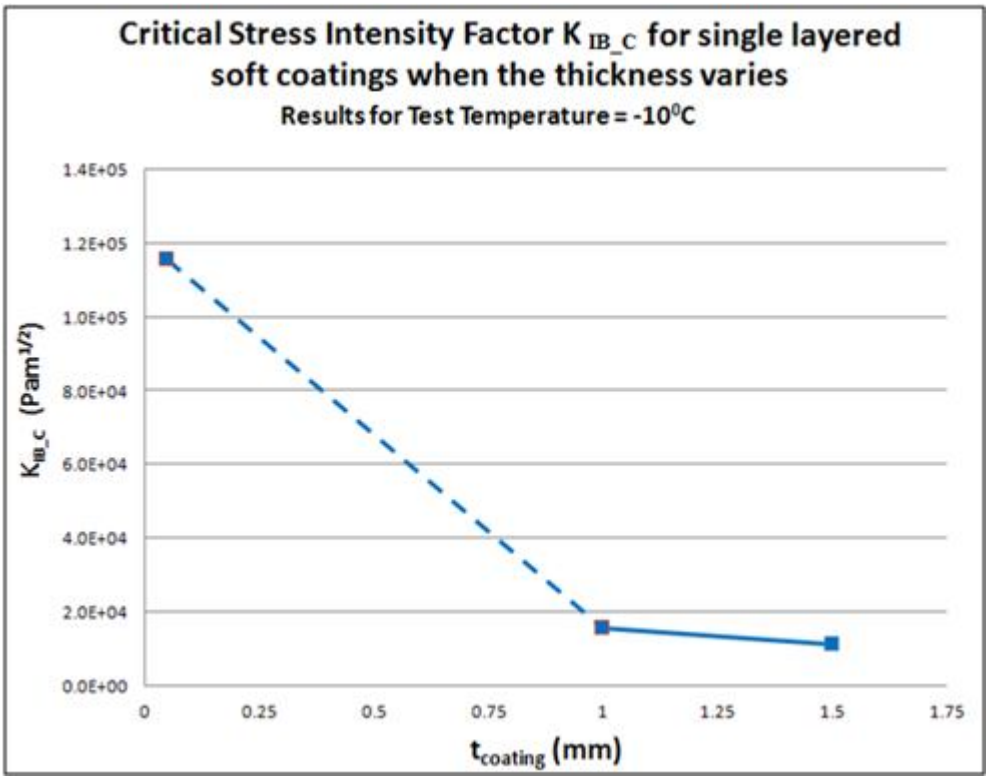

Fig 8.14. K_{IB_C} for single layered soft coatings for different thickness, for the case study of E = 1.5 GPa

Figure 8.14 shows the evolution of K_{IB_C} for different coating thickness in those Single-Layered experimental cases. K_{IB_C} is calculated from those cases where the underneath material was not considered to have an effect on the adhesion level.

It is observed that there is a large difference between K_{IB_C} obtained when the coating thickness is 0.05 mm and 1 mm. K_{IB_C} has a more gradual the coating thickness is larger than 1 mm. This influence in the Adhesion Level is related to the capacity of the larger volumes to generate larger strain fields, whereas the thinnest cases do not allow so large strains within, due to geometric restrictions.

The dashed trend line joining the data points from 0.05 mm to 1.0 mm coating thickness does not represent the K_{IB_C} trend line for the intermediate coating thickness values. Coatings thicker than 1 mm are disclosed to be enough to hide any underneath material effect and K_{IB_C} does not depend on the properties of any underneath material. However; the results from experimental tests carried out to thinner materials showed that the cases of coating thickness between 0.05 and 1 mm were not Single-Layered cases, the underneath material has an effect on the Adhesion Level.

Observing the results in Table 8.7, the K_{IB_C} obtained from the PP005 can be considered to be the same order as the K_{IB_C} obtained using Pervier equation for shear adhesion of ice to metals (Pervier, 2012). In this case, the thickness effect is minor, since the coating is unable to store large strain fields. Consequently, the strain fields generate within the volume of the ice (the “next” soft material). This shows that the thickness does have an influence on the Adhesions Level provided it is large to cope with the strain fields within.

8.5. Multi-layer case description

The Multi-layered is described as that case where the underneath materials have an effect on the load transfer between layers, that, ultimately can affect the Adhesion Level of ice. This situations led to carry out a study on the effect of the Stiffness of the underneath material on Ice Adhesion.

This "Multi-layered" case is not going to be fully disclosed in this work but discussed in this chapter to understand in which cases this double layer case applies in order to avoid comparing the results in the Multi-Layered case with the Single-Layered cases.

Four sets of FEA simulations were carried out in order to study how an underneath layer whose Stiffness varies along the tests, which is 0.5 mm thick, might have an effect in the Stress Intensity Factor in the ice-exposed coating junction. The series were:

1. Two series where the exposed coating was stiffer than the underneath one (E_{exp}= 5 GPa + E_{under} = 1.5 GPa and E_{exp} = 3 GPa + E_{under} = 1.5 GPa)
2. Two series where the underneath coating was stiffer than the exposed one (E_{exp}= 5 GPa + E_{under} = 8 GPa and E_{exp} = 3 GPa + E_{under} = 8 GPa)

The target is to find out which thickness must have the exposed coating so the stress state in the crack tip (in the interface) is not affected by the stiffness of the materials placed below. The results from the FEA simulations are showed in Figure 8.15.

The results show clearly that the softest exposed material (3 GPa) gives lower K_{IB}/σ results than the stiffer one (5 GPa), for thicker coating cases. Figure 8.15 also shows also that the underneath material does not affect K_B/σ when the exposed coating is thicker than a certain value, different for different Stiffness, named as "Effective Depth limit" in this work. "Effective Depth" is a theoretical concept used in this work to denote the distance from the ice-coating contact surface to the "Effective Depth limit". The materials within that Effective depth (and only those) have an effect on the Adhesion Level. It is graphically described in Figure 8.16.

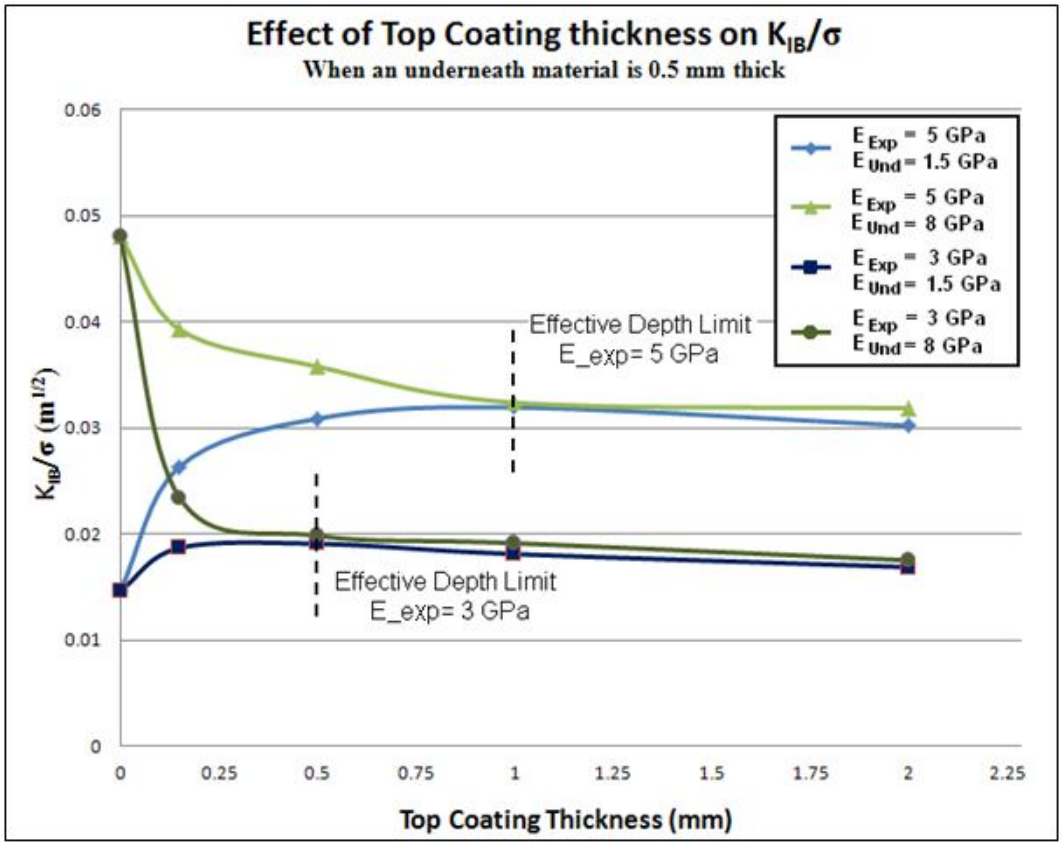

Fig 8.15. Effect of the coating thickness on the K_{IB}/σ obtained from FEA simulations

For coatings that are thicker than the Effective Depth limit (only one material within the Effective Depth), the K_{IB}/σ does not reflect any effect of the underneath material and both curves (exposed and underneath material) converge to a certain value as thickness increases. These are named "Single-Layered cases" (even though the substrate is composed by more than one material, only the exposed one has an effect on the adhesion)

In those cases where there is more than one material within the "Effective Depth Limit", every material (or portion of it) enclosed has an effect on the Adhesion Level, and this magnitude will be highly dependent on the volume of the softest material enclosed. The larger is the volume of the underneath material within the Effective Depth, the larger in going to be its effect on the stress state in the interface. According to Figure 8.16, in the Multi layered cases, the underneath materials increased the K_{IB}/σ if it is stiffer than the exposed material or decreased it if it was less stiff.

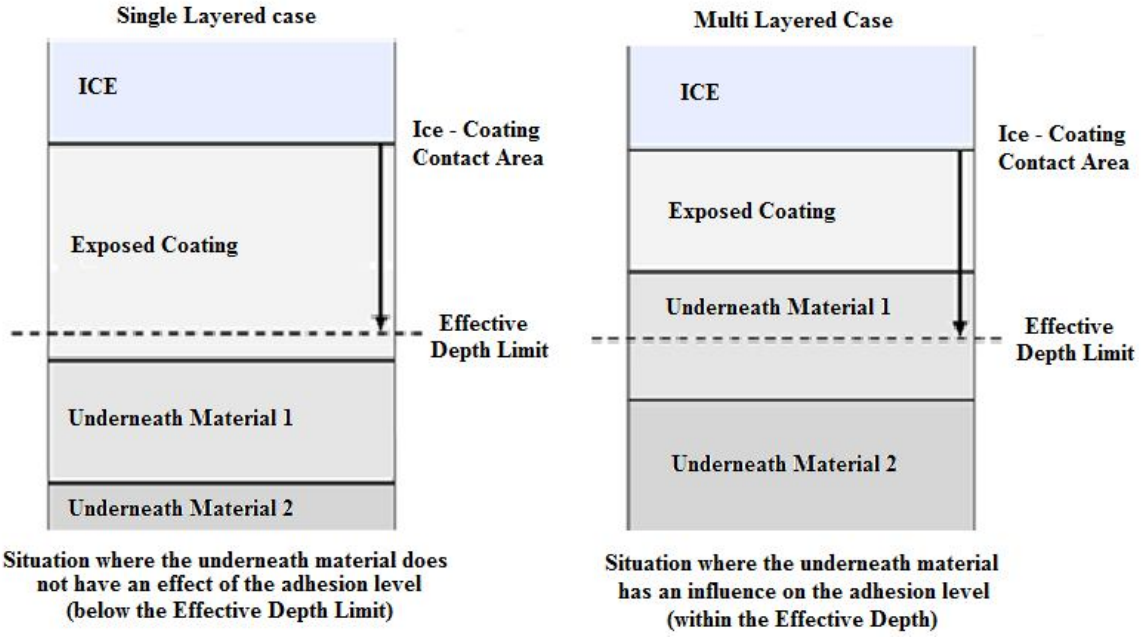

Fig 8.16. Situations where the underneath layer has no effect on the adhesion level, Single Layered cases (left) and Multi Layered cases where more than one material have an effect on the adhesion level (right).

In the experiment-tal graph of results, ice adhesion to the coupons labelled as PP02 and PP05 was lower when the underneath glue volume was larger. The adhesion was also found lower en the PP02 coupons, since there was more quantity of glue (very soft material) within the Effective Depth.

The double layer case might explain some of the results observed in Chapter 7, Figure 7.2 and 7.6, where it was observed mixed fracture mode. According to what has been observed in the experimental routines and FEA work, the fracture of ice when it attaches to less stiff materials, the least stiff material is the key in the fracture mode, as the strain fields generate within its volume. In these tables, ice attached to less stiff coatings was observed to shed in missed mode, this is, the strain fields also generated within the ice. The double layer case explains that situation: as the top coating layer was too thin (measured a thickness of 0.3-0.5 mm in the specimens whose results are showed in Figure 7.6), the volume cannot cope with large strain fields and, consequently, the new strain fields generate within the volume of the other material in the junction, causing the fracture to be likely to occur in cohesive way.

8.6. Conclusions of the Chapter (summary)

- The Ice Adhesion Level in Mode I, represented in this work through the K_{IB_C}, when testing impact ice to the polymers employed, is significantly lower than that one obtained by other authors who tested ice adhesion to metals. Softer materials allow larger strain fields for the same load. In the elastic domain, these larger strain fields result in larger retraction forces that aid to reduce the K_{IB_C} by peeling the ice off
- Because of this capacity to generate larger strains, the softest material is the one that leads the fracture type (adhesive or cohesive) and Adhesion Level in a bi-material junction
- K_{IB_C} depends on the Temperature only when ice attaches to materials stiffer than 3 GPa (PVC, 3 GPa), as it happened when ice attached to a metal. Nevertheless; it is independent on the Temperature when ice attaches to materials that are softer than 1.5 GPa. The influence of the retraction forces within the least Stiff materials on the Adhesion Level is so high that hides the effect that lower temperatures have strengthening the intermolecular bonds of ice to the coatings. On the other hand, the strain field generated within a 3 GPA stiff coating is larger than the one generated within the ice, but does not hide completely the effect of the temperature that strengthens the ice-to-coating bonds.
- By observing the results and comparing them with the ones obtained by other authors, it can be concluded that placing a soft coating over exposed surfaces reduces considerable the adhesion level. So that, it is found to be an interesting mitigation strategy. In the case studies, a 1.5 GPa Stiff, 1 mm Thick Coating can reduce the Adhesion Strength of Ice up to approximately 80%.
- The coating Thickness, in a Single-Layered case, has an effect on the adhesion level, K_{IB_C}. The change in the Adhesion Level is more abrupt in Plane Stress conditions, whereas the decrement is more gradual in Plane Strain conditions. The decrement on the Stress Intensity factor in Plane Strain conditions is not set forth in the Literature for fracture within bulk materials but observed by Andrews when testing ice adhesion to flexible substrates (Andrews, et al., 1984). This circumstance happens due to the storage capacity that the least stiff materials have, that aid the fracture by generating larger retraction forces.

- In the Single-Layered cases, the capacity of a coating to reduce the ice adhesion is lowered as the coating thickness approaches to zero. For a case tested, where the coating thickness was 0.05 mm, the K_{IB_C} obtained was observed to be the same order as the K_{IB_C} for an ice-metal junction. This situation occurs because the very thin materials cannot cope with large strain fields within, that would result in retraction forces to aid the ice shedding.
- The underneath material has an effect in the σ_C in the thinnest coatings (observed experimentally in Figure 8.6 and numerically in Figure 8.15). A concept is introduced in this study, the Effective Depth (Figure 8.16), This magnitude is the distance from the ice-exposed coating contact surface, for which every material within is having an effect on the ice adhesion
- The volume of the least stiff material within this Effective Depth is the one that has the most remarkable effect in the K_{IB}/σ as long as the load-strain state occurs in the Elastic zone. The softest material is capable to generate the larger strain fields that result in larger retraction forces as a reaction, aiding the stress state in the crack tip to be reduced.
- The Effective Depth depends on the exposed material stiffness and it is expected to be larger for stiff exposed coatings. As seen in Figure 8.15, in an exposed coating whose Stiffness is 3 GPa, the Effective Depth is found to be around 0.5 mm, whereas in the case of 5 GPa is found to be 1 mm approximately.

CHAPTER 9. EFFECT OF COATING STIFFNESS AND THICKNESS ON ICE ADHESION IN SHEAR DIRECTION

9.1. Motivation and Procedure

This chapter describes the effect of the coating Stiffness and Thickness on the Adhesion Level when the shear stresses in the interface dominate the fracture process. The metric chosen as representative of the Adhesion Level is the Critical Stress Intensity Factor, in shear direction, on a bi-material junction K_{IIB_C}.

The coating Stiffness and Thickness were observed to have an influence on the Critical Pressure, in shear direction, when the effect of the ambient conditions on the σ_C was studied in Chapter 7. Observing those results, in Figure 7.7, the Stiffness had an effect in the σ_C: the ice required lower pressure to shed when attached to coated specimens than the one required in the uncoated ones. The coatings were polyurethanes, whose Stiffness is around 0.7 GPa, and the uncoated specimen was a bare composite material whose upper-bound Stiffness was estimated to be around 275 GPa. In shear fracture tests, the load is applied in the direction of the fibbers of the composite; therefore, it is taken the upper-bound Stiffness from the Rule of Mixtures, unlike Mode I tests, where it was taken the lower-bound Stiffness. The complexity of the materials led the author to carry more tests over more simplistic materials as it was done for Mode I fracture tests.

This chapter will be carried out following the four steps procedure explained in Chapter 3 and employed in Chapter 8: Experimental routine to selected materials, Numerical work adapting those test fixtures in a FEA model, a Mathematical Methodology to obtain the Stress State in the vicinity of the crack tip and, finally, the calculation of the K_{IIB_C} combining these results

9.2. Experimental work to obtain σ_C in Mode II fracture tests

9.2.1. Effect of Stiffness in Mode II fracture tests

A set of tests is carried out in the Icing Tunnel Facilities; with the same materials tested in the tensile load study, modifying their geometry to fit them in the ISD employed in the Mode II tests: HDPE, 0.8 GPa; PP, 1.5 GPa; and PVC, 3 GPa. The materials are tested in the same conditions they were tested for Mode I fracture tests, in order to make them comparable: T = -10^{0}C, v = 50 m/s, LWC = 0.4 g/m^3 and MVD = 20 µm.

It is not placed any defect in the tests carried out for shear fracture (as it was for Mode I), however, it is supposed the existence of a crack in the ice-coating interface, at the point in contact with the plunger, whose size is the order of the grain size. Therefore, the fracture can be considered to occur in Mode II, starting from that assumed crack.

The experimental routine will register the Critical Pressure inside the piping system that caused the plunger of the ISD to move and break the ice. The σ_C values have been applied the correction factor α for shear tests (Chapter 4.3.2 and Equation 4-3):

The results for the σ_C for different materials are showed in Table 9.1 and Figure 9.1. The table and figure include the results obtained in Chapter 7 for the bare composite specimen and the results obtained by Pervier to rough and mirror polished Titanium specimens (Pervier, 2012). These added pressure values are acquired using the same facilities, ambient conditions controls and recording system. The results showed are the average of at least six data points

Material	Code	E (GPa)	σ_C (Mpa)	stdev
High Density Polyethilene	HDPE	0.8	0,509	0.021
Polyproplynene	PP150	1.5	0,550	0.069
Polyvynilchloride	PVC	3	0,587	0.088
Bare composite	-	275	1.114	
Titanium (Mirror Polished)	-	120	1.344	
Titanium (Ground)	-	120	1.874	

Table 9.1. Experimental Results for Critical Pressure for different materials

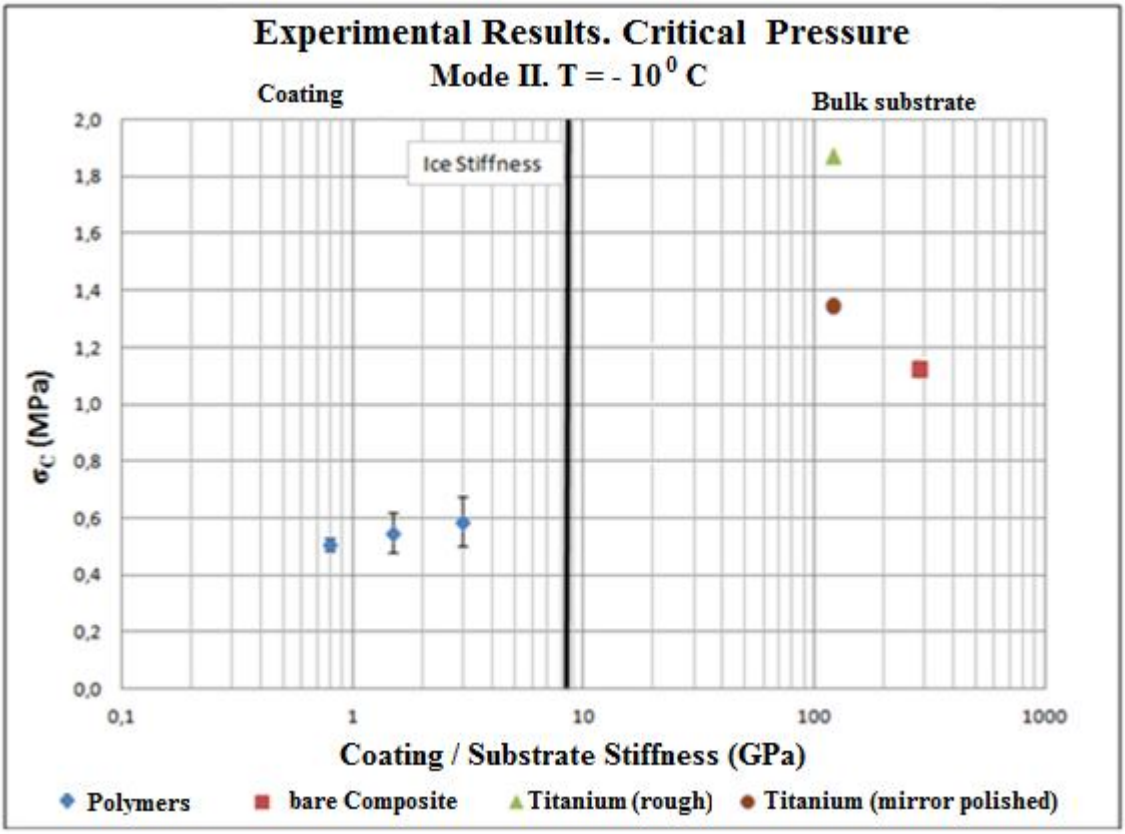

Fig 9.1. σ_C to break the ice in Mode II to different Materials

Unlike in Mode I study (Figure 8.5), the author considers more appropriate to use the σ_C values to make a comparison with the rather than the K_{IIB_C}. The results showed in Figure 9.1 by Pervier are obtained using the same facilities; however, the methodology to obtain the K_{IIB_C} employed by Pervier is different as it was ice attached to substrates that were stiffer than ice. The mathematical methodology developed in this work (Chapter 6) is based in the fact that the ice adheres to a less stiff substrate (polymeric coatings in this case). Making a comparing using the σ_C will reduce any possible divergence derived from the different Methodology.

Figure 9.1 shows a large difference between the Critical Pressure recorded to break the ice from the materials that are stiffer than ice and the Critical Pressure to break it from less stiff coatings. σ_C is lower than the required one in the stiffer materials cases. Among the polymers, there is a slight increment in the σ_C as the coating placed is stiffer, this is, PVC (3 GPa) results in larger σ_C, in average, than HDPE (0.8 GPa). However, this increment is gradual.

Surface Roughness is observed to have a strong influence in Mode II fracture tests, as studied by some authors (Laforte, et al., 2002). Pervier et al observed the effect of Roughness for the same test rig employed in this work, for metallic specimens (Pervier, et al., 2012). Roughness is not a material property but a condition and its level of influence not studied in this work, neither neglected tough. The influence of the Roughness is observed in the results from Mirror Polished and Realistic (rough) Titanium alloy samples (obtained by Pervier, in Figure 9.1). These results show a big difference in the σ_C provided the surface where the ice grows is rough or not.

The different nature of the metal and the composite is observed to have had an effect on the Adhesion level. The composite is stiffer than the metals in the direction of the fibbers but the ice formed over it requires lower amount of pressure to break. Metals are polar materials and the intermolecular bonds between ice and metal are much stronger than those between ice and a non-polar material (polymers, composite). Comparing the σ_C recorded in the fracture tests to polymers and composite, assuming that the polarity of the composite is the same order as the polarity of the polymers (ε_r of the epoxy is around 3), it is observed that the Stiffness does have an effect on the σ_C but the increment is gradual.

The roughness level of the three polymers tested was assumed to be of the same order as each other. This assumption was made after observing that all the specimens looked visually the same and felt smooth when rubbing the finger over them. It was also taken a special care when manipulating them in order not to modify their surface between tests. So that, the results obtained from these three samples reflect the influence of the Stiffness, without considering the effect of Roughness.

9.2.2. Effect of Thickness in Mode II Critical Pressure

The study of the effect of Thickness on Mode II fracture tests has been carried out using the same sheets employed when testing the effect of this parameter in Mode I: Polypropylene (E = 1.5 GPa) in four sheets whose thicknesses are: 0.18, 0.5, 1.0 and 1.5 mm. The σ_C represented is the pressure recorded after the correction factor α (Equation 4-3).

Material	Code	t (mm)	σ_C(Mpa)	stdev
Polyproplynene	PP018	0.2	0,508	0.0945
Polyproplynene	PP050	0.5	0,412	0.0738
Polyproplynene	PP100	1	0,507	0.0576
Polyproplynene	PP150	1.5	0,550	0.0689

Table 9.2. σ_C results for different Thickness values for Polypropylene

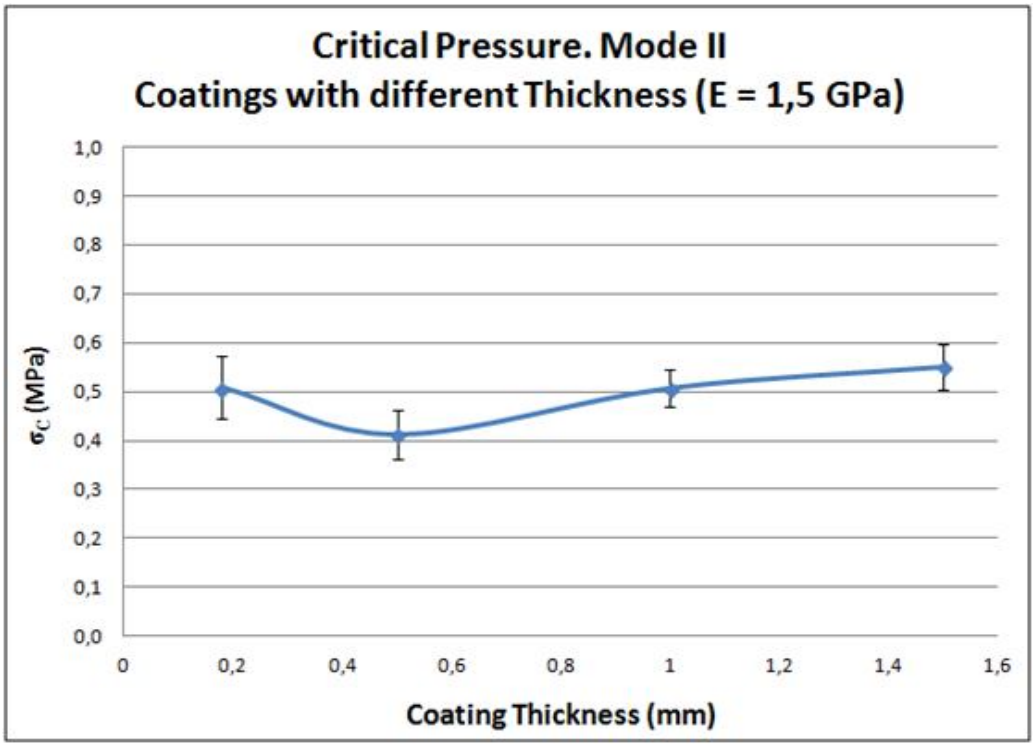

Fig 9.2. Effect of Thickness on the σ_C (same Stiffness)

It is observed that the σ_C trend did not vary considerably with the coating Thickness for the range of Thickness tested. The results do not show neither any effect of the underneath glue layer as it happened in Mode I tests in the specimens whose thickness was 0.2 and 0.5 mm.

9.3. Stress State calculation through Numerical Simulations, K_{IIB}/σ

9.3.1. Results from the Numerical Simulations, K_{IIB}/σ

A set of FEA simulations is run on the shear load model (described in Chapter 5) in order to obtain the Shear Stress field along the crack plane, for a range of coating Stiffness and Thickness scenarios. The Mathematical Methodology takes this Shear Stress field in the interface in order to obtain the Stress Intensity Factor in the vicinity of the crack tip, in shear direction, as a function of a Remote Load: K_{IIB}/σ.

The numerical results for the K_{IIB}/σ in all the cases of Stiffness and Thickness are showed in Table 9.3 and represented in Figure 9.3. The Stress State in an Ice-Aluminium junction, obtained with the same model, is also represented in the graph for comparison purposes.

K_{IIB}/σ is obtained for a given coating Stiffness, coating Thickness and geometry of the crack development area. The model designed in the FEA package does not reflect the Ambient Condition neither the Roughness, only the Mechanic Behaviour of Materials in a bi-material junction.

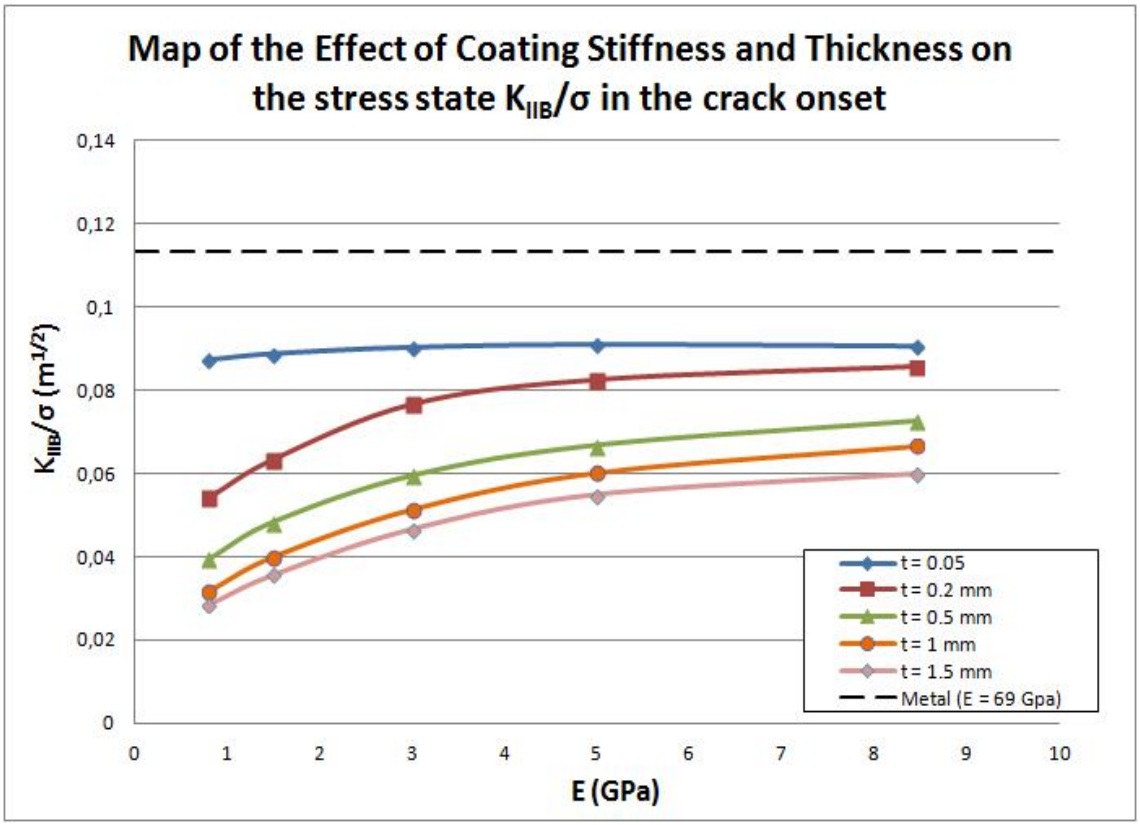

Fig 9.3. K_{IIB}/σ for the scenarios simulated in FEA

K_{IIB}/σ					
	t (mm)				
E (Gpa)	0.05	0.2	0.5	1	1.5
0.8	0.087	0.045	0.040	0.032	0.029
1.5	0.089	0.058	0.048	0.040	0.036
3	0.090	0.071	0.060	0.051	0.047
5	0.091	0.077	0.067	0.060	0.059
8.45	0.091	0.081	0.072	0.069	0.060

Table 9.3. K_{IIB}/σ in a range of Stiffness and Thickness Results

9.3.2. Observations on the Effect of Stiffness and Thickness on the K_{IIB}/σ

K_{IIB}/σ varies with Stiffness and Thickness according to Figure 9.3. It is found to be the largest for the stiffest coatings, in the cases when the coating was thicker than, approximately, 0.2 mm. For these cases, there is a substantial difference in the Stress State between the softest and the stiffest material.

The reason for this behaviour is the same reason stated for the tensile direction case study: less stiff materials and thicker coating (larger volume) allows larger strain fields within the material. Pure elastic behaviour is also assumed in shear direction as it was for tensile direction (isotropic materials used). The strain fields generated result in reaction forces, in the contrary direction, that aim to restore the original shape of the body. This scenario helps to peel the ice from the accretion surface in shear direction. A screenshot from the FEA software in Figure 9.4 shows that the Logarithmic Strain fields generate mostly within the volume of the least stiff material.

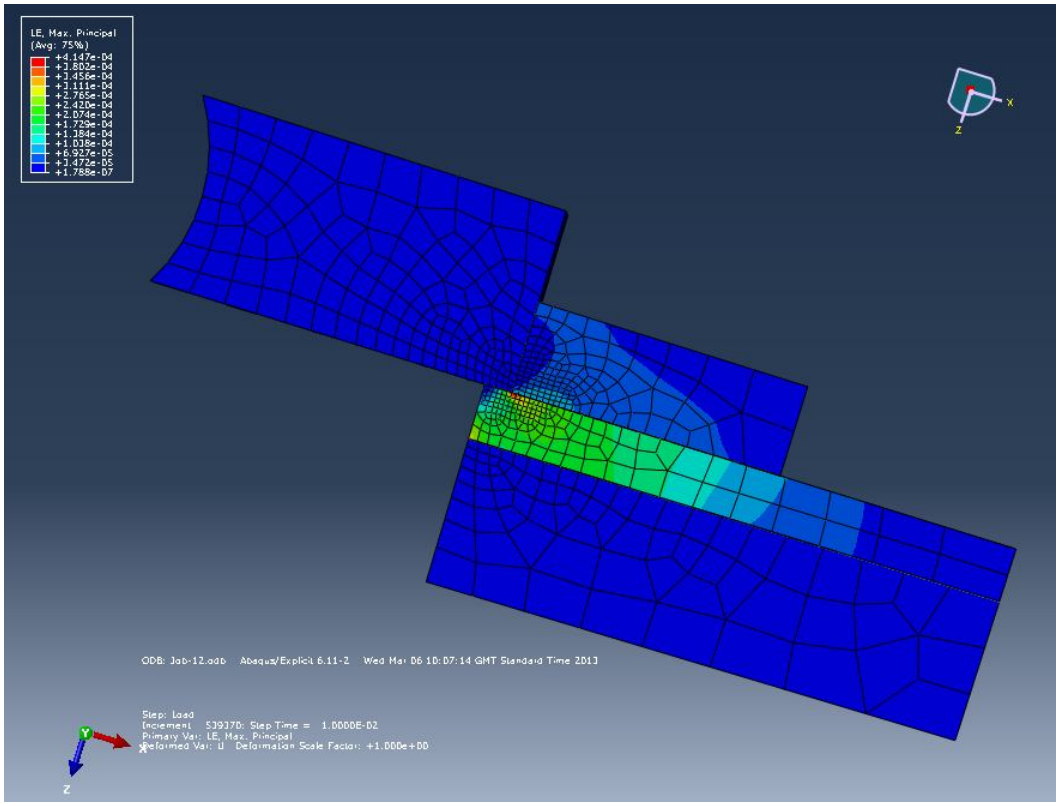

Fig 9.4. Strain distribution in the coating

On the other hand, the FEA simulations carried out for the thinnest case (t =0.05 mm) showed that the variation of the K_{IIB}/σ was not significantly affected by the Stiffness, resulting in a quasi horizontal line. However, the Stress State generated in the crack tip was lower than the one calculated for an ice-stiff material junction. Therefore, even a 0.05 mm thick coating can reduce the K_{IIB}/σ in the crack tip. As the coating material is less stiff than ice, the strain fields can still generated within the coating volume, even the small thickness.

This situation was not observed in tensile load cases (Figure 8.9), where very thin soft coatings resulted in having similar K_{IB}/σ than bare stiff materials. The reason might be that, in the cases where the fracture propagates in shear direction, there is more quantity of material in the direction of the Remote Load, and larger quantities of strain in the direction of the load can generate. This is sketched in Figure 9.5.

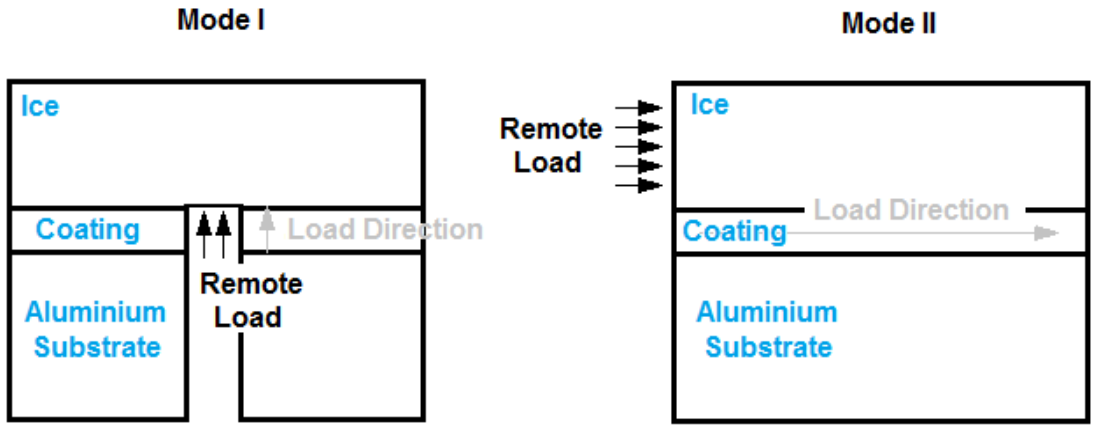

Fig 9.5. Sketch of the Load direction

More material in the Load direction might aid in the level of the retraction forces generated within and help the coating to peel the ice off. Consequently, the existence of a very thin layer in Mode II can reduce the stress state in the crack tip

This might explain the different observations in Figure 9.3 and Figure 8.9 respect the effect of a 0.05 mm coating on the Stress State. On the other hand, the Stiffness is not having a noticeable effect in the Stress State. This can be explained by the fact that the thin coating might be able to generate strain fields in shear direction to reduce the Stress State, however, this strain fields are low and might not reflect completely the influence of the less stiff materials on their scale.

It is observed in Figure 9.3 that the variation of K_{IIB}/σ with the Stiffness can be approximated to a mathematical function. A quadratic equation (Equation 9-1) has been considered accurate to fit the data, as it was chosen for tensile load case study, as a function of the coating Stiffness.

$$\frac{K_{IIB}}{\sigma} = C_1 * E^2 + C_2 E + C_3 \qquad [9\text{-}1]$$

C_1, C_2 and C_3 are quadratic constants that are affected by other variables, where Thickness is included. Unlike the tensile load case (Equation 8-1), $C_3 \neq 0$ in shear direction.

9.3.3. Methodology to obtain C_1, C_2 and C_3

A similar procedure to the one employed in the tensile load case (Chapter 8) is carried out to estimate the values of the C-Constants as a function of Thickness. Observing Figure 9.3, and considering that Equation 9-1 is a suitable choice to fit the data points obtained in the FEA, the C-constants in that equation, for the scenarios simulated, are showed in Table 9.4. The table includes the Coefficient of Determination R^2:

t (mm)	C_1	C_2	C_3	R^2
0,05	-0,0010	0,0016	0,0865	0,973
0,2	-0,0009	0,0119	0,0468	0,9842
0,5	-0,0007	0,0106	0,033	0,9901
1	-0,0007	0,0108	0,0244	0,996
1,5	-0,0007	0,0101	0,0215	0,9976

Table 9.4. C-Constants for Equation 9-1, affeected by Stiffness and Thickness

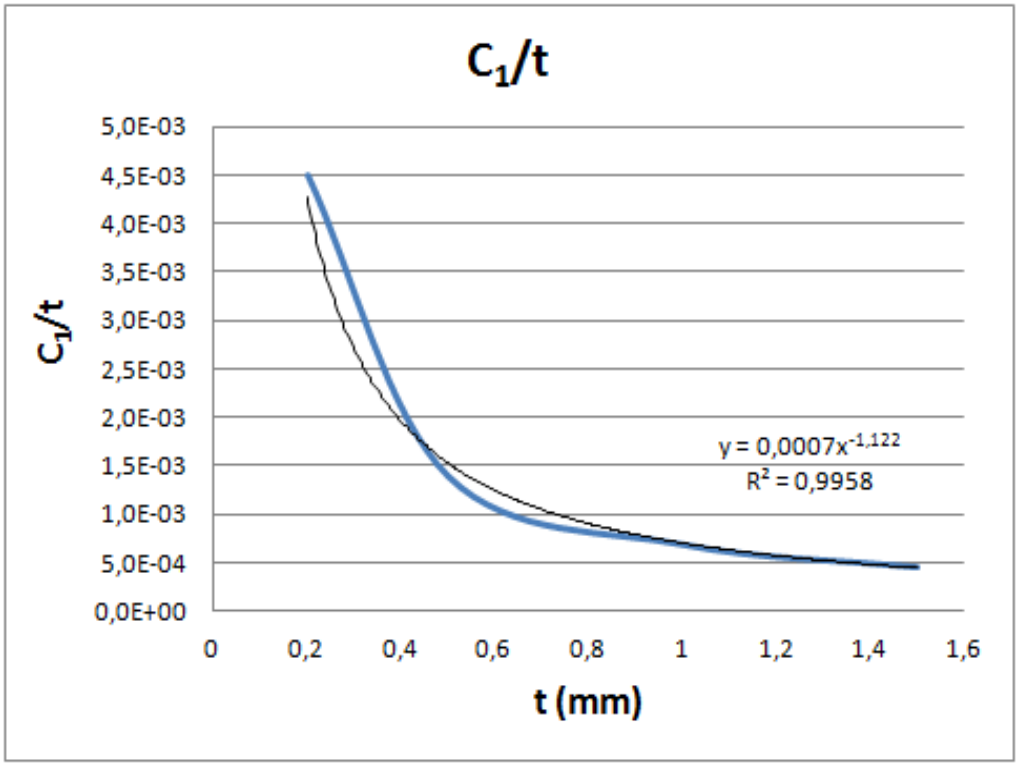

Fig 9.6. Estimation of C_1 as a function of Thickness

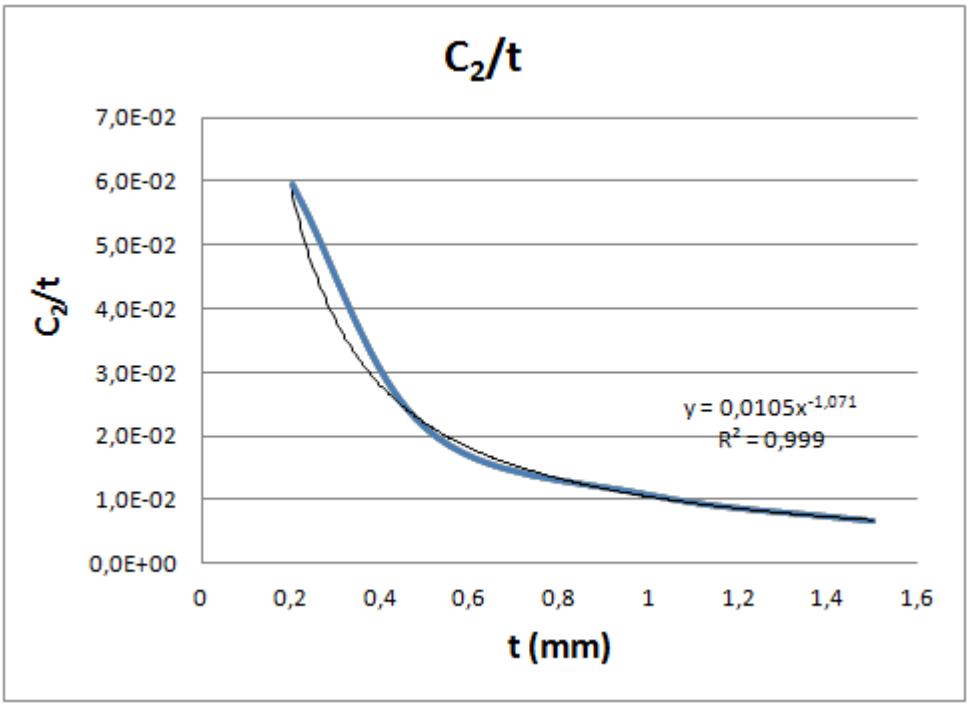

Fig 9.7. Estimation of C_2 as a function of Thickness

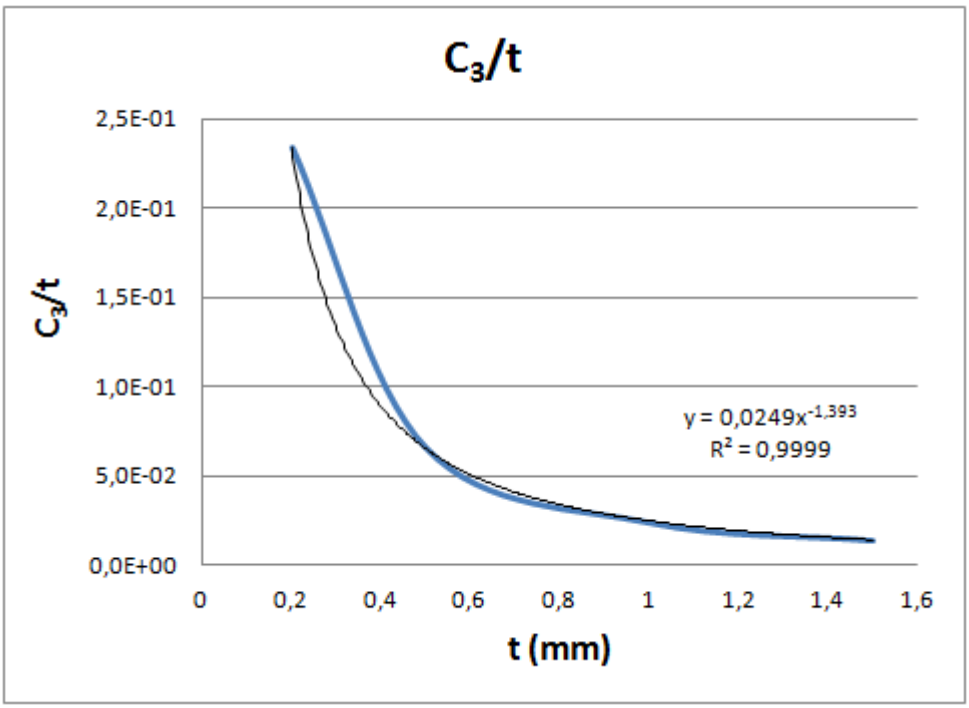

Fig 9.8. Estimation of C_3 as a function of Thickness

These graphs show that the relationship between the C-Constants and Thickness can be approximated to a power function:

$$\frac{C_1}{t} = 0.0007 * t^{-1.122}$$

$$\frac{C_2}{t} = 0.0105 * t^{-1.071}$$

$$\frac{C_3}{t} = 0.025 * t^{-1.393}$$

Solving the equations:

$$C_1 = 0.0007 * t^{-0.1}$$

$$C_2 = 0.0105 * t^{-0.071}$$

$$C_3 = 0.025 * t^{-0.4}$$

C_2 can be considered as independent from Thickness. C_1 and C_3 power factors over t can be round up to -0.1 and -0.4 respectively. Therefore, Equation 9-1 can be re-written as a function of coating Stiffness and Thickness as:

$$\frac{K_{IIB}}{\sigma} = -0.0007 * t^{-0.1} * E^2 + 0.0105 * E + 0.025 * t^{-0.4}$$

Assuming that the constants are related to other factors, the Equation 9-1 can be re-written as:

$$\frac{K_{IIB}}{\sigma} = K_1^{II} * t^{-0.1} * E^2 + K_2^{II} * E + K_3^{II} * t^{-0.4} \qquad [9\text{-}2]$$

Equation 9-2 describes mathematically the effect of Coating Stiffness (E) and Thickness (t) in the linear relationship between the Stress Intensity Factor and the Remote Load, in shear direction. The equation has three K^{II}-constants (superscript "II" since they refer to Mode II case) that can depend on other factors that were not studied in this Project, such as density, pressurization rate, etc.

Figure 9.9 shows the comparison between the results obtained numerically in FEA and the results obtained from Equation 9-2. The graph shows that the equation developed matches acceptably for any Stiffness value provided the material is less stiff than ice (E

< 10 GPa). The equation also matches with the trend line calculate for the Thickness described, except for the thinnest case (t = 0.05 mm).

The equation applies for any Stiffness between 0.8 and 8 GPa and any thickness value larger than 0.2 mm. Consequently, all the σ_C data points obtained experimentally (Table 9.1 and table 9.2) can be used in this equation to obtain the $K_{IIB\_C.}$

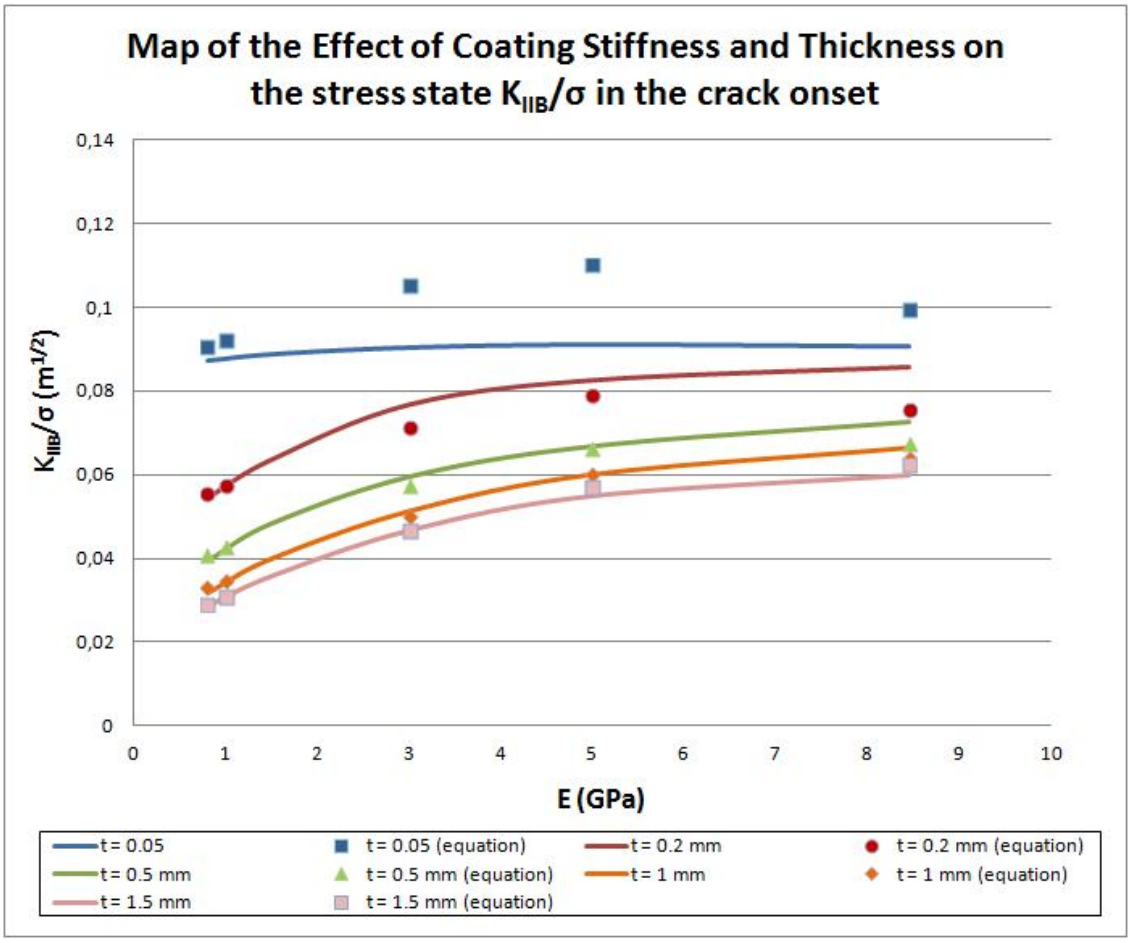

Fig 9.9. FEA and equation comparison results for K_{IIB}/σ

9.4. Ice Adhesion Level calculation, K_{IIB_C}

9.4.1. Results

As chosen for the Mode I scenario, the Fracture Criterion is the Critical Stress Intensity Factor in the interface between ice and coating, in shear direction, K_{IIB_C}. This K_{IIB_C} is obtained merging the σ_C obtained from the Icing Tunnel Facilities and the Stress State K_{IIB}/σ obtained in the Finite Elements package, through Equation 9-2, for a range of Stiffness and Thickness scenarios.

The σ_C is obtained for this chapter at T = -10^{0}C, v = 50 m/s and LWC = 0.4 g/m^3. The numerical value for K_{IIB_C} will change for other conditions. However, the trend line of the K_{IIB_C} with Stiffness and Thickness will be adequate to be extrapolated to other scenarios with different ambient conditions.

The results for K_{IIB_C} obtained are showed in Table 9.4 and Table 9.5. Figure 9.10 and Figure 9.11 show the effect of Stiffness and Thickness on K_{IIB_C}.

Code	E (GPa)	t (mm)	σ_C (Mpa)	K_{IIB}/σ (m$^{1/2}$)	K_{IIB_C} (Pam$^{1/2}$)
HDPE	0.8	1,5	0,509	0,0292	22300,11
PP150	1.5	1,5	0,55	0,0355	29283,09
PVC	3	1,5	0,587	0,0467	41149,23
Titanium (*)	120	-	1.2-1.8	-	≈250000

Table 9.4. K_{IIB_C} for different Stiffness scenarios.

Code	t (mm)	E (GPa)	σ_C (Mpa)	K_{IIB}/σ (m$^{1/2}$)	K_{IIB_C} (Pam$^{1/2}$)
PP018	0.2	1,5	0,508	0,0615	46917,88
PP050	0.5	1,5	0,412	0,0470	29076,69
PP100	1	1,5	0,507	0,0392	29773,00
PP150	1.5	1,5	0,55	0,0355	29283,09

Table 9.5. K_{IIB_C} for different Thickness scenarios.

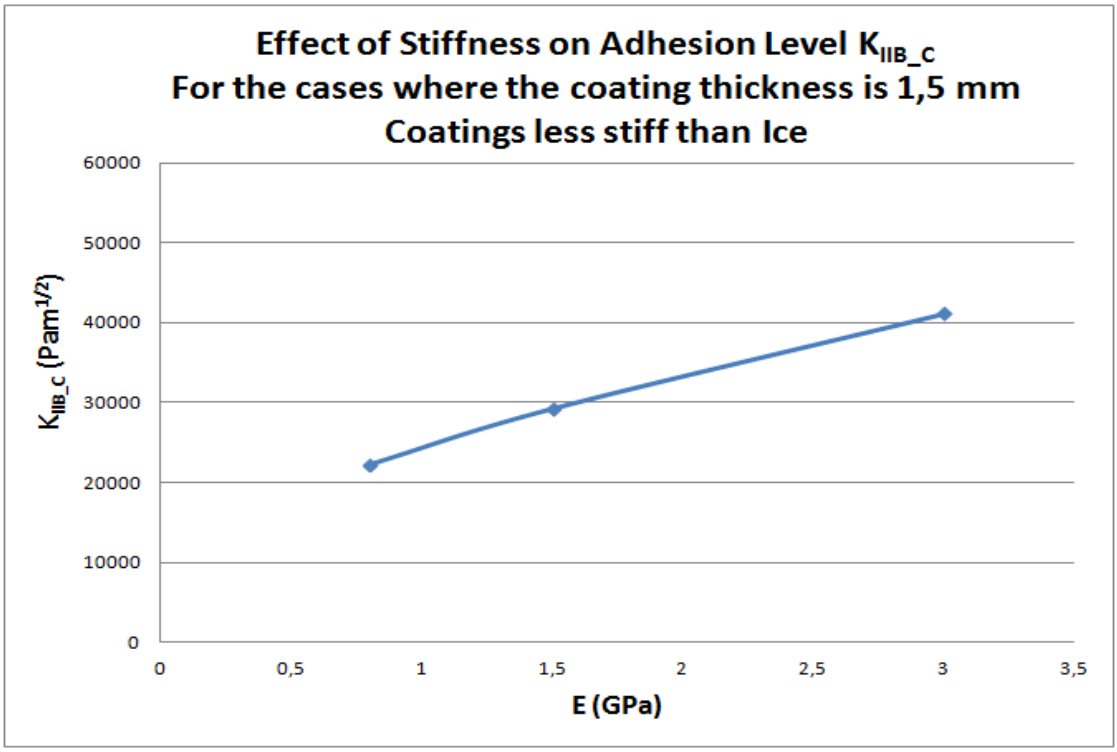

Fig 9.10. Effect of Adhesion Level with Coating Stiffness

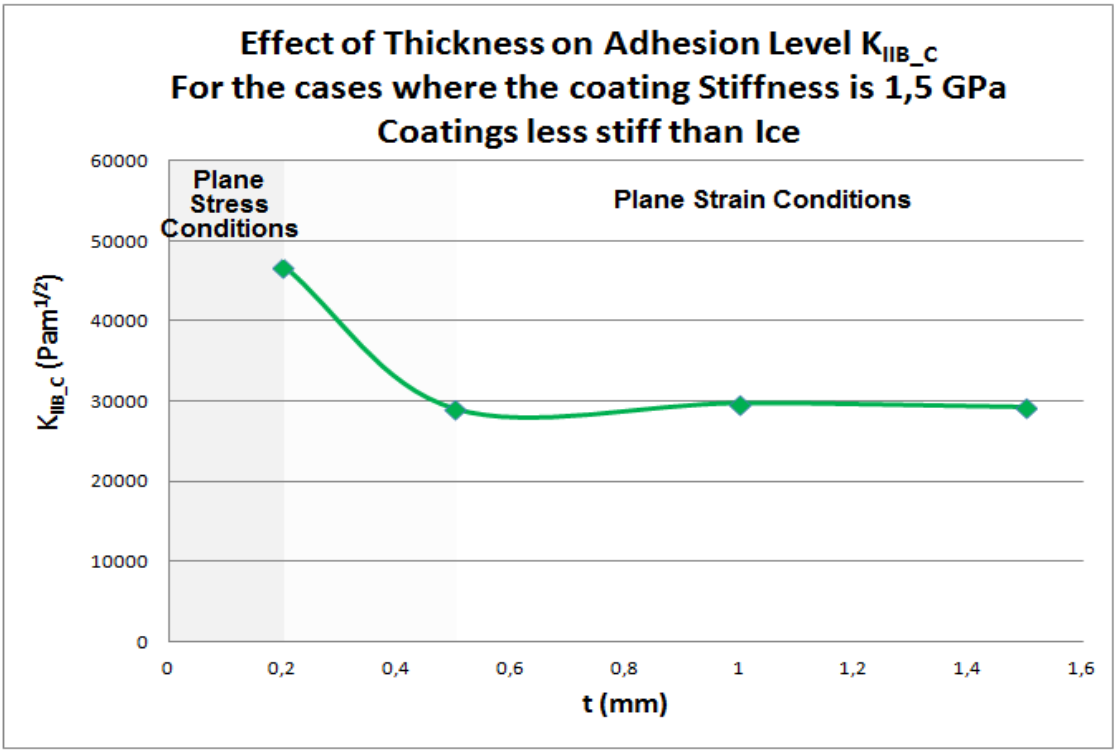

..

Fig 9.11. Effect of Coating Thickness on Ice Adhesion

9.4.2. Discussion on the Effect of Stiffness and Thickness on Ice Adhesion Level

The results in Figure 9.10 show that the Adhesion Level of ice can be lowered by reducing the Stiffness of the coating. The results of K_{IB_C}, taken from experimental values when the coating was 1.5 mm, show a gradual increment. For instance, the K_{IIB_C} doubles its value when the coating stiffness is increased from 0.8 to 3 GPa (Table 9.4), whereas the increment of K_{IB_C}, under the same conditions, for the same Stiffness increment, was 7 times larger (Table 8.3). Consequently, the influence of the coating Stiffness in reducing the ice Adhesion Level is larger in tensile adhesion.

In the study of the effect of coating Thickness, it is noticeable that the trend line of the σ_C recorded from the Tunnel and the trend line of the Adhesion Level calculations do not follow a similar pattern, as it happened in the tensile load case study (Figure 9 2 and Figure 9.11). This dissimilarity is observed when the coating is thinner than 0.5 mm. For thinner coatings than that value, the coating thickness is considered to affect the value for the K_{IIB_C} and, therefore, the range 0.2-0.5 mm thick indicates the borderline between Plane Stress and Plane Strain conditions in the coating.

In Plane Strain Conditions, the load is distributed along the three dimensions of the volume. The shear retraction forces generated in the coating volume distribute along the crack plane without a geometric restriction. The load distribution is not affected by the volume and, then, the shear Adhesion level does not vary with the Thickness.

In Plane Stress conditions, the retraction forces are restricted to two dimensions (low Thickness). As the Thickness decreases, the strain fields are restricted to a lower volume, the aid provided by the coating to peel the ice off decreases. Consequently, it is required larger Stress State to separate the ice from the coating in shear direction.

9.5. Conclusions (Summary)

9.5.1. On the Effect of Coating Stiffness on Ice Adhesion

- Putting a polymeric coating over a metallic substrate reduces the Adhesion Level of ice in Mode II. However, its influence is not as noticeable as it was in Mode I. The evolution of the K_{IIB_C} as the coating Stiffness increases is more gradual in shear direction. This consideration has been taken after observing the influence of the Stiffness on the K_{IIB_C} only in the cases of the three materials purchased, where the roughness of these materials was considered to be similar and other properties such as the polarity or the conductivity were discussed not to have a differentiating effect in these materials
- As it happened in Mode I, the retraction forces generated within the volume of the least stiff material of the junction (the coating in this case) are the key factor in the value of the K_{IIB_C}, as they cause an aid for the ice to be peel off. These retraction forces derive from the storage capacity of a body and are larger within the least stiff bodies

9.5.2. On the Effect of Coating Thickness on Ice Adhesion

- Coating Thickness does not have an effect on the K_{IIB_C} in the cases where it is thicker than the range 0.5 mm, this is, when the coating is loaded under Plane Strain conditions. In Plane Strain conditions, the retraction forces are not restricted due to the geometry of the volume and are constant for the same Stiffness
- On the other hand, the K_{IIB_C} increases when the coating is thinner than 0.2-0.5 mm. The coating is loaded in Plane Stress conditions in that case. In this scenario, one of the dimensions is very small compared to the other ones and the shear stresses are restricted to that one. When the load is restricted to transfer in one of the dimension, a Remote Load causes larger Stress State K_{IIB}/σ in the other two dimensions, resulting in larger Adhesion Level.
- The σ_C recorded in the test rig was the same range for every coating tested. According to the previous conclusion, the thinnest cases result in the largest K_{IIB}/σ. The same amount of Remote load σ will result consequently in larger K_{IIB_C} required to break the bonds between the ice and the coating.

- Despite the fact that reducing the coating Thickness results in an increment of the K_{IIB_C}, there is a noticeable difference between the K_{IIB}/σ in the case where there is a coating and an uncoated case. The K_{IIB}/σ obtained in FEA simulations of an ice-polymer junction, for a coating that was 0.05 mm thick, was lower than the K_{IIB}/σ obtained for an uncoated scenario. This situation was not observed in the tensile load case study, in that case, a coating whose thickness was 0.05 mm has and K_{IB_C} similar to the one resulting from an ice-metal junction. The reason was discussed to be due to the fact that there is more material in the same direction of the Remote Load. Therefore, the capacity to generate retraction forces, as a response for that Remote Load and in contrary direction, is larger. This situation was sketched in Figure 9.5

CHAPTER 10. CONCLUSION AND SUGGESTIONS

10.1. Comparison between Adhesion Level in tensile and shear direction

The Adhesion Level in Tensile and Shear direction has been studied in Chapter 8 and Chapter 9 respectively. The results are put together in order to establish whether there is a relationship between the Adhesion Level in both directions.

A comparison of the effect of Stiffness in the tensile and shear adhesion level is showed in Figure 10.1, for a Temperature of -10^0C. The comparison is made in two cases where the coating thickness was 1.5 mm. According to Figure 9.11, that value ensures Plain Strain conditions in the coating.

It is observed that shear and tensile Adhesion Level trend lines can be considered to be parallel.

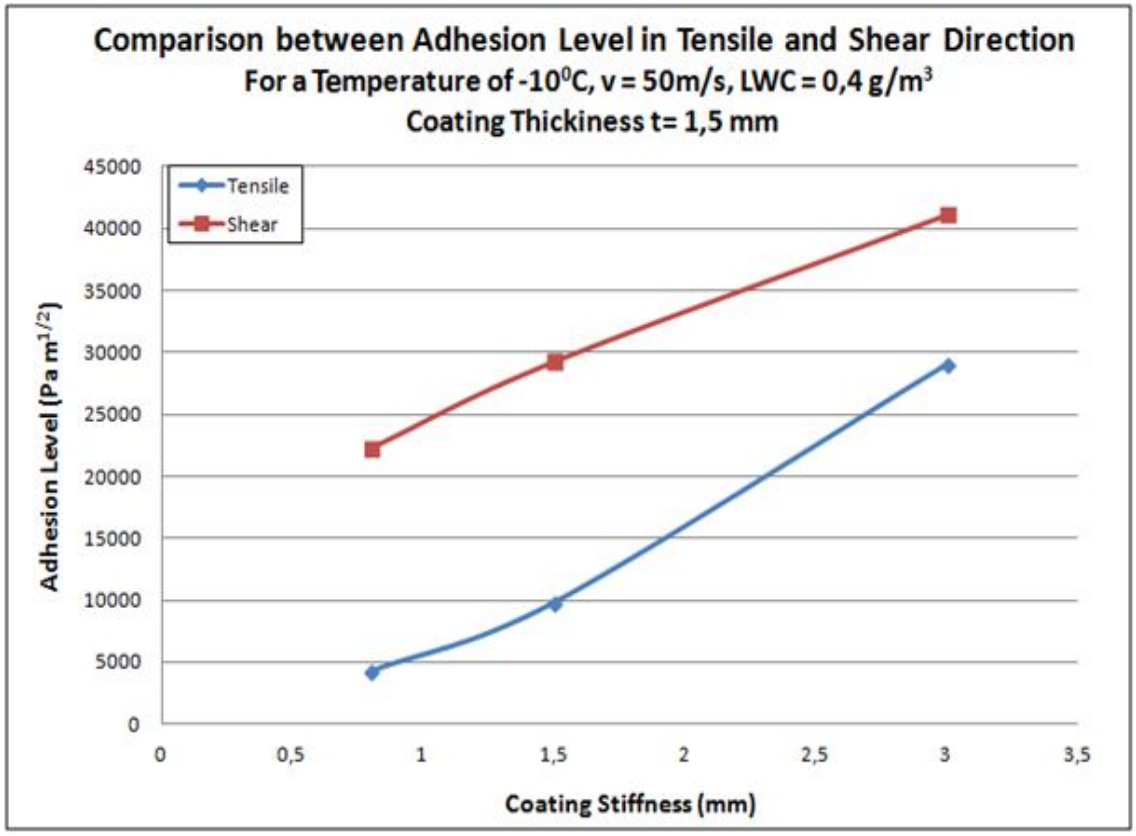

Fig 10.1. Comparison between tensile and shear Adhesion Level

According to the conclusions extracted in Chapters 8 and 9, the least stiff material in a junction is the one that has the largest influence in the Adhesion Level for both Mode I and Mode II fracture tests because it has a larger capacity to generate largest strain fields within its volume. Softer materials results in lower Adhesion Level.

Figure 10.1 shows that the Adhesion Level in shear direction is found to be larger than the Adhesion Level in tensile direction for the range of Stiffness between 0.8 and 3 GPa.

The Adhesion Level of a bi-material junction is related to the capacity of the least stiff material to generate strain fields within, provided the stress-strain behaviour is Linear Elastic. Bearing this in mind, provided that the body is isotropic and provided that it is loaded under Plane Strain conditions, the retraction forces due to an external load should be the same, regardless the direction.

That situation is not reflected in Figure 10.1, what is more, shows the contrary behaviour than the one observed by Jellinek (Jellinek, 1959). Jellinek observed that the Adhesion Level in tensile direction was larger than the one in shear and, according to these results; he developed the theory of a liquid-like layer between the ice and the substrate.

These disconformities in the results are justified due to the fact that Jellinek made his study on ice adhesion to metals, whereas this work has been done to ice adhesion to polymers. Jellinek´s work had the ice as the least stiff material in a bi-material junction, whereas this work has the polymeric coating as the least stiff material. So, it is having the largest influence on the Adhesion Level.

The liquid-like layer explained by Jellinek (Jellinek, 1959) has a considerable influence reducing the Adhesion Level in shear direction when ice attaches to metals. The properties of metals, such as Stiffness, polarity or thermal conductivity favour a high Adhesion Level of the ice. The existence of this liquid-like layer aids the block of ice to slide over the metallic surface, overcoming the strength of the intermolecular bonds between the ice and the metal.

In the case of ice attaching to polymers, the intermolecular bonds are not that strong, because polymers are not as much polar as metals. A liquid-like layer generated in between the ice and the coating will not have such a determining effect.

The difference between the Adhesion Level in tensile and shear direction might be due to the effect of the surface Roughness. The Roughness effect is carried with the σ_C values obtained experimentally. This effect is larger in shear direction than in tensile and that difference can be the perpendicular distance between the quasi parallel lines in Figure 10.1.

This hypothesis is applicable as long as the coating is loaded under Plane Strain conditions; for this particular case, when it is thicker than 0.5 mm. For thinner cases, the Adhesion Level depends on the thickness of the coating.

The effect of Thickness on Adhesion Level in both Mode I and Mode II is showed in Figure 10.2.

The graph in Figure 10.2 is plotted with the same numerical data points that create the graphs showed in Figure 8.14 and 9.11, however, the graph showed in Figure 10.2 has some variations:

The dashed line in Figure 9.11 denoted that the trend line did not have to follow necessarily that tendency, but the experimental results recorded for the points within that dashed line (results for 0.2 and 0.5 mm) were affected by the underneath material (glue, much least stiff material that any other in the junction) on the σ_C, this was a Multi-Layered case and the results obtained are not applicable to calculate K_{IB_C}.

On the other hand, the numerical results in Figure 8.9 showed that a coating thicker than 0.5 mm can be assumed to be work under Plane Strain conditions; so, K_{IB_C} is assumed to vary gradually with the Thickness.

Bearing in mind these considerations, the Figure 10.2 is with a dashed line with the assumed evolution of K_{IB_C} with the coating Thickness:

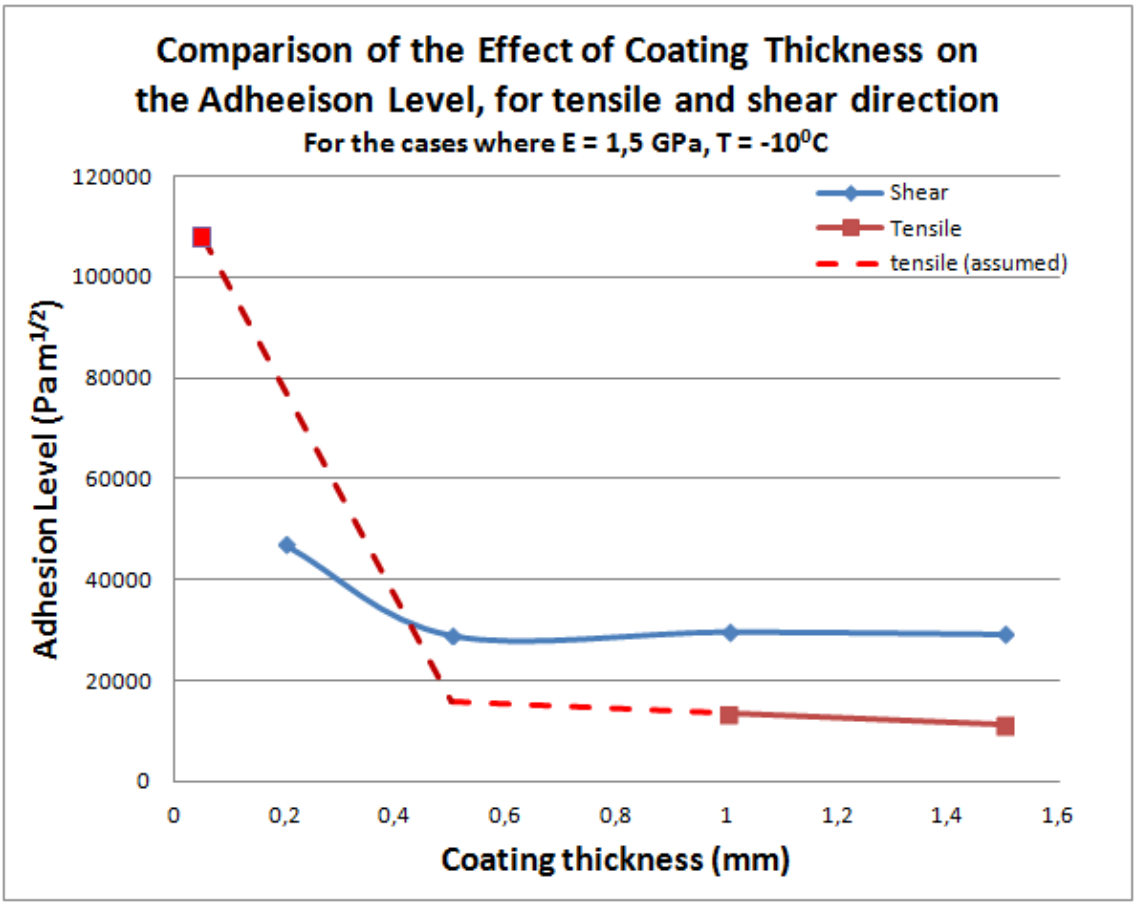

Fig 10.2. Comparison between tensile and shear Adhesion Level in Mode II

This figure corroborates what was observed in the comparison of tensile and shear Adhesion Level for different substrates: For those cases where the coating is loaded in Plane Strain conditions, this is, it is thicker than 0.5 mm, the thickness does not have an effect on the Adhesion Level in Mode II and has a gradual effect in Mode I (the adhesion level at t = 0.5 mm was estimated after observing the data points at t = 1 mm and t = 1.5 mm). The difference between shear and tensile Adhesion Level was attributed to the influence of the Roughness in the shear case

On the other hand, when the coating thickness is decreased up to a point where Plane Stress conditions apply, it is observed an abrupt change in the Adhesion Level in Mode I, whereas the Adhesion Level in Mode II increases more gradually.

This trend line explains why Jellinek observed that the Adhesion Level was larger in the tensile direction than in the shear direction. The existence of a liquid-like layer starts to have an effect in those cases where the thickness is below 0.2 mm. The reduced volume

of the coating cannot cope with larger strain fields, consequently, it cannot generate larger retraction forces that result in an increment on the Adhesion Level in Mode I, whereas the liquid-like layer keeps the increment of the Adhesion Level in Mode II more gradual. As the coating thickness approaches to zer, the Adhesion Level in Mode I is found to be larger than the one in Mode II

10.2. Application to gas turbine fan blades

The main interest of the sponsor of this Project is to understand how a polymeric coating might have an influence on the Adhesion Level of the ice to the blades

When the metallic blades are covered by a polymeric coating, the Adhesion Level of ice is reduced considerably according to the results in this Project. For instance, the Adhesion Level estimated for ice-to-polymeric coatings was found to be reduced around 60-80% when ice was attaching to Aluminium in the same conditions (Figure 8.4). This means that the ice will require lower levels of load to detach from the blades. This reduction on the Adhesion Level, in comparison with metals, will result in ice shedding in small pieces, consequently, less dangerous for the inner parts and more unlikely that fan nearby parts can be damaged in-flight, such as track liners or inlet guide vanes.

Icing is a phenomenon that aircraft manufacturers must deal with in order not to compromise the service and the in-flight safety. The gas turbines are designed with fan track liners assembled around the fan in order to protect the nacelle from ice impact and blade impact. These components must be robust to stand the impact of ice. The fact that the ice adhesion level is lower in coated blades might allow the manufacturer to create lighter fan track liner, resulting in a reduction of the fuel consumption.

WORKS CITED

Ahmad, J. & Majumdar, S., 1992. *An Engineering Fracture Mechanics Analysis of Metal/Ceramic and Ceramic/Ceramic Joints.* Philadelphia, Ernst, H.A; Saxena, A/ McDowell, D.L Editors. American Society for Testing Materials, pp. 590-614.

Anderson, T., 2005. *Fracture Mechanics: Fundaments and Applications (Third Edition).* s.l.:CRC Press. Taylor and Francis Group.

Andersson, L., Golander, C. & Persson, S., 1993. *Ice Adhesion to Rubber Substrates,* Ersmark, Sweden: Lulea University of Technology.

Andrews, E. & Lockington, N., 1983. The Cohesive and Adhesive Strength of Ice. *Journal of Materials Science, Volume 18, Number 5, DOI: 10.1007/BF01111965,* Volume 18, pp. 1455 - 1965.

Andrews, E., Majid, H. & Lockington, N., 1984. Adhesion of Ice to a Flexible Substrate. *Journal of Material Science,* Volume 19.

Andrews, E. & Stevenson, A., 1978. Fracture energy of epoxy resin under plane strain conditions. *Journal of Materials Science, Vol 13, Number 8.DOI: 10.1007/BF00548731,* 13(8), pp. 1860 - 1868.

Fortin, G. & Perron, J., 1996. *Spinning Rotor Blade Tests in Icing Wind Tunnel,* Universite du Quebec a Chicoutimi, Quebec, Canada: Anti-Icing Materials International Laboratory.

Frederking, R. & Karri, J., 1981. *Laboratory Tests on Ice Sheet Adhesion through on Piles of Different Materials,* Helsinki, Finland: Technical Research Center of Finland. Laboratory of Structural Engineering.

Gent, R., Dart, N. & Cansdale, J., 2000. *Aircraft Icing,* Farnborough, Hampshire, United Kingdom: Defense Evaluation and Research Agency.

Hammond, D., Luxford, G. & Ivey, P., 2003. *The Cranfield University Icing Tunnel,* Cranfield, United Kingdom: The School of Engineering, Cranfield University.

Hammond, D. W., 1996. *Microstructurea and mechanical properties of some small ice impact accretions.* Chicoutimi, British Aerospace (Operations), Sowerby Research Centre.

Jellinek, H., 1957. The Influence of Imperfections on the Strength of Ice. *Proceedings of the Physical Society,* 71(5), pp. 797-814.

Jellinek, H., 1959. Adhesive Properties of Ice. *Journal of Colloid Science,* Volume 14, pp. 268 - 280.

Jochel, C., Mueller-Hoppe, D. & Meadows, M., 2006. *Comparison of Tetrahedral and Brick Elements for Linear Elastic Analysis,* s.l.: s.n.

Laforte, C. & Beisswenger, A., 2005. *Icephobic Material Centrifuge Adhesion Test,* Chicoutimi, Quebec, Canada: Anti-Icing Materials International Laboratory, Universite du Quebec a Chicoutimi.

Laforte, C. & Laforte, J., 2009. *Tensile, Torsional and Bending Strain at the Adhesive Rupture of an Iced Substrat,* Chicoutimi, Quebec, Canada: Universite du Quebec a Chicoutimi. Anti-Icing Materials International Laboratory.

Laforte, C., Laforte, J. & Carriere, J., 2002. *How a Solid Coating can reduce the Adhesion of Ice on a Structure.* s.l., Dept. des Sciences Apliquees. University du Quebec a Chicoutimi. Quebec. Canada.

Landy, M. & Freiberger, A., 1966. *Studies of Ice Adhesion: Adhesion to Plastics,* Brooklyn, New York, USA: U.S. Naval Applied Science Laboratory.

Lou, D., 2010. *The Development Production Demonstration and Analysis of the Ice Shear Rig for the Study of Engine Icing.* s.l.:Cranfield University.

Mason, B., 1972. *The Physics of Clouds.* Oxford: Oxford Clarendon Press. ISBN: 0198516037.

New Zealand: Civil Aviation Authority. 2000. *Aircraft Icing Handbook,*

Pervier, M., Gurrutxaga-lerma, B., Piles Moncholi, E. & Hammond, D., 2012. *New test apparatus to measure the adhesive shear,* s.l.: Cranfield University.

Pervier, M. L., 2012. *Mechanics of Ice applied to turbgomachinery. PhD Thesis.* Cranfield: Cranfield University.

Raraty, L. & Tabor, D., 1958. *The Adhesion a d Strength Properties of Ice,* University of Cambridge, UK: Research Laboratory for Physics and Chemistry of Surfaces.

Reddy, J. N. & Gartling, D. K., 2010. *The Finite Element Method in Heat Transfer and Fluid Dynamics, Third Edition.* s.l.:CRC Press.

Spinks, G., Noakes, A., Egan, B. & Isles, N., 1993. Fracture Mechanics of Adhesive Joints. *Journal of Materials Science,* Volume 12., pp. 1065-1067.

Stallabrass, J. & Price, R., 1962. *On the Adhesion of Ice to Various Materials,* Ottawa, Canada: National Rsearch Laboratories, Division of Mechanical Engineering.

Stone, S. F., Westman, R. & Fourney, M., 1975. *Analytical and Experimental Studies in Adhesive Mechanics,* s.l.: UCLA-ENG-7556.

Zeus Industrial Products, I., 2005. *Dielectric Properties of Polymers. Technical Whitepaper,* s.l.: Zeus Inc..

APPENDIX A: LWC CALIBRATION AND SPECIMENS LOCATION IN THE TEST RIG

Cloud Generation

LWC is the content of super cooled droplets in the cloud generated due to the atomization of water sprayed in the Icing Tunnel. The elements whose duty is to create the cloud are some nozzles placed over a spray grid upstream the Test Area. The nozzles work the same way as spray atomizers. The nozzles have a water intake and an air intake. The correct combination of air and water pressure (P_A and P_W respectively), manipulated by the operator in the control room, together with a given air impact speed, gives a concentration of super cooled droplets in the cloud, or LWC. A schematic sketch of a single nozzle is showed in Figure A.1

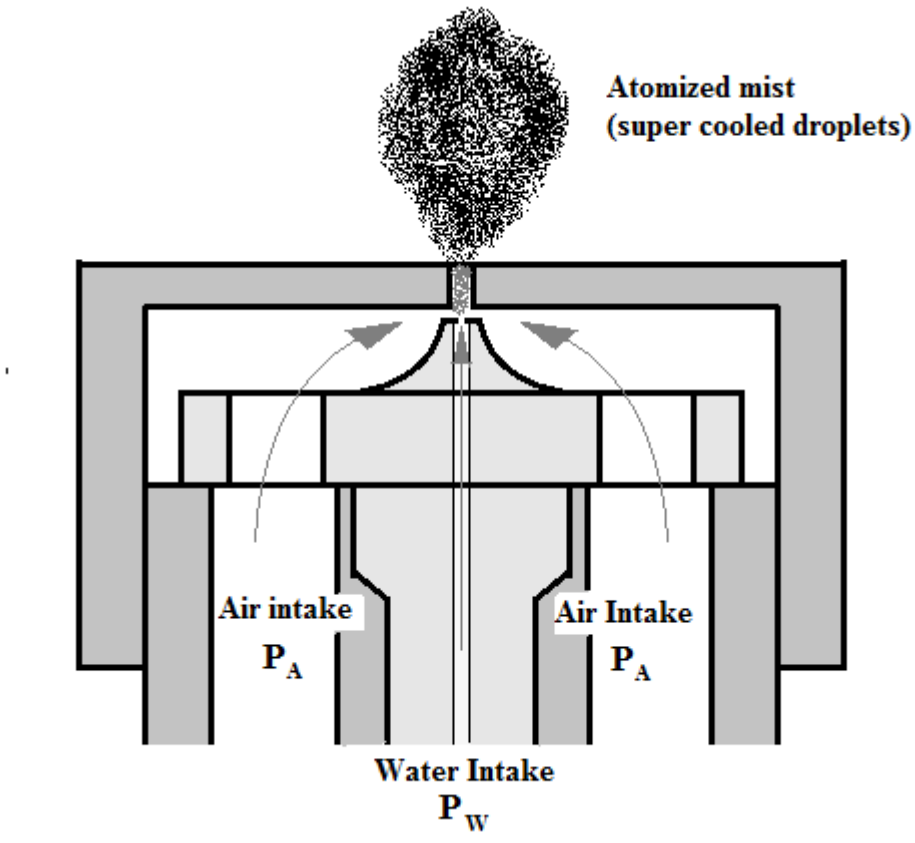

Fig A.1 Sketch of one of the atomizers employed

The LWC observed in the Test Section depends on the P_A and P_W that atomizes the water, on the number of nozzles placed in the grid and on the air speed that drives the cloud towards the Test Section.

The Icing Tunnel drives the air in a wide circuit and at large speeds, so that, the regime within the Tunnel is clearly turbulent. The turbulent regime is a purpose in the design of the Tunnel, as the atomized water from the nozzles must merge into a cloud as homogeneous as possible. However, this idealistic situation is not realistic and the cloud generated within tends to be quite heterogeneous. This variation in the LWC within does not allow placing the Test Specimens randomly inside the Tunnel, but in those places where the LWC is in the same range.

Cloud Set Up

A configuration of nozzles (number and position) must create a cloud whose LWC is as uniform as possible.

The tests carried out in this work are intended to be carried out at a LWC of around 0.4 g/m^3, in order to reproduce the Icing conditions typically found in stratus clouds.

The nozzles are placed randomly in the spray grid, and the tests are carried out continuously, doing small variation between them, until the results obtained are satisfactory enough.

The test fixtures for Mode I and Mode II require different nozzle configuration, since the LWC of the cloud registered in the Test Section can be different, due to the different shape of the bodies placed there.

The configuration employed for Mode I is the one that Pervier used in her work, the configuration for Mode II was developed by the author following the guidelines explained previously. Both Configurations are showed in Figure A.2

Nozzle Configuration Employed for Mode I tests
Cloud configurated by Pervier (Pervier, 2012)
Estimated LWC = 0.4 ± 0.1 g/m³

v (m/s)	P_W (bar)	P_A (bar)
30	16.1	22.6
40	16.6	23.1
50	17	24
60	17.4	24.4

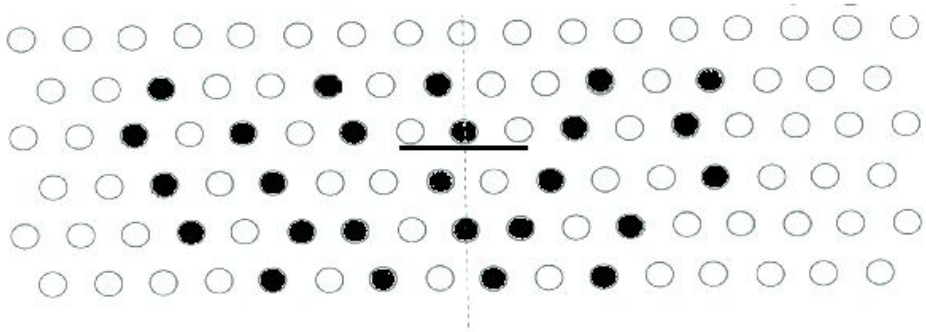

Nozzle Configuration Employed for Mode II tests
Cloud configurated for this work
Estimated LWC = 0.3 ± 0.1 g/m³

v (m/s)	P_W (bar)	P_A (bar)
30	17.5	24.5
40	18.5	25.3
50	19.5	26.2
60	20	26.5

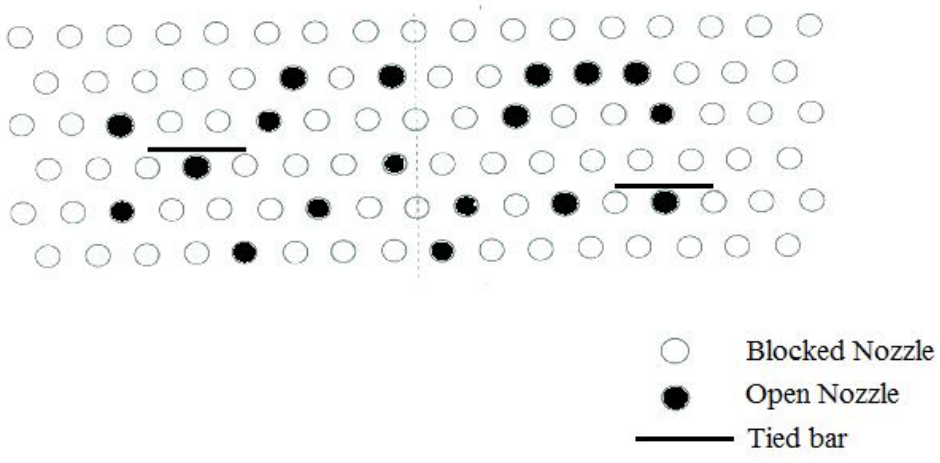

Fig A.2. Nozzle Configurations employed in this work, for Mode I and Mode II tests

The configuration of the spray grid can contains also metallic bars tied transversally over the nozzles. The bars cover three nozzles in the configurations chosen, although its length is variable. The bars are prepared in situ by cutting a larger tube. The bars allow small changes in the cloud distribution, where changing nozzles might cause larger variation. The position of the bars is chosen when the LWC in the cloud is nearby the desired value although its distribution is not entirely satisfactory. The bars create a depression in the immediate zone upstream. This depression causes the suction of the atomized water, causing the cloud to distribute as showed in Figure A.3

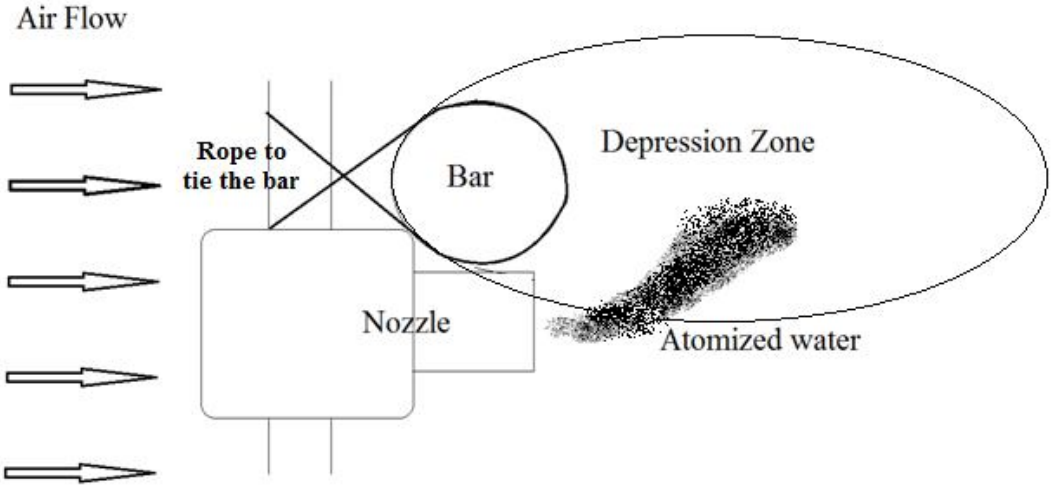

Fig A.3. Sketch explaining the effect of the bar in the LWC distribution

LWC Measurements

These configurations create different clouds in the Section Area. The LWC is calculated following the guidelines by Pervier: A thin blade is placed transversally in the Tunnel when it is running and nozzles are working. This blade is placed from outside, in small holes practised in the walls of the Tunnel and held in slots found in the opposite wall. The blade is left inside for one minute. During that minute, the ice grows on the blade. In order to obtain this, the blade is kept in a freezer at sub zero Temperature, in order to make the super cooled droplets to freeze over it simulating icing conditions. When the blade is taken off, it is measured the thickness of the ice grown on the exposed face in intervals of 5 cm. The LWC in those points is calculated through the equation suggested by Pervier (Pervier, 2012):

$$LWC = \frac{h * \rho}{v * t}$$

Where h is the ice thickness at that point, ρ is the density of the ice, v is the impact speed and t is the time (60 seconds)

Therefore, the LWC of the cloud is measured for 30 points, 10 points along the width of the Tunnel (10 points read from the blade) at 3 altitudes. However, the test fixtures employed are larger than the distance used in the blade points. This work employs the same cloud calibrated by Pervier for Mode I, therefore, the locations of Mode I tests specimens are the ones used by Pervier (Pervier, 2012)

On the other hand, the ISD for Mode II tests and the bar have been modified for this work and another cloud for these fixtures should be calibrated. The ISD size is larger than the Mode I cylinders and can cover up to 3 measurement point positions. Figure A.4 shows a sketch of the Test Section in the Icing Tunnel, where it is distinguished the Test Points and the Test Fixtures allowed locations for Mode II.

The LWC of interest is the value read in the LWC Measurement point corresponding to every possible ISD slot or the average of them in case a ISD slot covers more than one LWC Measurement Point. The Values for LWC in the ISD placing slots are shoed in Table A.2. The table highlights the valid LWC values (those one in the range 0.25 – 0.55 g/m^3 are considered valid enough to consider a test LWC of 0.4 g/m^3) and the chosen ones.

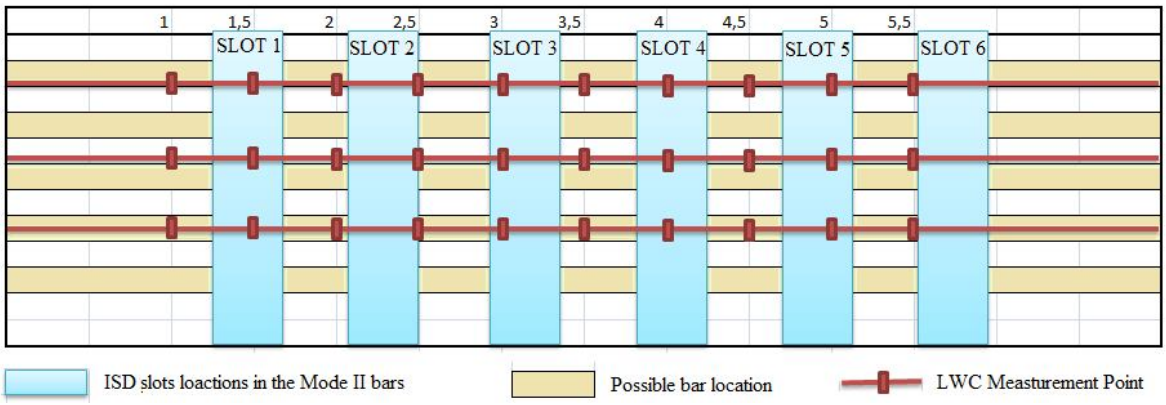

Fig A.4. Locations of the LWC Measurement Points and Mode II ISD location slots

	LWC Measured in allowed ISD locations (g/m^3)					
Blade altitude	SLOT 1	SLOT 2	SLOT 3	SLOT 4	SLOT 5	SLOT 6
top	0,26535	0,281275	0,1641	0,54158	0,38715	0,85695
medium	0,0957	0,131225	0,1537	0,2668	0,58145	0,2639
bottom	0,21605	0,4843	0,3422	0,29145	0,54375	0,56405

chosen valid

Table A.1. LWC measurement in every allowed ISD location and chosen spaces

Having in mind this results, and having chosen the preferred locations for ISD, the layout for Mode II is the one showed in Figure A.5

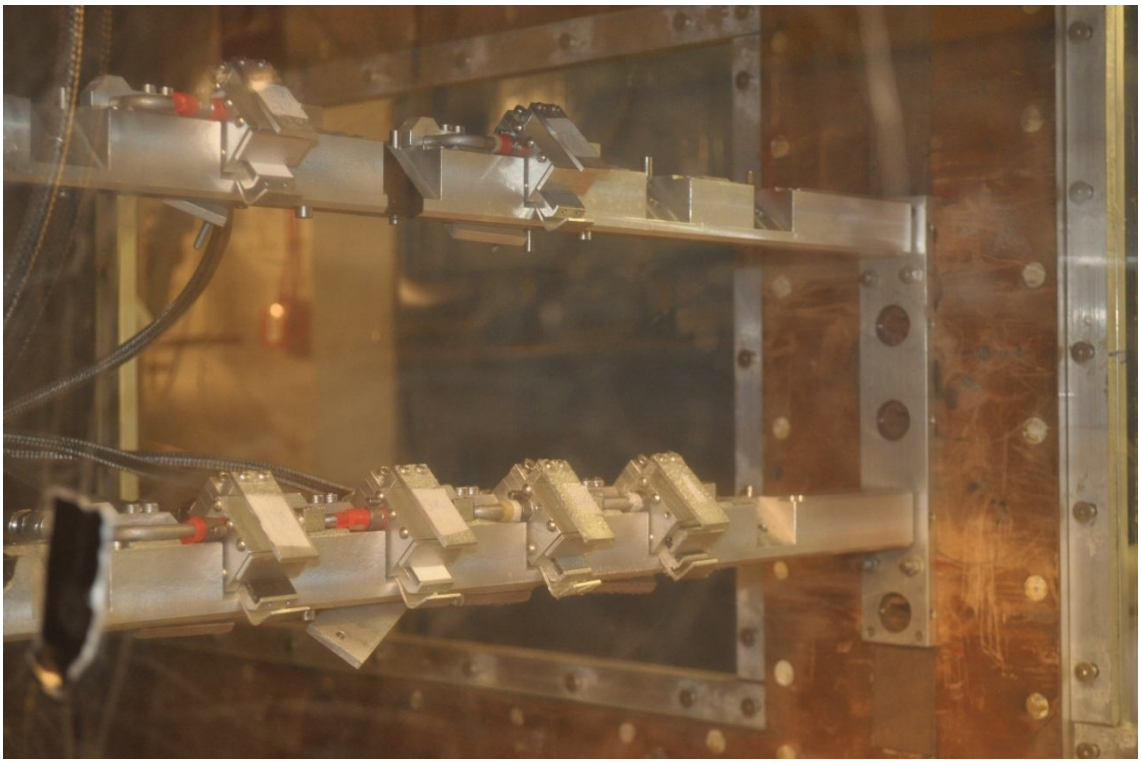

Fig A.5. ISD chosen locations inside the Tunnel, according to LWC measurments